EXTENDED HIGHER ORDER THEORY FOR SANDWICH PLATES OF ARBITRARY ASPECT RATIO

A Thesis
Presented to
The Academic Faculty

by

Faisal Siddiqui

In Partial Fulfillment
of the Requirements for the Degree
Doctor of Philosophy in the
School of Aerospace Engineering

Georgia Institute of Technology
December 2015

EXTENDED HIGHER ORDER THEORY FOR SANDWICH PLATES OF ARBITRARY ASPECT RATIO

Approved by:

Professor George Kardomateas,
Advisor
School of Aerospace Engineering
Georgia Institute of Technology

Professor Graeme J Kennedy
School of Aerospace Engineering
Georgia Institute of Technology

Professor Abdul-Hamid Zureick
School of Civil and Environmental
Engineering
Georgia Institute of Technology

Dr Raghu Pucha
School of Mechanical Engineering
Georgia Institute of Technology

Professor Dewey H. Hodges
School of Aerospace Engineering
Georgia Institute of Technology

Date Approved: July 10 2015

To my late father and sister,

I wish you were alive

to witness this proud

moment

ACKNOWLEDGEMENTS

I am very thankful to Professor Kardomateas for being my mentor and always being considerate and patient with me. His support, guidance and inspiration in each phase of my work has been instrumental in my academic success. He has always been a strong motivational figure and I will always be indebted to him for teaching me the philosophy of research and inculcating a constant urge for academic excellence.

Professor Hodges has always been kind and has helped me whenever I asked for his support and guidance. I am also very thankful to Professor Zureich, Professor Kennedy and Dr. Pucha for agreeing to be a part of my thesis committee and providing their invaluable support and expertise.

I would also take this opportunity to thank Professor Jagoda and all administrative staff of School of Aerospace Engineering for their continued support during my stay at Georgia Tech.

I would like to especially thank my parents for their undying support and belief in me. Their prayers and guidance have always been with me at each step of my life.

Finally, I am heartily thankful to my wife and kids for their support and love. My wife has been instrumental in my ability to complete my research. She has always provided encouragement, personal sacrifices and patience throughout my studies. Thank you for being such a great part of this journey.

Contents

List of Tables

List of Figures

Nomenclature

a	plate length
b	plate width
c	core half thickness
h_{tot}	total plate thickness
q_0	peak value of the sinusoidally distributed transverse load
x	in-plane coordinate along length
y	in-plane coordinate along width
z	thickness wise coordinate
u	in-plane x displacement
v	in-plane y displacement
w	transverse displacement along z-axis

Subscript

0	middle surface

Superscripts

b	bottom face sheet
c	core
t	top face sheet

SUMMARY

In recent years advances in technology have allowed the transition of composite structures from secondary to primary structural components. Consequently, a lot of applications demand development of thicker composite structures to sustain heavier loads. Typical sandwich panels consist of two thin metallic or composite face sheets separated by a honeycomb or foam core. This configuration gives the sandwich panel high stiffness and strength and enables excellent energy absorption capabilities with little resultant weight penalty. This makes sandwich structures a preferred design for a lot of applications including aerospace, naval, wind turbines and civil industries. Most aerospace structures can be analyzed using shell and plate models and many such structures are modeled as composite sandwich plates and shells. Accurate theoretical formulations that minimize the CPU time without penalties on the quality of the results are thus of fundamental importance.

The classical plate theory (CPT) and the first order shear deformation theory (FSDT) are the simplest equivalent single-layer models, and they adequately describe the kinematic behavior of most laminates where the difference between the stiffnesses of the respective phases is not huge. However, in the case of sandwich structures where the core is a much more compliant and softer material as compared to the face sheets the results from CPT and FSDT becomes highly inaccurate. Higher order theories in such cases can represent the kinematics better, may not require shear correction factors, and can yield much more accurate results.

An advanced Extended Higher-order Sandwich Panel Theory (EHSAPT) which is a two-dimensional extension of the EHSAPT beam model that Phan [2] presented is

developed. Phan [2] had extended the HSAPT theory[3] for beams that allows for the transverse shear distribution in the core to acquire the proper distribution as the core stiffness increases as a result of non-negligible in-plane stresses. The HSAPT model is incapable of capturing the in-plane stresses and assumes negligible in-plane rigidity. The current research extends that concept and applies it to two-dimensional plate structures with variable aspect ratios. The theory assumes a transverse displacement in the core that varies as a second order equation in z and the in-plane displacements that are of third order in z, the transverse coordinate. This approach allows for five generalized coordinates in the core (the in-plane and transverse displacements and two rotations about the x and y-axes respectively).

The major assumptions of the theory are as follows:

1. The face sheets satisfy the Euler-Bernoulli assumptions, and their thicknesses are small compared to the overall thickness of the sandwich section; they undergo small strains with moderate rotations.

2. The core is compressible in the transverse and axial directions; it has in-plane, transverse and shear rigidities.

3. The bonding between the face sheets and the core is assumed to be perfect.

The kinematic model is developed by assuming a displacement field for the soft core and then enforcing continuity of the displacement field across the interface between the core and facesheets. The constitutive relations are then defined, and variational and energy techniques are employed to develop the governing equations and associated boundary conditions.

A static loading case for a simply supported sandwich plate is first considered, and the results are compared to existing solutions from Elasticity theory [4, 5], Classical Plate Theory (CPT) and First-Order Shear Deformation Plate Theory (FSDT) [6, 7, 8].

Subsequently, the governing equations for a dynamic analysis are developed for a laminated sandwich plate. A free vibration problem is analyzed for a simply supported laminated sandwich plate, and the results for the fundamental natural frequency are compared to benchmark elasticity solutions provided by Noor [9]. After validation of the new Extended Higher Order Sandwich Panel Theory (EHSAPT), a parametric study is carried out to analyze the effect of variation of various geometric and material properties on the fundamental natural frequency of the structure.

After the necessary verification and validation of the theory by comparing static and free vibration results to elasticity solutions, a nonlinear static analysis for square and rectangular plates is carried out under various sets of boundary conditions. The analysis was carried out using variational techniques, and the Ritz method was used to find an approximate solution. The kinematics were developed for a sandwich plate undergoing small strain and moderate rotations and nonlinear strain displacement relations were evaluated.

Approximate and assumed solutions satisfying the geometric boundary conditions were developed and substituted in the total potential energy relations. After carrying out the spatial integrations, the total potential energy was then minimized with respect to the unknown coefficients in the assumed solution resulting in nonlinear simultaneous algebraic equations for the unknown coefficients. The simultaneous nonlinear equations were then solved using the Newton-Raphson method.

A convergence study was carried out to study the effect of varying the number of terms in the approximate solution on the overall result and rapid convergence was observed. The rapid convergence can be attributed to the fact that the assumed approximate solution not only satisfies the geometric boundary conditions of the problem but also the natural boundary conditions.

During calculations four cases of boundary conditions were considered

1. Simply Supported with moveable edges.

2. Simply Supported with fixed edges.

3. Clamped with moveable edges.

4. Clamped with fixed edges.

For movable boundary conditions, in-plane displacements along the normal direction to the supported edges are allowed whereas the out-of-plane displacement is fixed. For the immovable boundary condition cases, the plate is prevented from both in-plane and out-of-plane displacements along the edges. For the simply supported cases rotations about the tangential direction are allowed, and for the clamped cases no rotations are allowed.

Chapter I

LITERATURE REVIEW

The classical plate theory also known as the Kirchhoff plate theory [10] assumes a non-compressible plate model. It has the advantage of being simple and reliable for thin plates. However, if there is strong anisotropy of mechanical properties, or if the composite plate is relatively thick other advanced models such as the first order shear model is required which assumes a linear distribution of shear effects [11, 6, 7]. Higher-order Shear Deformation Theories (HSDT) have also been used , giving the possibility to increase the accuracy of numerical evaluations for moderately thick plates [12, 13, 14]. But even these theories are not sufficient if local effects are important or accuracy in the calculation of transverse stresses is sought. Therefore, more advanced plate theories have been developed to include zig-zag effects [15, 16, 17, 18, 19]. In some challenging cases the previous type of theories are not sufficiently accurate. Therefore, Layerwise theories have been introduced [20, 21, 22, 23, 24, 25]. In these theories the quantities are layer-dependent and the number of required degrees of freedom is much higher than the case of Equivalent Single Layer Models.

The assumptions on these theories are restrictive and only adequate if the core is made of a high-strength and stiff material, but in many cases when the core is more compliant and is made of a softer material, the evaluations from these theories become more and more inaccurate especially under quasi-static loading [2]. Experimental

results have also shown that the core can undergo significant transverse deformation under a sudden impulsive load and the core plays an important role in the absorption of the impact energy [26, 27, 28, 29, 30]. This implies that in order to get accurate results, the transverse deformation and shear stresses in the core must be taken into consideration. Therefore, a more accurate sandwich panel model should account for the transverse compressibility of the core, and consideration of the core compressibility also implies that the displacements of the upper and lower face sheets may not be identical.

1.1 Static Model

Many refined theories have been proposed in which various assumptions are made in order to better model the behavior of composite sandwich structure. Equivalent single layer, layer-wise, zig-zag, and mixed layer theories have been proposed for the analysis of sandwich beams and plates [31] These theories typically make the same assumption in each layer regarding the distribution of displacements and/or stresses through the thickness coordinate z, and enforce compatibility and/or traction reciprocity at the interfaces. Layer-wise theories with displacement and stress assumptions of $O(z^2)$ to $O(z^4)$ presented in [31] give accurate displacements, stresses (longitudinal and shear), and natural frequencies compared to elastostatic and elastodynamic benchmarks; however, transverse normal stress/strain results were not shown. Furthermore, these theories are often presented in an integral sense because they rely on symbolic mathematical software to evaluate a particular application [32].

Berdichevsky [33, 34] offers an approximate universal asymptotic theory for linear and nonlinear sandwich beams and plates with geometric and material symmetry about the mid-plane of the structure subject to static loads. This theory can give accurate results for the structural response to a static loading or even to a dynamic loading of long-duration, but is not suitable for highly transient loading problems. Hodges also presented an application of the Variational-Asymptotical Method to Laminated Composite Plates [1, 35, 36, 37, 38, 39].

Many different higher order shear deformation theories have been proposed that use higher order terms in the Taylor's series expansion of the displacements in the transverse coordinate [40, 41]. Frostig et al [3] proposed a theory for sandwich panels in which the resulting shear strain in the core is constant and the resulting transverse normal strain in the core is linear in z. However, this model was only formulated for a one-dimensional beam (HSAPT). Hohe et al. [42] developed a model for sandwich plates in which the transverse normal strain is constant along the transverse coordinate z, and the shearing strains are first order in z. Also Li and Kardomateas [43] explored a higher order theory for plates in which the transverse normal strain in the core is cubic in z, and the shear strains in the core are quartic in z.

The accuracy of these models can be assessed because an elasticity solution for the static case already exists. Pagano [4] presented a three-dimensional elasticity solution for laminated rectangular plates for the cases of:

1. *Orthotropic Material:* The cubic characteristic equation has a negative discriminant and results in real and unequal roots

2. *Isotropic Material:* The cubic characteristic equation has a zero discriminant and results in real and equal roots

Kardomateas [5] then presented a closed-form solution for the case of positive discriminant in which case two of the roots are complex conjugates. This is actually a case frequently encountered in sandwich construction in which the core is orthotropic and stiffer in the transverse direction than in the in-plane directions. This elasticity solution is extremely useful in the current context as it allows one to make direct comparison to EHSAPT for various different configurations and validate the theory. While making the analysis, the Classical Plate Theory (CPT) and the First Order Shear Deformation Theory (FSDT) Models are also compared to quantitatively assess the shortcomings of these theories in case of sandwich structures.

1.1.1 Wrinkling of Sandwich Plates

Sandwich plates experience some failure modes not occurring in metallic sheets or laminated plates. Face wrinkling is one of the important behaviors of these plates subjected to in-plane compressive loads. In this phenomenon, the faces buckle in shorter wavelength than those associated with overall buckling of the plate [44].

The first studies on wrinkling analysis of soft-core sandwich panels began in 1930s decade Gough et al. [45] used the Winkler elastic foundation model to study sandwich panels with a compliant core material. They neglected the compressive stresses of the core in the direction of the applied load. The symmetric and anti- symmetric wrinkling for sandwich struts with isotropic facings and solid cores were investigated by Hoff and Mautner [46] using a new model. In this model, the through thickness

deformation decays linearly from the face sheet into the core. Plantema [6] proposed an exponential decay for the through thickness deformation in his book. Allen [7] studied the 2D wrinkling problem of sandwich beams or plates in cylindrical bending. He solved the governing differential equation and assumed that the core stress field has to satisfy the Airy's stress function under 2D conditions. Also, Zenkert [47] and Vinson [48] summarized sandwich wrinkling statements in their textbooks.

Frostig [49] developed a theory using the classical laminated plate theory (CLPT) for the face sheets and postulated a stress distribution in the core for overall and local buckling analysis of soft core sandwich plates. Analytical solutions were presented for simply supported soft-core sandwich plates, but the transverse stress continuity conditions were neglected. In two papers, Dawe and Yuan [50, 51] provided a model which uses a quadratic and linear expansion of the in-plane and transverse displacements of the core and represented the face sheets as either FSDT or CLPT. Vonach and Rammer- storfer [52] studied the problem of the wrinkling of orthotropic sandwich panels under general loading. They assumed infinite thickness for the core and a sinusoidal wrinkling wave at the interface of the face sheet and the core. A high-order layer-wise model was proposed by Dafedar et al. [53] for buckling analysis of multi-core sandwich plates. They assumed cubic polynomial functions for all displacement components in any layer. As a large number of unknowns were involved, they proposed a simplified model and calculated critical loads based on the geometric stiffness matrix concept.

Kardomateas [54] presented a 2D elasticity solution for the wrinkling analysis of sandwich beams or wide sandwich panels subjected to axially compressive loading.

The sandwich section was assumed symmetric and the facings and the core were considered to be orthotropic. Aiello and Ombres [55] presented an analytical approach for evaluating the buckling load of sandwich panels made of hybrid laminated faces and a transversely flexible core. A priori assumption of the displacement field through the thickness was applied which was a superposition of symmetric and anti-symmetric components besides a pure compressive mode.

Noor et al. [56] presented three-dimensional elasticity solutions for global buckling of simply supported sandwich panels with composite face sheets. But, they did not present a wrinkling analysis of the sandwich plates.

Based on the above discussions, it can be concluded that initial works on wrinkling of sandwich plates modeled the supporting action of the core by a simple Winkler elastic foundation. In these models, the effect of the other face sheet is neglected and face sheets are assumed isotropic. Also, in this approach, the sandwich plate wrinkles in a 2D manner such as a sandwich beam or a sandwich plate in cylindrical bending. Some investigators assumed the layered sandwich plates consisting of two laminated composite face sheets and a soft flexible core and postulated polynomial functions for in-plane and transverse displacements of each layer.

Wrinkling has not been studied in the present research work and is proposed as a future work in Section 4.2.

1.2 Dynamic Model

The Classical Laminate Plate Theory (CLPT) which is an extension of the Classical Plate theory neglects the effects of out of plane strains because of the restrictive

a priori assumptions on thhe displacement field. The greater differences in elastic properties between the fiber filaments and the matrix materials lead to a significant difference between the in plane stiffness and the transverse shear modulus which causes the transverse shear deformations to be much more pronounced for laminated and soft core sandwich plates. In general CLPT often under predicts deflections and over predicts natural frequencies. The First Order Shear Deformation Theories (FSDT) assumes linear in-plane stresses and displacements through the laminate thickness. Since the FSDT accounts for layer wise constant states of transverse shear stress, shear correction factors are needed to rectify the unrealistic variation of the shear stress/strain through the thickness.

In order to overcome the limitations of FSDT, higher-order theories that involve higher-order terms in the Taylor's series expansions of the displacements in the thickness coordinate were developed. In these higher-order theories with each additional power of the thickness coordinate an additional dependent unknown is introduced into the theory. Hildebrand et al.[57] were the first to introduce this approach to derive improved theories of plates and shells. Nelson and Lorch [58] and Librescu [59] presented higher-order displacement based shear deformation theories for the analysis of laminated plates. Lo et al.[60, 61] also presented a closed-form solution for a laminated plate with higher-order displacement model which also considers the effect of transverse normal deformation.

Reddy [62] presented a simple higher order theory for laminated composite plates using the kinematic model originally proposed by Levinson and Murthy [63, 64].

Using the theory of Reddy, Senthilnathan et al. [65] presented a simplified higher-order theory by introducing a further reduction of the functional degrees of freedom by splitting up the transverse displacement into bending and shear contributions. Reddy and Phan [66] then used the theory of Reddy [62] to present the free vibration analysis of isotropic, orthotropic and laminated plates. Lee and Hodges then presented the asymptotic method for the analysis of composite shells undergoing high-frequency vibrations using the asymptotic method [67] but no numerical results were presented.

Noor [9] presented exact three dimensional elasticity solutions for the free vibration analysis of isotropic, orthotropic and anisotropic composite laminated plates which serve as a benchmark solutions for comparison and validation of new theories.

1.3 Nonlinear Static Analysis

Nonlinear problems are of interest to the scientific and engineering communities because most physical systems are inherently nonlinear in nature. The sources of nonlinear behavior can be classified into three main categories i.e., geometrical nonlinearity, material nonlinearity and boundary condition nonlinearity. The geometrical nonlinearity category is important to systems with large deflections. When plates are deflected beyond a certain magnitude linear theory loses its validity and produces incorrect results.

In plates geometrical nonlinearity may arise because of the nonlinear strain-displacement relationship, and the nonlinearity in the governing differential equations due to the coupling of in-plane and transverse displacement fields. As a result, mid-plane stretching of the plate may occur. When the deflection of the plate increases,

the stretching effects becomes more pronounced than the bending effect particularly when the edges of the plate are restricted.

Another important category of nonlinearity relates to material properties. Such nonlinearity would render the stress strain relationship of the material of the structure nonlinear. In the case of nonlinear material behavior, linearity occurs up to the yield point and beyond that point the response becomes nonlinear.

Nonlinear systems are also caused by nonlinear boundary conditions. Examples of such phenomena include the use of a nonlinear spring or damper on the edge of a plate. Besides these categories, inertia, impacts, backlash, fluid effects and damping are also capable of categorizing other types of nonlinearities which exist in structures [68].

Plate structures undergoing deformation can be classified into three main regimes that describe the nature of their behavior and thus the characteristics of the mathematical problem, namely [69]:

1. Small deflection theory (linear).

2. Moderately large deflection theory (nonlinear-stretching nonlinearities dominates).

3. Very large deflection theory (highly nonlinear-curvature nonlinearities become important).

This behavior can generally be classified by observation of the amount of deflection in comparison to the plate dimensions. Small deflection theory can typically be used

for deflections less than twenty percent of the plate thickness. Moderately large deflection theory is applied when the deflection is a multiple of the plate thickness but much less than the plate side length, whereas very large deflection theory is applied when the deflection of the plate is similar in order to the magnitude of the plate side length. Depending on the plate classification the solution to these problems can be relatively simple or highly complex, and typically impossible without the implementation of approximating techniques.

1.3.1 Nonlinear Theory of Plates

G. Kirchhoff (1824-1887) discovered the theory of plates that accounts for both bending and stretching of plate structures. After Kirchhoff established the classical linear plate theory, Von Karman[70] developed a nonlinear plate theory. In his study the final form of the nonlinear differential equations governing the moderately large deflection behavior of a statically deflected plate was developed. Solutions for these sets of nonlinear equations have been examined extensively in the literature. Following an approximation by Berger [71], the coupled von Kármán equations were replaced by a simplified set of equations describing the large deflection of plates. Berger solved several problems in the static deflection of plates and concluded that his simplified theory gave results in substantial agreement with more elaborate methods. The Berger formulation can be used to investigate nonlinear vibrations when the strain energy due to the second strain invariant in the middle surface can justifiably by ignored. This then results in decoupling and linearization of the governing equations.

Wah [72] used the simplified Berger equation by imposing the condition that the in-plane displacements u and v can be assumed to disappear at the external boundaries, and therefore applied this assumption for the vibration analysis of rectangular plates with large amplitudes, and with various boundary conditions. In Leissa's monograph [73] other techniques are illustrated which extend the Berger technique to include the vibrational behavior of these nonlinear plates. Hodges et al.[74] also presented a geometrically nonlinear theory for elastic plates.

For nonlinear analysis of plates, Chia [75] has carried out a great deal of work [75]. He made a systematical effort into the large deflection and postbuckling behavior as well as the nonlinear flexural vibration of the isotropic, anisotropic and laminated plates for various boundary conditions. His work not only helped to solve a lot of problems in engineering practice but also established a base for nonlinear numerical method of plates. A bibliography on the geometric nonlinear analysis of plates can be found in the literature [75]. Nayfeh and Mook [76] and Sathyamoorthy [77] have also presented various cases of nonlinear analysis of plates.

1.3.2 Solution Techniques

The solution of a set of nonlinear simultaneous equations is often the final step in the solution of engineering problems. These equations can be expressed as the simultaneous zeroing of a set of functions, where the number of functions to be zeroed is equal to the number of independent variables. The solution techniques for nonlinear equations have interested many researchers for a very long time. A variety of solution techniques can be found in the literature such as the incremental method, the

Newton-Raphson iteration method, the direct minimization of potential energy and incremental iteration technique. Reviews and different classifications of the methods of solving nonlinear structural systems may be found in articles by Riks [78] and Gadala [79]. A great deal of effort has since been made in improving the efficiency of these methods [80, 81, 82, 83] and mathematical software use these techniques for finding the roots of nonlinear equations [84].

Chapter II

THEORY

A sandwich plate with two face sheets of thickness f^b and f^t and a core of thickness $2c$ respectively is considered. The Cartesian coordinate system is placed at the middle plane of the sandwich plate as shown in Figure 1.

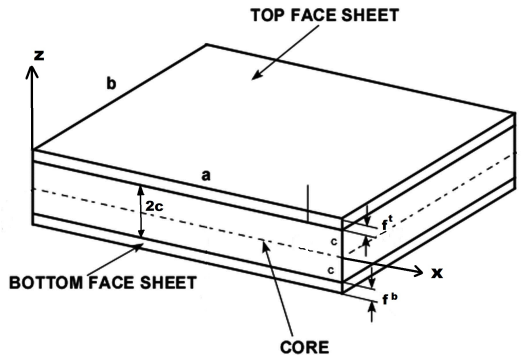

Figure 1: Geometric configuration of the plate

The corresponding displacements are denoted (u, v, w). The superscripts t, b and c refer to the top face sheet, bottom face sheet and the core, respectively. Similarly, the subscript 0 refers to the middle surface of the respective phase.

2.1 Displacements and Strains

The following functions depend on x, y, z and t and this functional dependence will not be explicitly documented in the equations that follow in favor of conserving writing space.

$$u^{t,b,c} = u^{t,b,c}(x, y, z, t), \quad u_0^{t,b,c} = u_0^{t,b,c}(x, y, t), \quad \psi_0^c = \psi_0^c(x, y, t), \quad u_2^c = u_2^c(x, y, t),$$

$$u_3^c = u_3^c(x,y,t)$$

$$v^{t,b,c} = v^{t,b,c}(x,y,z,t), \quad v_0^{t,b,c} = v_0^{t,b,c}(x,y,t), \quad \phi_0^c = \phi_0^c(x,y,t), \quad v_2^c = v_2^c(x,y,t),$$

$$v_3^c = v_3^c(x,y,t)$$

$$w^{t,b,c} = w^{t,b,c}(x,y,z,t), \qquad w_1^c = w_1^c(x,y,t), \qquad w_2^c = w_2^c(x,y,t)$$

2.1.1 Displacements of the Face Sheets

The face sheets are assumed to satisfy the Kirchhoff-Love assumptions and their thickness is assumed to be small as compared to the overall thickness of the plate. The displacements are represented as follows for the top facesheet:

$$u^t = u_0^t - \zeta^t w_{,x}^t \tag{1a}$$

$$v^t = v_0^t - \zeta^t w_{,y}^t \tag{1b}$$

$$w^t = w^t \tag{1c}$$

and similarly for the bottom face sheet:

$$u^b = u_0^b - \zeta^b w_{,x}^b \tag{2a}$$

$$v^b = v_0^b - \zeta^b w_{,y}^b \tag{2b}$$

$$w^b = w^b \tag{2c}$$

where $\zeta^{t,b} = z \mp (c + \frac{f^{t,b}}{2})$

The strain-displacement relations are as follows:

$$\left\{\epsilon\right\} = \begin{Bmatrix} \epsilon_{xx} \\ \epsilon_{yy} \\ \gamma_{xy} \end{Bmatrix} = \left\{\epsilon_0\right\} + \zeta \left\{\kappa\right\} = \begin{Bmatrix} \epsilon_{0x} + \zeta\kappa_x \\ \epsilon_{0y} + \zeta\kappa_y \\ \gamma_{0xy} + \zeta\kappa_{xy} \end{Bmatrix} \tag{3a}$$

$$\left\{\epsilon_0\right\} = \begin{Bmatrix} \epsilon_{0x} \\ \epsilon_{0y} \\ \gamma_{0xy} \end{Bmatrix} = \begin{Bmatrix} u_{0,x} \\ v_{0,y} \\ u_{0,y} \end{Bmatrix} \tag{3b}$$

moreover, $\{\kappa\}$ is the curvature matrix

$$\{\kappa\} = \begin{Bmatrix} \kappa_x \\ \kappa_y \\ \kappa_{xy} \end{Bmatrix} = \begin{Bmatrix} -w_{,xx} \\ -w_{,yy} \\ -2w_{xy} \end{Bmatrix} \tag{3c}$$

2.1.2 Displacements for the Higher-Order Core

As a first order approximation the classical sandwich panel theory neglects the transverse deformation of the core and thus leads to erroneous results in many practical cases. In order to capture the core compressibility effects a higher-order definition of the in-plane and transverse deformation of the core in terms of the transverse coordinate is used.

$$u^c = u_0^c + \psi_0^c z + u_2^c z^2 + u_3^c z^3 \tag{4a}$$

$$v^c = v_0^c - \phi_0^c z + v_2^c z^2 + v_3^c z^3 \tag{4b}$$

$$w^c = w_0^c + w_1^c z + w_2^c z^2 \tag{4c}$$

In these equations $u_0^c,\ v_0^c$ and w_0^c are the in-plane and transverse displacements and ϕ_0^c and ψ_0^c are the rotations about the x-axis and y-axis at the centroid of the core respectively. Also, $u_2^c,\ u_3^c,\ v_2^c,\ v_3^c\ w_1^c$ and w_2^c are the in-plane and transverse unknown functions to be determined by enforcing displacement compatibility conditions at the core/facesheets interface $z = \pm c$. After some algebraic manipulation, the following

core displacement field is obtained.

$$u^c = u_0^c + z\psi_0^c - \frac{z^3}{4c^3}[2u_0^b - 2u_0^t + 4c\psi_0^c - f^b w_{,x}^b - f^t w_{,x}^t] - \frac{z^2}{4c^2}[-2u_0^b - 2u_0^t + 4u_0^c + f^b w_{,x}^b - f^t w_{,x}^t] \tag{5a}$$

$$v^c = v_0^c - z\phi_0^c - \frac{z^3}{4c^3}[2v_0^b - 2v_0^t - 4c\phi_0^c - f^b w_{,y}^b - f^t w_{,y}^t] - \frac{z^2}{4c^2}[-2v_0^b - 2v_0^t + 4v_0^c + f^b w_{,y}^b - f^t w_{,y}^t] \tag{5b}$$

$$w^c = w_0^c - \frac{z^2}{2c^2}[-w^b - w^t + 2w_0^c] - \frac{z}{2c}[w^b - w^t] \tag{5c}$$

This leads to the following strain-displacement relations. It is highlighted that Phan [2] and Li [85] in developing their higher order theories assumed that the core is undergoing moderate rotation with a small displacement and therefore neglected the in-plane strains. The current theory does not make any such assumptions and we consider all six strains in the core. This leads to the following six strain-displacement relations for the core.

$$\epsilon_{xx}^c = u_{0,x}^c + z\psi_{0,x}^c - \frac{z^3}{4c^3}[2u_{0,x}^b - 2u_{0,x}^t + 4c\psi_{0,x}^c - f^b w^b{}_{,xx} - f^t w^t{}_{,xx}] - \frac{z^2}{4c^2}[-2u_{0,x}^b + 4u_{0,x}^c - 2u_{0,x}^t + f^b w^b{}_{,xx} - f^t w^t{}_{,xx}]\psi_{0,x}^c \tag{6a}$$

$$\epsilon_{yy}^c = v_{0,y}^c - z\phi_{0,y}^c - \frac{z^3}{4c^3}[2v_{0,y}^b - 2v_{0,y}^t - 4c\phi_{0,y}^c - f^b w^b{}_{,yy} - f^t w^t{}_{,yy}] - \frac{z^2}{4c^2}[-2v_{0,y}^b + 4v_{0,y}^c - 2v_{0,y}^t + f^b w^b{}_{,yy} - f^t w^t{}_{,yy}] \tag{6b}$$

$$\epsilon_{zz}^c = -\frac{z}{c^2}[2w_0^c - w^b - w^t] - \frac{1}{2c}[w^b - w^t] \tag{6c}$$

$$\gamma_{xy}^c = u_{0,y}^c + z\psi_{0,y}^c + v_{0,x}^c - z\phi_{0,x}^c - \frac{z^3}{4c^3}[2u_{0,y}^b - 2u_{0,y}^t + 4c\psi_{0,y}^c - f^b w^b{}_{,xy} - f^t w^t{}_{,xy}] - \frac{z^3}{4c^3}[2v_{0,x}^b - 2v_{0,x}^t - 4c\phi_{0,x}^c - f^b w^b{}_{,xy} - f^t w^t{}_{,xy}] - \frac{z^2}{4c^2}[-2u_{0,y}^b + 4u_{0,y}^c - 2u_{0,y}^t + f^b w^b{}_{,xy} - f^t w^t{}_{,xy}] - \frac{z^2}{4c^2}[-2v_{0,x}^b + 4v_{0,x}^c - 2v_{0,x}^t + f^b w^b{}_{,xy} - f^t w^t{}_{,xy}] \tag{6d}$$

$$\gamma^c_{xz} = \psi^c_0 + w^c_{0,x} - \frac{z^2}{2c^2}[2w^c_{0,x} - w^b{}_{,x} - w^t{}_{,x}] - \frac{z}{2c}[w^b{}_{,x} - w^t{}_{,x}] - \frac{3z^2}{4c^3}[2u^b_0 - 2u^t_0 + 4c\psi^c_0 - f^b w^b{}_{,x} - f^t w^t{}_{,x}] - \frac{z}{2c^2}[-2u^b_0 + 4u^c_0 - 2u^t_0 + f^b w^b{}_{,x} - f^t w^t{}_{,x}] \quad (6e)$$

$$\gamma^c_{yz} = -\phi^c_0 + w^c_{0,y} - \frac{z^2}{2c^2}[2w^c_{0,y} - w^b{}_{,y} - w^t{}_{,y}] - \frac{z}{2c}[w^b{}_{,y} - w^t{}_{,y}] - \frac{3z^2}{4c^3}[2v^b_0 - 2v^t_0 - 4c\phi^c_0 - f^b w^b{}_{,y} - f^t w^t{}_{,y}] - \frac{z}{2c^2}[-2v^b_0 + 4v^c_0 - 2v^t_0 + f^b w^b{}_{,y} - f^t w^t{}_{,y}] \quad (6f)$$

2.2 Static Model

2.2.1 Constitutive Relations

The face sheets are composite laminates, and the core is fully orthotropic. The stress-strain relations for the top and bottom sheets read as follows:

$$\begin{Bmatrix} \sigma^{t,b}_{xx} \\ \sigma^{t,b}_{yy} \\ \tau^{t,b}_{xy} \end{Bmatrix} = \begin{bmatrix} C^{t,b}_{11} & C^{t,b}_{12} & C^{t,b}_{16} \\ C^{t,b}_{12} & C^{t,b}_{22} & C^{t,b}_{26} \\ C^{t,b}_{16} & C^{t,b}_{26} & C^{t,b}_{66} \end{bmatrix} \begin{Bmatrix} \epsilon^{t,b}_{xx} \\ \epsilon^{t,b}_{yy} \\ \gamma^{t,b}_{xy} \end{Bmatrix} \quad (7a)$$

where C_{ij} $(i,j = 1,2,6)$ are the plane stress reduced stiffness coefficients. The core is considered to be fully orthotropic, so that

$$\begin{Bmatrix} \sigma^c_{xx} \\ \sigma^c_{yy} \\ \sigma^c_{zz} \\ \tau^c_{yz} \\ \tau^c_{xz} \\ \tau^c_{xy} \end{Bmatrix} = \begin{bmatrix} C^c_{11} & C^c_{12} & C^c_{13} & 0 & 0 & 0 \\ C^c_{12} & C^c_{22} & C^c_{23} & 0 & 0 & 0 \\ C^c_{13} & C^c_{23} & C^c_{33} & 0 & 0 & 0 \\ 0 & 0 & 0 & C^c_{44} & 0 & 0 \\ 0 & 0 & 0 & 0 & C^c_{55} & 0 \\ 0 & 0 & 0 & 0 & 0 & C^c_{66} \end{bmatrix} \begin{Bmatrix} \epsilon^c_{xx} \\ \epsilon^c_{yy} \\ \epsilon^c_{zz} \\ \gamma^c_{yz} \\ \gamma^c_{xz} \\ \gamma^c_{xy} \end{Bmatrix} \quad (7b)$$

The stress and moment resultants are defined in Appendix A.

2.2.2 Governing Differential Equations

The governing differential equations can be derived using the principle of minimum total potential energy. The sandwich panel is assumed to be transversely loaded on the top and bottom face sheets respectively. Let the strain energy be denoted by U and the external work by W, then the principle of minimum total potential energy states the following

$$\delta(U - W) = 0 \tag{8}$$

in which the first variation of the energy functionals can be written as follows

$$\begin{aligned}\delta U = \int_0^b \int_0^a \Bigg[& \int_{-c-f}^{-c} (\sigma_{xx}^t \delta\epsilon_{xx}^t + \sigma_{yy}^t \delta\epsilon_{yy}^t + \tau_{xy}^t \delta\gamma_{xy}^t)\, dz + \int_{-c}^{c} (\sigma_{xx}^c \delta\epsilon_{xx}^c + \sigma_{yy}^c \delta\epsilon_{yy}^c \\ & + \sigma_{zz}^c \delta\epsilon_{zz}^c + \tau_{xy}^c \delta\gamma_{xy}^c + \tau_{xz}^c \delta\gamma_{xz}^c + \tau_{yz}^c \delta\gamma_{yz}^c)\, dz + \int_{c}^{c+f} (\sigma_{xx}^b \delta\epsilon_{xx}^b + \sigma_{yy}^b \delta\epsilon_{yy}^b \\ & + \tau_{xy}^b \delta\gamma_{xy}^b)\, dz \Bigg]\, dxdy \end{aligned} \tag{9}$$

and

$$\begin{aligned}\delta W = \int_0^b \int_0^a & \left[q^t(x,y)\delta w^t + q^b(x,y)\delta w^b \, dxdy + \int_V b_x \left(\delta u^b + \delta u^c + \delta u^t\right) \right. \\ & \left. + b_y \left(\delta v^b + \delta v^c + \delta v^t\right) + b_z \left(\delta w^b + \delta w^c + \delta w^t\right) \right] dv \end{aligned} \tag{10}$$

where q^b and q^t are the distributed loads on the top and bottom face sheets respectively and b_x, b_y and b_z are the body forces in the x, y and z directions respectively.

The governing equations and associated boundary conditions can be obtained by substituting the stress-strain relations (7) into equation (9). The stress and moment resultants defined by equations (77) and (78) are then substituted into the resulting equations followed by substitution of equations (3) and (6). Integration by parts in

2D is then carried out which results in eleven governing equations and the associated boundary conditions: three for each face sheet and five for the core as shown in Appendix B.

2.3 Dynamic Model

2.3.1 Constitutive Relations

We assume that the face sheets are laminated plates with several orthotropic layers. The material axes of the individual laminae are oriented arbitrarily with respect to the laminate coordinates. The constitutive relations for the kth lamina in the principal material coordinates of a lamina are

$$\begin{Bmatrix} \sigma_{xx} \\ \sigma_{yy} \\ \tau_{xy} \end{Bmatrix} = \begin{bmatrix} C_{11} & C_{12} & 0 \\ C_{12} & C_{22} & 0 \\ 0 & 0 & C_{66} \end{bmatrix} \begin{Bmatrix} \epsilon_{xx} \\ \epsilon_{yy} \\ \gamma_{xy} \end{Bmatrix} \tag{11a}$$

where C_{ij} $(i, j = 1, 2, 6)$ are the plane stress reduced stiffness coefficients. Since the laminate is made of several orthotropic layers, with their material axes oriented arbitrarily with respect to the laminate coordinates, the constitutive equations for each layer must be transformed to the laminate coordinate system. The stress-strain relations when transformed to the laminate coordinates relate the stresses $(\sigma_{xx}, \sigma_{yy}, \sigma_{xy})$ to the strains $(\epsilon_{xx}, \epsilon_{yy}, \gamma_{xy})$ as follows:

$$\begin{bmatrix} \sigma_{xx} \\ \sigma_{yy} \\ \tau_{xy} \end{bmatrix} = \begin{bmatrix} Q_{11} & Q_{12} & Q_{16} \\ Q_{12} & Q_{22} & Q_{26} \\ Q_{16} & Q_{26} & Q_{66} \end{bmatrix} \begin{bmatrix} \epsilon_{xx} \\ \epsilon_{yy} \\ \gamma_{xy} \end{bmatrix} \tag{11b}$$

Where

$$Q_{11} = C_{11} \sin^4\theta + 2(C_{12} + 2C_{66}) \sin^2\theta \cos^2\theta + C_{22} \sin^4\theta \tag{11c}$$

$$Q_{12} =(C_{11} + C_{22} - 4C_{66}) \sin^2\theta \cos^2\theta + C_{12}(\sin^4\theta + \cos^4\theta) \tag{11d}$$

$$Q_{22} =C_{11} \sin^4\theta + 2(C_{12} + 2C_{66}) \sin^2\theta \cos^2\theta + C_{22} \cos^4\theta \tag{11e}$$

$$Q_{16} =(C_{11} - C_{12} - 2C_{26}) \sin\theta \cos^3\theta + (C_{12} - C_{22} + 2C_{66}) \sin^3\theta \cos\theta \tag{11f}$$

$$Q_{26} =(C_{11} - C_{12} - 2C_{26}) \sin^3\theta \cos\theta + (C_{12} - C_{22} + 2C_{66}) \sin\theta \cos^3\theta \tag{11g}$$

$$Q_{66} =(C_{11} + C_{22} - 2C_{12} - 2C_{66}) \sin^2\theta \cos^2\theta + C_{66}(\sin^4\theta + \cos^4\theta) \tag{11h}$$

The core is considered to be fully orthotropic

$$\begin{Bmatrix} \sigma^c_{xx} \\ \sigma^c_{yy} \\ \sigma^c_{zz} \\ \tau^c_{yz} \\ \tau^c_{xz} \\ \tau^c_{xy} \end{Bmatrix} = \begin{bmatrix} C^c_{11} & C^c_{12} & C^c_{13} & 0 & 0 & 0 \\ C^c_{12} & C^c_{22} & C^c_{23} & 0 & 0 & 0 \\ C^c_{13} & C^c_{23} & C^c_{33} & 0 & 0 & 0 \\ 0 & 0 & 0 & C^c_{44} & 0 & 0 \\ 0 & 0 & 0 & 0 & C^c_{55} & 0 \\ 0 & 0 & 0 & 0 & 0 & C^c_{66} \end{bmatrix} \begin{Bmatrix} \epsilon^c_{xx} \\ \epsilon^c_{yy} \\ \epsilon^c_{zz} \\ \gamma^c_{yz} \\ \gamma^c_{xz} \\ \gamma^c_{xy} \end{Bmatrix} \tag{11i}$$

Next the stress and moment resultants for the laminated facesheets are evaluated and are defined in Appendix C.

2.3.2 Governing Differential Equations

The governing differential equations and associated boundary conditions can be derived using Hamilton's principle. The sandwich panel is subjected to a transverse load $q(x, y, t)$ on the top face sheet. Let the strain energy be denoted by U, the kinetic energy by K and the external work by W, then Hamilton's principle states the following:

$$\delta[T - (U - W)] = 0 \tag{12}$$

in which the first variations of the energy functionals can be written as follows

$$\delta U = \int_0^t \int_0^b \int_0^a \Bigg[\int_c^{c+f^t} (\sigma_{xx}^t \delta\epsilon_{xx}^t + \sigma_{yy}^t \delta\epsilon_{yy}^t + \tau_{xy}^t \delta\gamma_{xy}^t)\ dz + \int_{-c}^{c} (\sigma_{xx}^c \delta\epsilon_{xx}^c + \sigma_{yy}^c \delta\epsilon_{yy}^c + \sigma_{zz}^c \delta\epsilon_{zz}^c + \tau_{xy}^c \delta\gamma_{xy}^c + \tau_{xz}^c \delta\gamma_{xz}^c + \tau_{yz}^c \delta\gamma_{yz}^c)\ dz + \int_{-c-f^b}^{-c} (\sigma_{xx}^b \delta\epsilon_{xx}^b + \sigma_{yy}^b \delta\epsilon_{yy}^b + \tau_{xy}^b \delta\gamma_{xy}^b)\ dz \Bigg]\ dxdy \tag{13}$$

$$\delta T = \int_0^t \int_0^b \int_0^a \Bigg[\int_c^{c+f^t} \rho^t (\dot{u}^t \delta\dot{u}^t + \dot{v}^t \delta\dot{v}^t + \dot{w}^t \delta\dot{w}^t) dz + \int_{-c}^{c} \rho^c (\dot{u}^c \delta\dot{u}^c + \dot{v}^c \delta\dot{v}^c + \dot{w}^c \delta\dot{w}^c) dz + \int_{-c-f^b}^{-c} \rho^b (\dot{u}^b \delta\dot{u}^b + \dot{v}^b \delta\dot{v}^b + \dot{w}^b \delta\dot{w}^b) dz \tag{14}$$

and the work done by the external forces is:

$$\delta W = \int_0^b \int_0^a \left[q^t(x,y,t) \delta w^t + q^b(x,y,t) \delta w^b \right.\ dxdy \tag{15}$$

where ρ is the mass density. The superscript t in the above equations denotes the corresponding values for the top face sheet whereas t appearing in the variable list of the functions refers to time.

The governing equations and associated boundary conditions can be obtained by using a similar approach as used for the static case which results in eleven governing equations: three for each face sheet and five for the core as shown in Appendix D.

2.4 Nonlinear Static Analysis

2.4.1 Variational Techniques

Variational Methods are not only used to obtain the governing differential equations and the associated boundary conditions of the problem but they can also be used to obtain approximate solutions to the governing equations and associated boundary conditions of a problem. These methods are also referred to as classical variational

methods. In these one seeks an approximate solution to the problem in terms of adjustable parameters that are determined by substituting an assumed solution into a variational statement equivalent to the governing equations of the problem. Such solution methods are called direct methods because the approximate solutions are obtained directly by applying the same variational principle that is used to derive the governing equations.

The assumed solutions in the variational methods are in the form of a linear combination of undetermined parameters with adjustable functions. This amounts to representing a continuous function by a finite set of functions. Since the solution of a continuum problem in general cannot be represented by a finite set of functions, error is introduced into the solution. Therefore, the solution obtained is an approximation to the true solution of the equations describing a physical problem. As the number of linearly independent terms in the assumed solution is increased, the error in the approximation will be reduced and the assumed solution converges to the exact solution.

2.4.1.1 Ritz Method

The Ritz method is a procedure for applying the principle of minimum total potential energy to obtain approximate solutions of elastic problems. In the Ritz method the dependent unknown of the problem (e.g., the displacement) u of a given problem is given by a finite linear combination of the form:

$$u^0 = \sum_{m=1}^{M} \sum_{n=1}^{N} A_{mn} u_{mn}(x, y) \tag{16}$$

In the above expression A_{mn} are the unknown parameters and u_{mn} are known functions, each of which may be expressed as $F_m(x)G_n(y)$. The total potential energy of the elastic system, denoted by Π, is

$$\Pi = U + V \tag{17}$$

in which U is the strain energy and $V = -W$ is the potential of the externally applied loads, both being functions of the displacement components. Substituting equation (16) into equation (17), the total potential energy Π becomes a function of the unknown parameters A_{mn}. These parameters are then determined from the condition that the total potential energy of the system is a minimum with respect to them.

$$\Pi_{,A_{mn}} = 0 \tag{18}$$

These conditions state that the incremental energy due to a variation in any of these parameters be zero. Equation (18) gives the same number of equations for A_{mn} as the number of parameters taken in the assumed solution. Evidently the accuracy of the of the method depends upon the choice of the number of parameters and the approximating shape functions u_{mn}.

2.4.1.2 Properties of the Approximation Functions

In order to ensure that the algebraic equations resulting from the Rayleigh-Ritz approximation have a solution, and the approximate solution converges to the true solution of the problem as the number of parameters m and n are increased, we must choose the shape functions so that they meet the following requirements.

1. The shape functions should satisfy the geometric boundary conditions of the problem.

2. The shape functions should be continuous functions as required by the variational statement (i.e., u_{mn} should be such that it has a nonzero contribution to the virtual work statement.

3. The shape functions should be linearly independent and form a complete set

The completeness property is mathematically defined as follow: Given a function u and a real number $\epsilon > 0$, the sequence u_{mn} is said to be complete if there exists an integer N and scalar c_1, c_2, ..., c_N such that

$$||u - \sum_{j=1}^{N} c_j u_{mn}|| < \epsilon \tag{19}$$

The set u_j is called the spanning set. A sequence of algebraic polynomials is called complete if it contains terms of all degrees up to the highest degree N.

Linear independence of a set of functions refers to the property that there exists no nontrivial relation among them i.e.,

$$\alpha_1 u_1 + \alpha_2 u_2 + \cdots + \alpha_N u_N = 0$$

holds for only all $\alpha_j = 0$.

For polynomial approximation functions, the linear independence and completeness properties require u_j to be increasingly higher order polynomials. For example if u_1 is a linear polynomial then u_2 should be a quadratic polynomial and so on (but each u_j may not be complete by itself).

The completeness property is essential for the convergence of the Ritz approximation. Since the natural boundary conditions of the problem are included in the variational statement, we require the Rayleigh Ritz approximation to satisfy the essential boundary conditions of the problem only. These requirements are generally referred to as admissible.

2.4.2 System of Algebraic Equations

Once the approximation shape functions have been selected, the parameters c_j are determined by requiring U_N to minimize the total potential energy functional Π of the problem $\delta\Pi(U_N) = 0$. Hence minimization of the functional $\Pi(U_N)$ is reduced to the minimization of a function of several variables.

$$\delta\Pi(U_N) = \delta\Pi(c_i) = \sum_{i=1}^{N} \frac{\partial \Pi}{\partial c_i} \delta c_i = 0 \tag{20a}$$

or

$$\frac{\partial \Pi}{\partial c_i} = 0 \tag{20b}$$

This gives N algebraic equations in the N coefficients $(c_1, c_2, \cdots, c_n)$

$$\frac{\partial \Pi}{\partial c_i} = \sum_{j=1}^{N} R_{ij} c_j - F_i = 0 \tag{21a}$$

or

$$[R]\{c\} = \{F\} \tag{21b}$$

where R_{ij} and F_i are known coefficients that depend on the problem parameters and the approximation functions.

Some general features of the Ritz method are as follows:

1. If the coordinate functions u_i are selected such that they are complete and linearly independent, the assumed approximation for the displacements converge to the true solution with an increase in the number of parameters (i.e., as $N \to \infty$).

2. For increasing values of N ($N \to \infty$), the previously calculated coefficients of the algebraic equations remain unchanged, provided the previously selected coordinate functions are not changed.

3. If the variational statement is nonlinear in u, then the resulting algebraic equations will also be nonlinear in the parameters c_i. In order to solve these nonlinear equations a variety of numerical techniques may be employed.

4. Since the strains are computed from an approximate displacement field, the strains and stresses are generally less accurate than the displacement.

5. The equilibrium equations of the problem are satisfied only in the energy sense, not in the differential equation sense. Therefore, the displacements obtained in general do not satisfy the equations of equilibrium point wise, unless the solution converged to the exact solution.

6. Since a continuous system is approximated by a finite number of coordinates (or DOFs), the approximate system is less flexible than the actual system. Consequently, the displacements obtained from the total potential energy by the Ritz method converge to exact displacement from below:

$$U_1 < U_2 < \cdots < U_M < U_N < \cdots < u(\text{exact}), \quad \text{for} \quad N > M \tag{22}$$

where U_N denotes the N-parameter Ritz approximation of u obtained using the principle minimum total potential energy. It should be noted that the displacements obtained from the Ritz method based on the total complimentary energy principle are the upper bounds.

2.4.3 Nonlinear Strains

A deformable body under the action of external forces develops internal forces and undergoes deformation. In discussing internal forces, the state of stress at a point within the body is specified by nine components of stress. The deformation is characterized by extension of line elements and distortion of angles between line elements.

For finite deformations both stress and strain can be described by two different reference systems namely the eulerian coordinate system and the lagrangian coordinate system. The eulerian system employs the deformed configuration to describe the coordinate system whereas the lagrangian system utilizes the undeformed configuration to describe the coordinate system. Hence the initially straight material lines are deformed into curves and curved surfaces in the lagrangian coordinate system. The strain tensor in the lagrangian coordinate system is also referred to as the Green strain tensor and the corresponding stress tensor is also called as the Kirchhoff stress tensor.

In the lagrangian description, for finite deformations of an elastic body, the strain displacement relations can be written as follows;

$$\epsilon_{xx} = \frac{\partial u}{\partial x} + \frac{1}{2}\left[\left(\frac{\partial u}{\partial x}\right)^2 + \left(\frac{\partial v}{\partial x}\right)^2 + \left(\frac{\partial w}{\partial x}\right)^2\right]$$

$$
\begin{aligned}
\epsilon_{yy} &= \frac{\partial v}{\partial y} + \frac{1}{2}\left[\left(\frac{\partial u}{\partial y}\right)^2 + \left(\frac{\partial v}{\partial y}\right)^2 + \left(\frac{\partial w}{\partial y}\right)^2\right] \\
\epsilon_{zz} &= \frac{\partial w}{\partial z} + \frac{1}{2}\left[\left(\frac{\partial u}{\partial z}\right)^2 + \left(\frac{\partial v}{\partial z}\right)^2 + \left(\frac{\partial w}{\partial z}\right)^2\right] \\
\epsilon_{xy} &= \frac{1}{2}\left(\frac{\partial u}{\partial y} + \frac{\partial v}{\partial x} + \frac{\partial u}{\partial x}\frac{\partial u}{\partial y} + \frac{\partial v}{\partial x}\frac{\partial v}{\partial y} + \frac{\partial w}{\partial x}\frac{\partial w}{\partial y}\right) \\
\epsilon_{xz} &= \frac{1}{2}\left(\frac{\partial u}{\partial z} + \frac{\partial w}{\partial x} + \frac{\partial u}{\partial x}\frac{\partial u}{\partial z} + \frac{\partial v}{\partial x}\frac{\partial v}{\partial z} + \frac{\partial w}{\partial x}\frac{\partial w}{\partial z}\right) \\
\epsilon_{yz} &= \frac{1}{2}\left(\frac{\partial v}{\partial z} + \frac{\partial w}{\partial u} + \frac{\partial u}{\partial y}\frac{\partial u}{\partial z} + \frac{\partial v}{\partial y}\frac{\partial v}{\partial z} + \frac{\partial w}{\partial y}\frac{\partial w}{\partial z}\right)
\end{aligned} \tag{23}
$$

where ϵ_{ij} are the tensorial strains.

If the components of the displacement gradients are of the order ϵ, i.e.,

$$
\frac{\partial u}{\partial x}, \frac{\partial u}{\partial y}, \frac{\partial v}{\partial x}, \frac{\partial u}{\partial y}, \frac{\partial w}{\partial z} = O(\epsilon) \tag{24}
$$

then the small strain assumption implies that terms of the order ϵ^2 are negligible. Terms of order ϵ^2 are

$$
\begin{gathered}
\left(\frac{\partial u}{\partial x}\right)^2, \left(\frac{\partial u}{\partial y}\right)^2, \left(\frac{\partial u}{\partial z}\right)^2, \left(\frac{\partial u}{\partial x}\right)\left(\frac{\partial u}{\partial y}\right), \left(\frac{\partial u}{\partial x}\right)\left(\frac{\partial u}{\partial z}\right), \left(\frac{\partial u}{\partial y}\right)\left(\frac{\partial u}{\partial z}\right), \\
\left(\frac{\partial v}{\partial x}\right)^2, \left(\frac{\partial v}{\partial y}\right)^2, \left(\frac{\partial v}{\partial z}\right)^2, \left(\frac{\partial v}{\partial x}\right)\left(\frac{\partial v}{\partial y}\right), \left(\frac{\partial v}{\partial x}\right)\left(\frac{\partial v}{\partial z}\right), \left(\frac{\partial v}{\partial y}\right)\left(\frac{\partial v}{\partial z}\right), \\
\left(\frac{\partial w}{\partial x}\right)\left(\frac{\partial w}{\partial z}\right), \left(\frac{\partial w}{\partial y}\right)\left(\frac{\partial w}{\partial z}\right), \left(\frac{\partial w}{\partial z}\right)^2
\end{gathered} \tag{25}
$$

If the rotations $\frac{\partial w}{\partial x}$ and $\frac{\partial w}{\partial y}$ are moderate then the following terms are small but not negligible compared to ϵ

$$
\left(\frac{\partial w}{\partial x}\right)^2, \left(\frac{\partial w}{\partial y}\right)^2, \frac{\partial w}{\partial x}\frac{\partial w}{\partial y} \tag{26}
$$

and they should be included in the strain-displacement relations. Thus for small strains and moderate rotations case the strain-displacement relations (23) take the

form;

$$\epsilon_{xx} = \frac{\partial u}{\partial x} + \frac{1}{2}\left(\frac{\partial w}{\partial x}\right)^2,\ \epsilon_{xy} = \frac{1}{2}\left(\frac{\partial u}{\partial y} + \frac{\partial v}{\partial x} + \frac{\partial w}{\partial x}\frac{\partial w}{\partial y}\right)$$
$$\epsilon_{xz} = \frac{1}{2}\left(\frac{\partial u}{\partial z} + \frac{\partial w}{\partial x}\right),\ \epsilon_{yy} = \frac{\partial v}{\partial y} + \frac{1}{2}\left(\frac{\partial w}{\partial y}\right)^2$$
$$\epsilon_{yz} = \frac{1}{2}\left(\frac{\partial v}{\partial z} + \frac{\partial w}{\partial y}\right),\ \epsilon_{zz} = \frac{\partial w}{\partial z} \tag{27}$$

2.4.4 Kinematics

The displacement field for the facesheets is defined by equations (1) and the displacement field for the higher order core is defined by equations (4a). The non-linear strains for the facesheets are computed using relations (2.4.3).

$$\epsilon^t_{xx} = u^t_{0,x} + \frac{1}{2}{w^t}^2_{,x} - \left(z - \frac{f^t}{2} - c\right){w^t}_{,xx} \tag{28a}$$
$$\epsilon^t_{yy} = v^t_{0,y} + \frac{1}{2}{w^t}^2_{,y} - \left(z - \frac{f^t}{2} - c\right){w^t}_{,yy} \tag{28b}$$
$$\gamma^t_{xy} = u^t_{0,y} + v^t_{0,x} + {w^t}_{,x}{w^t}_{,y} - 2\left(z - \frac{f^t}{2} - c\right){w^t}_{,xy} \tag{28c}$$

similarly for the bottom facesheet

$$\epsilon^b_{xx} = u^b_{0,x} + \frac{1}{2}{w^b}^2_{,x} - \left(z + \frac{f^b}{2} + c\right){w^b}_{,xx} \tag{29a}$$
$$\epsilon^b_{yy} = v^b_{0,y} + \frac{1}{2}{w^b}^2_{,y} - \left(z + \frac{f^b}{2} + c\right){w^b}_{,yy} \tag{29b}$$
$$\gamma^b_{xy} = u^b_{0,y} + v^t_{0,x} + {w^b}_{,x}{w^b}_{,y} - 2\left(z + \frac{f^t}{2} + c\right){w^b}_{,xy} \tag{29c}$$

The nonlinear strain displacement relations for the core are as follows:

$$\epsilon^c_{xx} = u^c_{0,x} + z\psi^c_{0,x} - \frac{z^3}{4c^3}[2u^b_{0,x} - 2u^t_{0,x} + 4c\psi^c_{0,x} - f^b{w^b}_{,xx} - f^t{w^t}_{,xx}]$$
$$- \frac{z^2}{4c^2}[-2u^b_{0,x} + 4u^c_{0,x} - 2u^t_{0,x} + f^b{w^b}_{,xx} - f^t{w^t}_{,xx}]$$

$$+\frac{1}{2}[w^c_{0,x}-\frac{z^2}{2c^2}(2w^c_{0,x}-w^b{}_{,x}-w^t{}_{,x})-\frac{z}{2c}(w^b{}_{,x}-w^t{}_{,x})]^2 \tag{30a}$$

$$\begin{aligned}\epsilon^c_{yy}=&v^c_{0,y}-z\phi^c_{0,y}-\frac{z^3}{4c^3}[2v^b_{0,y}-2v^t_{0,y}-4c\phi^c_{0,y}-f^bw^b{}_{,yy}-f^tw^t{}_{,yy}]\\&-\frac{z^2}{4c^2}[-2v^b_{0,y}+4v^c_{0,y}-2v^t_{0,y}+f^bw^b{}_{,yy}-f^tw^t{}_{,yy}]\\&+\frac{1}{2}[w^c_{0,y}-\frac{z^2}{2c^2}(2w^c_{0,y}-w^b{}_{,y}-w^t{}_{,y})-\frac{z}{2c}(w^b{}_{,y}-w^t{}_{,y})]^2\end{aligned} \tag{30b}$$

$$\epsilon^c_{zz}=-\frac{z}{c^2}[2w^c_0-w^b-w^t]-\frac{1}{2c}[w^b-w^t] \tag{30c}$$

$$\begin{aligned}\gamma^c_{xy}=&u^c_{0,y}+z\psi^c_{0,y}+v^c_{0,x}-z\phi^c_{0,x}-\frac{z^3}{4c^3}[2u^b_{0,y}-2u^t_{0,y}+4c\psi^c_{0,y}-f^bw^b{}_{,xy}-f^tw^t{}_{,xy}]\\&-\frac{z^3}{4c^3}[2v^b_{0,x}-2v^t_{0,x}-4c\phi^c_{0,x}-f^bw^b{}_{,xy}-f^tw^t{}_{,xy}]-\frac{z^2}{4c^2}[-2u^b_{0,y}+4u^c_{0,y}\\&-2u^t_{0,y}+f^bw^b{}_{,xy}-f^tw^t{}_{,xy}]-\frac{z^2}{4c^2}[-2v^b_{0,x}+4v^c_{0,x}-2v^t_{0,x}+f^bw^b{}_{,xy}-f^tw^t{}_{,xy}]\\&+\frac{1}{4c^2}[2(c^2-z^2)w^c_{0,y}+z\{(z-c)w^b{}_{,y}+(z+c)w^t{}_{,y}\}]\\&\quad[2(c^2-z^2)w^c_{0,x}+z\{(z-c)w^b{}_{,x}+(z+c)w^t{}_{,x}\}]\end{aligned} \tag{30d}$$

$$\begin{aligned}\gamma^c_{xz}=&\psi^c_0+w^c_{0,x}-\frac{z^2}{2c^2}[2w^c_{0,x}-w^b{}_{,x}-w^t{}_{,x}]-\frac{z}{2c}[w^b{}_{,x}-w^t{}_{,x}]-\frac{3z^2}{4c^3}[2u^b_0-2u^t_0\\&+4c\psi^c_0-f^bw^b{}_{,x}-f^tw^t{}_{,x}]-\frac{z}{2c^2}[-2u^b_0+4u^c_0-2u^t_0+f^bw^b{}_{,x}-f^tw^t{}_{,x}]\end{aligned} \tag{30e}$$

$$\begin{aligned}\gamma^c_{yz}=&-\phi^c_0+w^c_{0,y}-\frac{z^2}{2c^2}[2w^c_{0,y}-w^b{}_{,y}-w^t{}_{,y}]-\frac{z}{2c}[w^b{}_{,y}-w^t{}_{,y}]-\frac{3z^2}{4c^3}[2v^b_0-2v^t_0\\&-4c\phi^c_0-f^bw^b{}_{,y}-f^tw^t{}_{,y}]-\frac{z}{2c^2}[-2v^b_0+4v^c_0-2v^t_0+f^bw^b{}_{,y}-f^tw^t{}_{,y}]\end{aligned} \tag{30f}$$

2.4.5 Constitutive Relations

The face sheets are composite laminates and the core is fully orthotropic.The stress-strain relations for the top and bottom sheets read as follows:

$$\begin{bmatrix}\sigma^{t,b}_{xx}\\ \sigma^{t,b}_{yy}\\ \tau^{t,b}_{xy}\end{bmatrix}=\begin{bmatrix}C^{t,b}_{11} & C^{t,b}_{12} & C^{t,b}_{16}\\ C^{t,b}_{12} & C^{t,b}_{22} & C^{t,b}_{26}\\ C^{t,b}_{16} & C^{t,b}_{26} & C^{t,b}_{66}\end{bmatrix}\begin{bmatrix}\epsilon^{t,b}_{xx}\\ \epsilon^{t,b}_{yy}\\ \gamma^{t,b}_{xy}\end{bmatrix} \tag{31a}$$

where C_{ij} $(i,j = 1,2,6)$ are the plane stress reduced stiffness coefficients. The core is considered to be fully orthotropic

$$\begin{bmatrix} \sigma^c_{xx} \\ \sigma^c_{yy} \\ \sigma^c_{zz} \\ \tau^c_{yz} \\ \tau^c_{xz} \\ \tau^c_{xy} \end{bmatrix} = \begin{bmatrix} C^c_{11} & C^c_{12} & C^c_{13} & 0 & 0 & 0 \\ C^c_{12} & C^c_{22} & C^c_{23} & 0 & 0 & 0 \\ C^c_{13} & C^c_{23} & C^c_{33} & 0 & 0 & 0 \\ 0 & 0 & 0 & C^c_{44} & 0 & 0 \\ 0 & 0 & 0 & 0 & C^c_{55} & 0 \\ 0 & 0 & 0 & 0 & 0 & C^c_{66} \end{bmatrix} \begin{bmatrix} \epsilon^c_{xx} \\ \epsilon^c_{yy} \\ \epsilon^c_{zz} \\ \gamma^c_{yz} \\ \gamma^c_{xz} \\ \gamma^c_{xy} \end{bmatrix} \tag{31b}$$

2.4.6 Principle of Minimum Total Potential Energy

The strain energy for the plate is given by the following relation;

$$\begin{aligned} U = \frac{1}{2}\int_0^b \int_0^a \Bigg[& \int_{-c-f}^{-c} (\sigma^t_{xx}\epsilon^t_{xx} + \sigma^t_{yy}\epsilon^t_{yy} + \tau^t_{xy}\gamma^t_{xy})\ dz + \int_{-c}^{c} (\sigma^c_{xx}\epsilon^c_{xx} + \sigma^c_{yy}\epsilon^c_{yy} \\ & + \sigma^c_{zz}\epsilon^c_{zz} + \tau^c_{xy}\gamma^c_{xy} + \tau^c_{xz}\gamma^c_{xz} + \tau^c_{yz}\gamma^c_{yz})\ dz + \int_{c}^{c+f} (\sigma^b_{xx}\epsilon^b_{xx} + \sigma^b_{yy}\epsilon^b_{yy} \\ & + \tau^b_{xy}\gamma^b_{xy})\ dz \Bigg]\ dxdy \end{aligned} \tag{32}$$

The potential of the externally applied load q_0 on the top facesheet is given by is given by

$$W = \int_0^b \int_0^a q(x,y) \sin\frac{\pi x}{a} \sin\frac{\pi y}{b} w^t\ dxdy \tag{33}$$

The total potential energy is described by:

$$\Pi = U - W \tag{34}$$

The total potential energy is integrated with respect to the thickness coordinate z to obtain a relationship which is only a function of the inplane coordinates x and y.

Substituting the assumed solution into $\Pi = \Pi(x, y)$, the total potential energy Π now becomes a function of the unknown parameters A_{mn} in the assumed solution. These parameters are then determined by the condition that the total potential energy of the system is a minimum with respect to them. After the differentiations are carried out we are left with $M \times N$ simultaneous nonlinear algebraic equations which are then solved using the Newton-Raphson method.

2.4.7 Newton-Raphson Method for Nonlinear System of Equations

The Newton-Raphson method gives a very efficient means of converging to a root if a sufficiently good initial guess is available.

A typical problem gives N functional relations to be zeroed, involving variables x_i, $i = 1, 2, \cdots, N$.

$$F_i(x_1, x_2, \cdots, x_N) = 0 \qquad i = 1, 2, \cdots, N \tag{35}$$

If $\mathbf{x}$ denotes the entire vector of values x_i and $\mathbf{F}$ denotes the entire vector of functions F_i. In the neighborhood of $\mathbf{x}$, each of the functions F_i can be expanded in a Taylor's series exapnsion.

$$F_i(x + \delta x) = F_i(x) + \sum_{j=1}^{N} \frac{\partial F_i}{\partial x_j} \delta x_j + O(\delta x^2) \tag{36}$$

The matrix of partial derivatives appearing in equation (36) is the *Jacobian* matrix $\mathbf{J}$:

$$J_{ij} = \frac{\partial F_i}{\partial x_j} \tag{37}$$

In matrix notation equation (37) is;

$$\mathbf{F}(x + \delta x) = \mathbf{F}(x) + \mathbf{J}.\delta x + O(\delta x^2) \tag{38}$$

By neglecting terms of order δx^2 and higher and by setting $\mathbf{F}(x + \delta x) = 0$, we obtain a set of linear equations for the corrections δx that move each function closer to zero simultaneously, namely;

$$\mathbf{J}.\delta x = -\mathbf{F} \tag{39}$$

Matrix equation (39) can be solved by LU decomposition and the corrections are then added to the solution vector;

$$x_{new} = x_{old} + \delta x \tag{40}$$

and the process is iterated to convergence.

Chapter III

RESULTS

3.1 Static Model

The numerical results for several typical sandwich configurations are evaluated and compared to established elasticity solutions, the existing classical model and the first order shear model. The case of a simply supported plate which is subjected to sinusoidal transverse loading on the top face sheet will be studied.

$$q(x,y) = q_0 \sin\frac{\pi x}{a}\sin\frac{\pi y}{b}, \qquad 0 \le x \le a, \qquad 0 \le y \le b \tag{41}$$

The following boundary conditions are applied: For $x = 0,\ a$

$$v_0^b = v_0^c \quad = v_0^t \quad = 0 \tag{42a}$$

$$w^b = w_0^c \quad = w^t \quad = 0 \tag{42b}$$

$$w^b{}_{,y} = \phi_0^c \quad = w^t{}_{,y} = 0 \tag{42c}$$

$$\tilde{N}_{xx}^b = \tilde{N}_{xx}^c \ = \tilde{N}_{xx}^t = 0 \tag{42d}$$

$$\tilde{M}_{xx}^b = \tilde{M}_{xx}^c = \tilde{M}_{xx}^t = 0 \tag{42e}$$

similar boundary conditions can be written for the other two edges of the plate at $y = 0$ and b.

According to the Navier's solution technique the following displacement functions are assumed that satisfy the boundary conditions of the problem.

$$u_0^t = U^T \cos\frac{\pi x}{a}\sin\frac{\pi y}{b}, \quad u_0^c = U^C \cos\frac{\pi x}{a}\sin\frac{\pi y}{b}, \quad u_0^b = U^B \cos\frac{\pi x}{a}\sin\frac{\pi y}{b} \tag{43a}$$

$$v_0^t = V^T \sin\frac{\pi x}{a}\cos\frac{\pi y}{b}, \quad v_0^c = V^C \sin\frac{\pi x}{a}\cos\frac{\pi y}{b}, \quad v_0^b = V^B \sin\frac{\pi x}{a}\cos\frac{\pi y}{b} \tag{43b}$$

$$w^t = W^T \sin\frac{\pi x}{a}\sin\frac{\pi y}{b}, \quad w_0^c = W^C \sin\frac{\pi x}{a}\sin\frac{\pi y}{b}, \quad w^b = W^B \sin\frac{\pi x}{a}\sin\frac{\pi y}{b} \tag{43c}$$

$$\phi_0^c = \Phi \sin\frac{\pi x}{a}\cos\frac{\pi y}{b}, \quad \psi_0^c = \Psi \cos\frac{\pi x}{a}\sin\frac{\pi y}{b} \tag{43d}$$

where U^T, U^C, U^B, V^T, V^C, V^B, W^T, W^C, W^B, Φ and Ψ are constants to be determined. Substituting equations Eqn.(43) into Eqn.(79) results in a system of eleven equations for the eleven unknown constants U^T, U^C, U^B, V^T, V^C, V^B, W^T, W^C, W^B, Φ and Ψ.

3.1.1 Numerical Results

We first consider a sandwich configuration consisting of unidirectional graphite/epoxy faces with moduli (in GPa) of $E_1^f = 181.0$, $E_2^f = E_3^f = 10.3$, $G_{12}^f = G_{31}^f = 7.17$, and $G_{23}^f = 5.96$ and Poisson's ratio of $\nu_{12}^f = 0.277$, $\nu_{31}^f = 0.016$ and $\nu_{32}^f = 0.4$. The core is made up of hexagonal glass/phenolic honeycomb with moduli (in GPa) of $E_1^c = E_2^c = 0.032$, $E_3^c = 0.300$, $G_{23}^c = G_{31}^c = 0.048$ and $G_{12}^c = 0.013$ and Poisson's ratio of $\nu_{12}^c = \nu_{31}^c = \nu_{32}^c = 0.250$.

The two face sheets are identical with a thickness of $f = 2$ mm. The core thickness is $2c = 16$ mm. The total thickness of the plate is defined to be $h_{tot} = 2f + 2c$. In the following results, the displacements are normalized with $100h_{tot}\frac{q_0}{E_1^f}$ and the stresses with $q_0\frac{a^2}{h_{tot}^2}$. Two plate configurations are considered with $a = b = 5h_{tot}$ and $a = b = 20h_{tot}$, respectively.

Plotted in Figure 2 is the normalized displacement at the top face sheet as a function of x at $y = b/2$. In this figure we also show the predictions of the CPT as well as FSDT; for the latter, there are two versions: one that is based only on the

core shear stiffness and one that includes the face sheet stiffnesses. From Figure 2, one can see that both CPT and FSDT seem to be inadequate. The classical theory is too non-conservative and the first order shear with faces added can hardly make a difference. On the other hand the first order shear theory where shear is assumed to be carried exclusively by the core is too conservative; this clearly demonstrates the need for higher order theories in dealing with sandwich plate structures. In this regard the EHSAPT theory gives a profile which is essentially identical to the elasticity solution. In Figure 2 we can also see the effect of transverse shear, which is an important feature of sandwich structures.

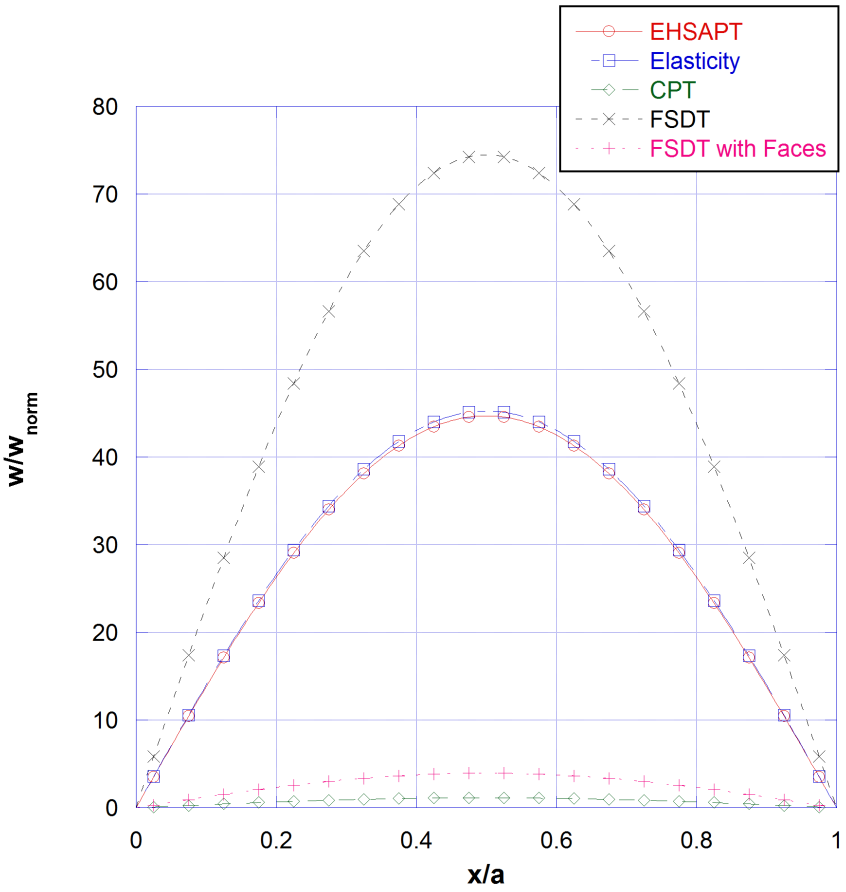

Figure 2: Transverse displacement w^t, at the top face $z = c + f^t$ at $y = \frac{b}{2}$ for $a = b = 5h_{tot}$

The distribution of the axial stresses σ_{xx} and σ_{yy} in the core as a function of z at the midspan location, $x = \frac{a}{2}$ and $y = \frac{b}{2}$ (where the bending moment is maximum) is plotted in Figures 3 and 4. Note that for both elasticity and EHSAPT, there is no symmetry with regard to the mid-plane ($z = 0$).

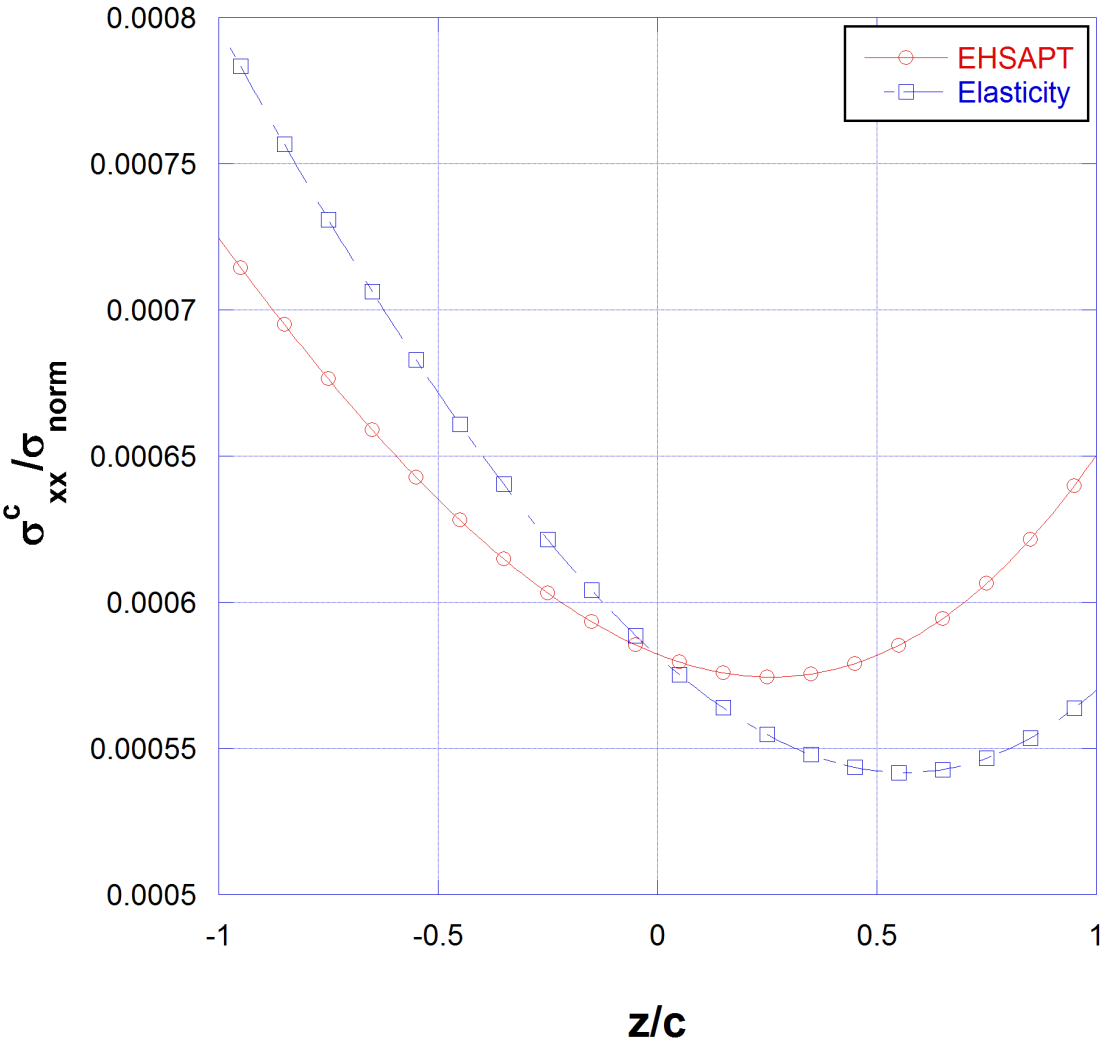

Figure 3: Through-thickness distribution in the core of the axial stress, σ^c_{xx}, at $x = a/2$ and $y = b/2$; case of $a = b = 5h_{tot}$

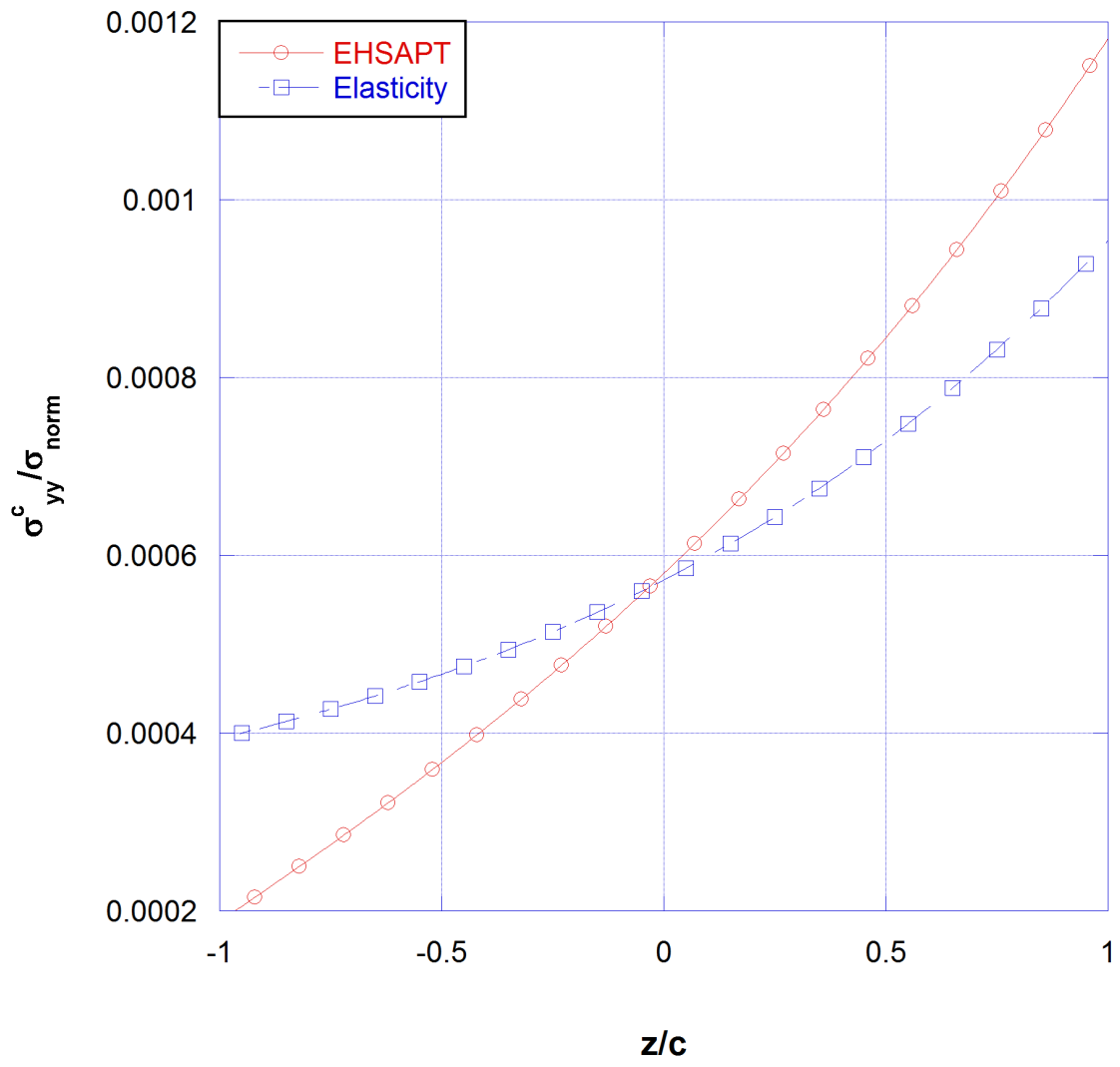

Figure 4: Through-thickness distribution in the core of the axial stress, σ^c_{yy}, at $x = a/2$ and $y = b/2$; case of $a = b = 5h_{tot}$

The through-thickness distribution of the transverse normal stress in the core, σ_{zz}, at the midspan location, $x = a/2$ and $y = b/2$, is shown in Figure 5. It can be seen that the elasticity curve is in perfect agreement with the EHSAPT curve and both are nearly linear.

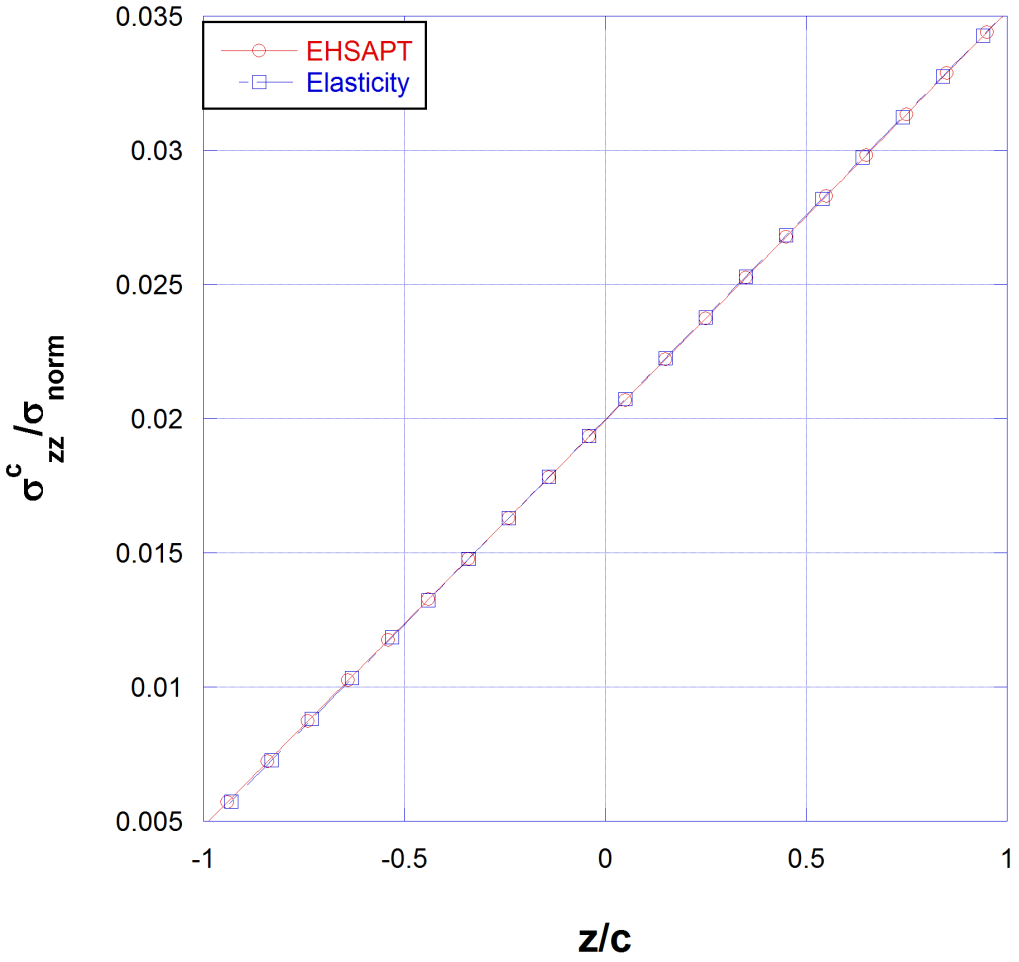

Figure 5: Through-thickness distribution in the core of the transverse normal stress, σ^c_{zz}, at $x = a/2$ and $y = b/2$; case of $a = b = 5h_{tot}$

Plotted in Figs. 6, 7, 8 and 9 are the normalized displacement, axial stresses and the transverse normal stress respectively for the case of $a = b = 20h_{tot}$.

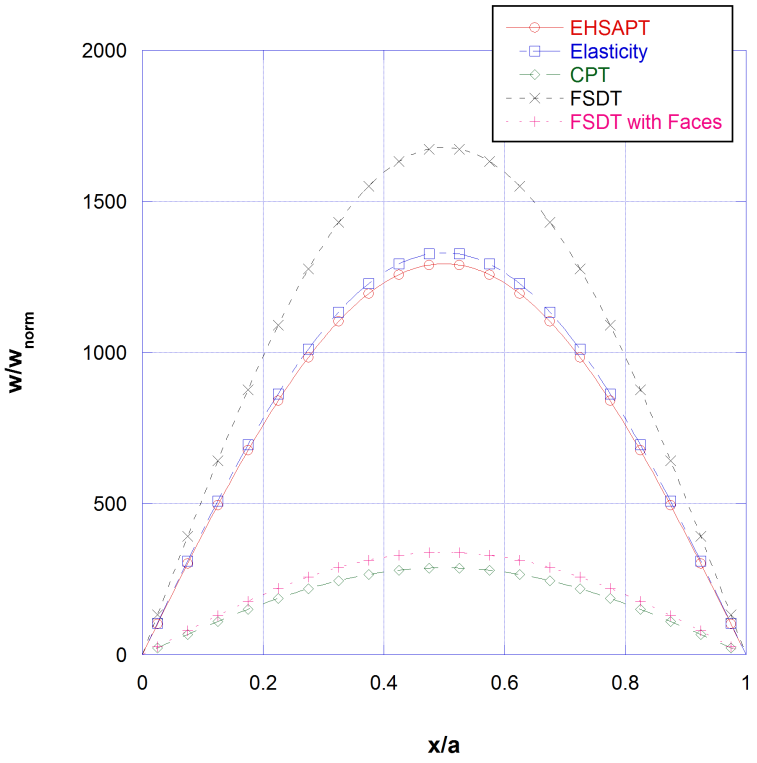

Figure 6: Transverse displacement w^t, at the top face $z = c + f^t$ at $y = \frac{b}{2}$ for $a = b = 20h_{tot}$

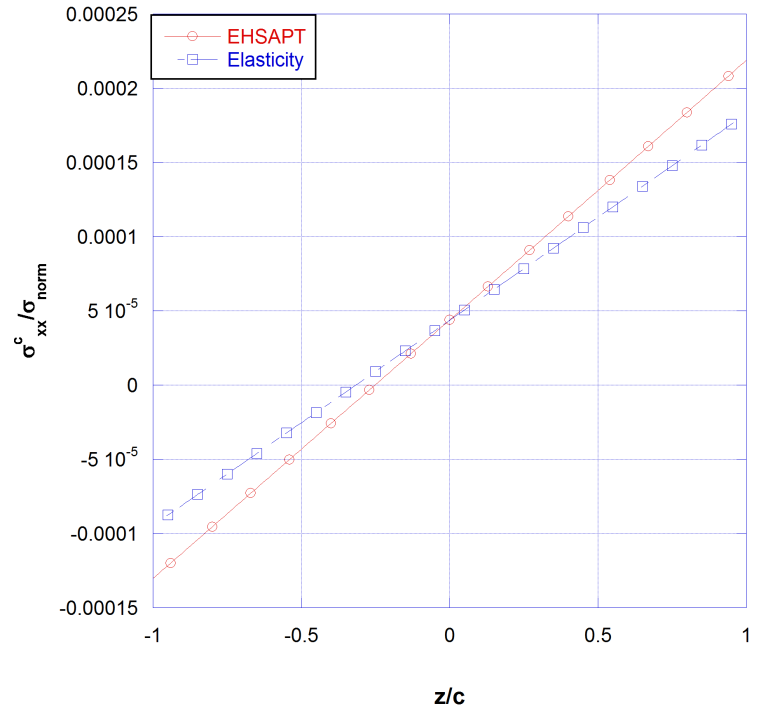

Figure 7: Through-thickness distribution in the core of the axial stress, σ^c_{xx}, at $x = a/2$ and $y = b/2$; case of $a = b = 20h_{tot}$

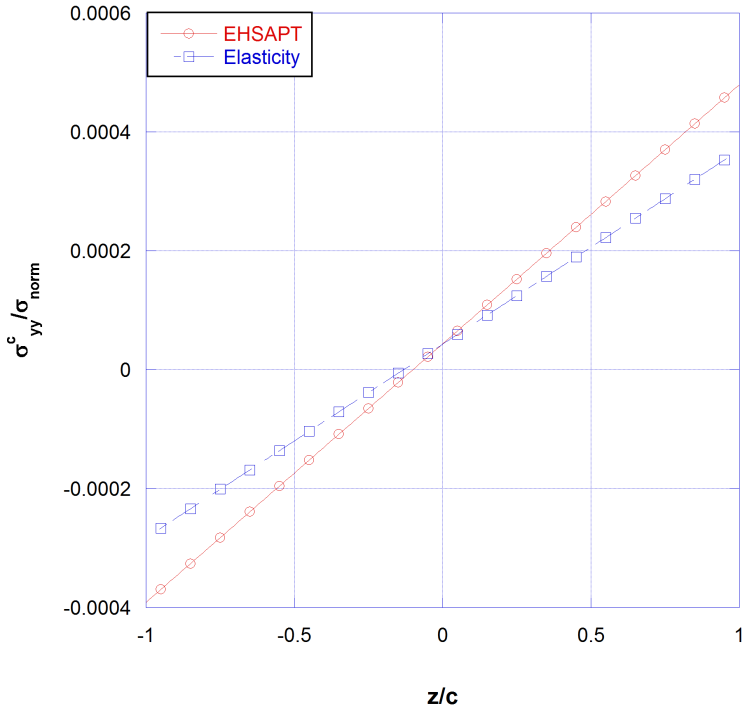

Figure 8: Through-thickness distribution in the core of the axial stress, σ^c_{yy}, at $x = a/2$ and $y = b/2$; case of $a = b = 20h_{tot}$

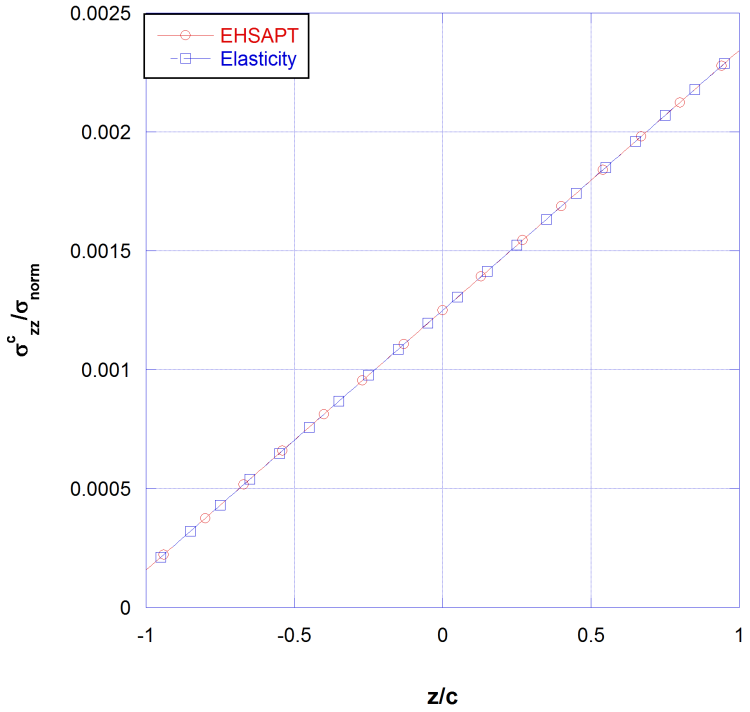

Figure 9: Through-thickness distribution in the core of the transverse normal stress, σ^c_{zz}, at $x = a/2$ and $y = b/2$; case of $a = b = 20h_{tot}$

3.1.1.1 Comparison with CLPT and FSDT theories

In the classical sandwich model, the core is assumed to be incompressible in the transverse direction, and the transverse displacements of the face sheets and the core are considered to be the same. As such, the governing equation for a plate subject to transverse loading $q^t(x, y)$ of the top face sheet reads as:

$$D_{11}\frac{\partial^4 w(x,y)}{\partial x^4} + 2(D_{12} + 2D_{66})\frac{\partial^4 w(x,y)}{\partial^2 x \partial^2 y} + D_{22}\frac{\partial^4 w(x,y)}{\partial y^4} = q(x,y) \tag{44}$$

where the stiffness matrix is defined as

$$D_{ij} = C_{ij}\left(2fc^2 + 2f^2c + \frac{2}{3}f^3\right) \tag{45}$$

and

$$q^t(x,y) = q_0 \sin\frac{m\pi x}{a}\sin\frac{n\pi y}{b} \tag{46}$$

For a simply supported rectangular plate, the transverse displacements can be expressed as

$$w(x,y) = \sum_{m,n} W_{mn}\sin\frac{m\pi x}{a}\sin\frac{n\pi y}{b} \tag{47}$$

Which leads to

$$W_{mn} = q_0 \Big/ \left[D_{11}\left(\frac{m\pi}{a}\right)^4 + 2(D_{12} + 2D_{66})\left(\frac{m\pi}{a}\right)^2\left(\frac{n\pi}{b}\right)^2 + D_{22}\left(\frac{n\pi}{b}\right)^4\right] \tag{48}$$

If we let $\bar{\alpha}_x$ be the shear deformation in the x direction and $\bar{\alpha}_y$ be the shear deformation in the y direction, then the governing equations with shear effects can be written as:

$$D_{11}\frac{\partial^2 \bar{\alpha}_x}{\partial x^2} + D_{66}\frac{\partial^2 \bar{\alpha}_x}{\partial y^2} + (D12 + D_{66})\frac{\partial^2 \bar{\alpha}_y}{\partial x \partial y} - \kappa D_{55}\left(\bar{\alpha}_x + \frac{\partial w}{\partial x}\right) = 0 \tag{49a}$$

$$(D12 + D_{66})\frac{\partial^2 \bar{\alpha}_x}{\partial x \partial y} + D_{66}\frac{\partial^2 \bar{\alpha}_y}{\partial x^2} + D_{22}\frac{\partial^2 \bar{\alpha}_y}{\partial x^2} - \kappa D_{44}\left(\bar{\alpha}_y + \frac{\partial w}{\partial y}\right) = 0 \tag{49b}$$

$$\kappa D_{55}\left(\frac{\partial \bar{\alpha}_x}{\partial x} + \frac{\partial^2 w}{\partial x^2}\right) + \kappa D_{44}\left(\frac{\partial \bar{\alpha}_y}{\partial y} + \frac{\partial^2 w}{\partial y^2}\right) + q^t(x, y) = 0 \tag{49c}$$

where $\kappa = \pi^2/12$ or $\kappa = 5/6$ is the transverse shear correction factor, the bending stiffness matrix is defined in Equation (45). and as follows:

$$D_{44} = 2G^c_{xz}c, \quad D_{55} = 2G^c_{yz}c \tag{50}$$

For a simply supported rectangular plate, the solution to Equations (49) can be set in the following form:

$$w(x, y) = \sum_{m,n} W_{mn} \sin\frac{m\pi x}{a} \sin\frac{n\pi y}{b} \tag{51a}$$

$$\bar{\alpha}_x(x, y) = \sum_{m,n} A_{mn} \cos\frac{m\pi x}{a} \sin\frac{n\pi y}{b} \tag{51b}$$

$$\bar{\alpha}_y(x, y) = \sum_{m,n} B_{mn} \sin\frac{m\pi x}{a} \cos\frac{n\pi y}{b} \tag{51c}$$

Let us assume a loading of the form

$$q(x, y) = q_0 \sin\frac{\pi x}{a} \sin\frac{\pi y}{b}, \qquad 0 \le x \le a, \qquad 0 \le y \le b \tag{52}$$

if

$$\lambda_m = \frac{m\pi}{a}, \quad \lambda_n = \frac{n\pi}{b} \tag{53a}$$

$$L_{11} = D_{11}\lambda_m^2 + D_{66}\lambda_n^2 + \kappa D_{55}, \quad L_{12} = (D_{12} + D_{66})\,\lambda_m\lambda_n \tag{53b}$$

$$L_{22} = D_{66}\lambda_m^2 + D_{22}\lambda_n^2 + \kappa D_{44}, \quad L_{13} = \kappa D_{55}\lambda_m \tag{53c}$$

$$L_{33} = \kappa D_{55}\lambda_m^2 + \kappa D_{44}\lambda_n^2, \quad L_{23} = \kappa D_{44}\lambda_n \tag{53d}$$

then substituting Equations (51) in Equations (49) leads to

$$\begin{bmatrix} L_{11} & L_{12} & L_{13} \\ L_{12} & L_{22} & L_{23} \\ L_{13} & L_{23} & L_{33} \end{bmatrix} \begin{Bmatrix} A_{mn} \\ B_{mn} \\ W_{mn} \end{Bmatrix} = \begin{Bmatrix} 0 \\ 0 \\ q_0 \end{Bmatrix} \tag{54}$$

which yields the solution

$$A_{mn} = \left(L_{12}L_{23} - L_{22}L_{13}\right)\frac{q_0}{\Delta} \tag{55a}$$

$$B_{mn} = \left(L_{12}L_{23} - L_{11}L_{23}\right)\frac{q_0}{\Delta} \tag{55b}$$

$$W_{mn} = \left(L_{11}L_{22} - L_{12}^2\right)\frac{q_0}{\Delta} \tag{55c}$$

where Δ is the determinant of matrix $[L]$. Notice that it has been assumed that the shear is carried exclusively by the core. If the shear of the facesheets is included then:

$$D_{44} = 2G_{xz}^c c + G_{xz}^t f^t + G_{xz}^b f^b \tag{56a}$$

$$D_{55} = 2G_{yz}^c c + G_{yz}^t f^t + G_{yz}^b f^b \tag{56b}$$

Using the material and geometric properties from Section 3.1.1 a comparative analysis of the elasticity and EHSAPT results against CLPT and FSDT theories has been presented in Figures 6, 2. It can be seen that the predictions of CLPT are too non-conservative and the FSDT results are highly conservative. The effect of inclusion of the shear stiffness of the faces is also very negligible.

An effective shear modulus for the sandwich section, $\bar{G}$, which includes the contribution of the face sheets, is derived based on the compliances of the constituent phases [86]. The expression for $\bar{G}$ is given by:

$$\frac{f^t + f^b + 2c}{\bar{G}_{xy}} = \frac{f^t}{G_{xy}^{f^t}} + \frac{f^b}{G_{xy}^{f^b}} + \frac{2c}{G_{xy}^c} \tag{57a}$$

$$\frac{f^t + f^b + 2c}{\bar{G}_{xz}} = \frac{f^t}{G^{f^t}_{xz}} + \frac{f^b}{G^{f^b}_{xz}} + \frac{2c}{G^c_{xz}} \tag{57b}$$

$$\frac{f^t + f^b + 2c}{\bar{G}_{yz}} = \frac{f^t}{G^{f^t}_{yz}} + \frac{f^b}{G^{f^b}_{yz}} + \frac{2c}{G^c_{yz}} \tag{57c}$$

The results from FSDT are again computed using the updated shear stiffnesses and are presented in Figure 10 below:

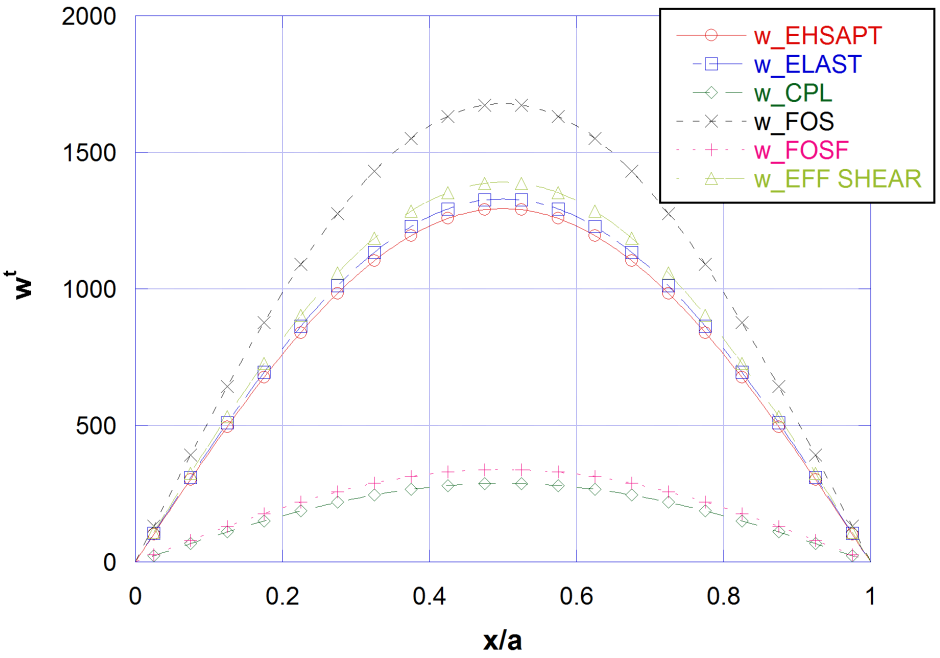

Figure 10: Transverse displacement w^t, at the top face $z = c + f^t$ at $y = \frac{b}{2}$ for $a = b = 20h_{tot}$

It can be seen in Figure 10 that the results from FSDT using effective shear are much more accurate as compared to the other cases considered.

If a thicker plate is now considered with $a/h_{tot} = 5$, the results from FSDT with effective shear are not as accurate as the case for a thinner plate with $a/h_{tot} = 20$ as shown in Figure 11. However, FSDT with the use of effective shear stiffnesses still results in a more accurate result as compared to the other two cases of FSDT considered.

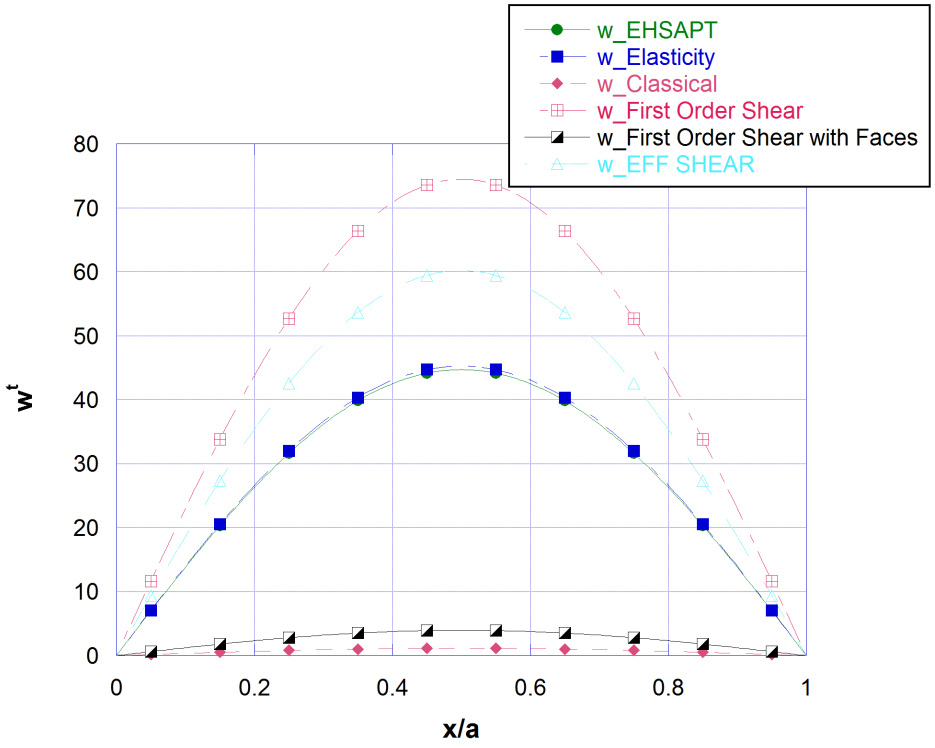

Figure 11: Transverse displacement w^t, at the top face $z = c + f^t$ at $y = \frac{b}{2}$ for $a = b = 5h_{tot}$

It can be seen in Table 1 that as the thickness of the plate decreases and the a/h_{tot} ratio increases the results from FSDT with effective shear become more accurate.

Table 1: Transverse displacement w^t at $z = c + f^t,\ x = a/2,\ y = b/2$

a/h	FSDT (Effective Shear)	EHSAPT	Err.%
5	60.18	44.70	34.60
6	88.31	68.29	29.31
7	122.77	97.76	25.29
8	164.07	133.65	22.76
10	269.36	227.06	18.63
12	408.61	353.40	15.62
15	690.72	615.73	12.18
20	1391.13	1293.74	7.53

3.1.2 Comparison of EHSPAT Results Against Other Theories [1]

Range of applicability of EHSAPT can be assessed by comparing EHSAPT results against several other higher order, zig- zag, layerwise theories and VAM (Variational Asymptotic Method) [87]. Results from the following theories are compared against EHSAPT:

- Advanced Higher-order Shear Deformation Theories (AHSDT). These are equivalent single layer models.
- Advanced Higher-order Shear Deformation Theories with Zig-Zag effects included (AHSDTZ). These are equivalent single layer models and the so called Zig-Zag form of the displacement is taken into account.
- Advanced Layerwise Theories (ALWT). The displacements have a layerwise description.
- VAPAS (Variational Asymptotic Plate and Shell Analysis) is a computer program based on the variational asymptotic method [88].

The order of expansion of the displacements u_x, u_y and u_z along the thickness coordinate defines the class of theories.

3.1.2.1 Acronyms Used to Identify a Generic Theory

A AHSDT with orders of expansion N_{u_x}, N_{u_y} and N_{u_z} for the displacements u_x, u_y and u_z respectively is denoted as $ED_{N_{u_x}N_{u_y}N_{u_z}}$. "E" stands for "Equivalent Single Layer" and "D" stands for "Displacement-based" theory.

With a similar logic, it is possible to define acronyms for the second type (Advanced Higher-order Shear Deformation Theories with zig-zag effects included (AHSDTZ)) and the third type of theories (Advanced LayerWise theories (ALWT)). The acronyms are $EDZ_{N_{ux}N_{uy}N_{uz}}$ and $LD_{N_{ux}N_{uy}N_{uz}}$. For example, a $AHSDTZ$ theory with cubic orders for all displacements is indicated as EDZ_{333} whereas a $ALWT$ theory with parabolic orders for all displacements is indicated as LD_{222}.

The relative error $Err\%$ used in the tables is defined as follows:

$$Err\% = 100 \cdot \frac{\text{Result current theory} - \text{Result elasticity solution}}{\text{Result elasticity solution}} \tag{58}$$

3.1.2.2 Results

Two test cases are analyzed. Test case 1 is a sandwich plate Figure 12 made of two skins and a core [$h_{lowerskin} = h/10;\ h_{upperskin} = 2h/10;\ h_{core} = (7/10)h$]. It is also $\frac{E_{lowerskin}}{E_{upperskin}} = 5/4$. The plate is simply supported and the load is sinusoidal pressure applied at the top surface of the plate ($m = n = 1$). Different Face-to-Core Stiffness Ratio (FCSR) are considered:

- Face-to-Core Stiffness Ratio = $FCSR = \frac{E_{lowerskin}}{E_{core}} = 10^1;\ a/h = 4,\ 10,\ 100$
- Face-to-Core Stiffness Ratio = $FCSR = \frac{E_{lowerskin}}{E_{core}} = 10^5;\ a/h = 4,\ 100$

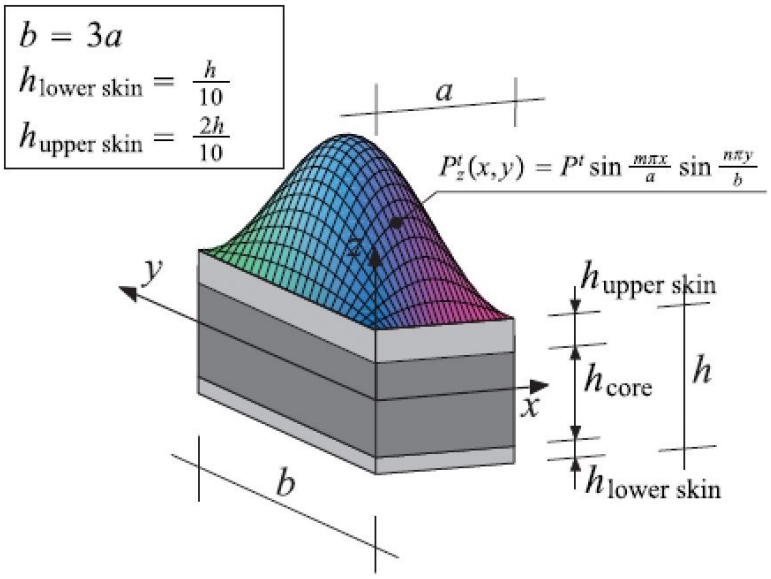

Figure 12: Case 1: Geometric configuration of the plate

As far as Poisson's ratio is concerned, the following values are used: $\nu_{lowerskin} = \nu_{upperskin} = \nu_{core} = 0.34$. The middle plane of the plate is a rectangle with $b = 3a$. In this test case there is *no symmetry* with respect to the plane $z = 0$.

Test case 2 is represented by a *symmetric* sandwich structure and the details can be obtained from Figure 13.

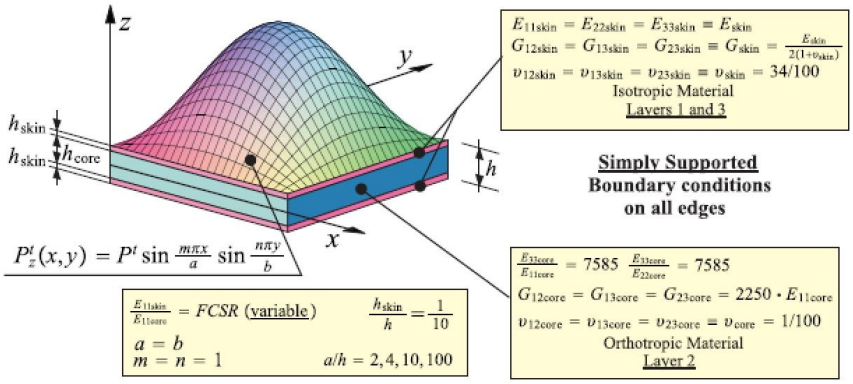

Figure 13: Case 2: Geometric configuration of the plate

3.1.2.3 Test Case 1: Numerical Results

Table 2 indicates that when the FCSR is small i.e. when the difference between the stiffness of the core and the facesheets is small indicating a stiff core the results from EHSAPT are not very accurate. However, when FCSR is larger i.e. when the stiffness of the core is much smaller than the stiffness of the face sheets which is mostly the case for sandwich structures, the results from EHSAPT are very accurate as indicated by Table 3.

Table 2: Transverse displacement $\hat{w}^t = w^t \frac{100E_{core}}{q_0 h_{tot}\left(\frac{a}{h_{tot}}\right)}$ at $z = c,\ x = a/2,\ y = b/2,\ \frac{E_{\text{lower skin}}}{E_{\text{core}}} \equiv FCSR = 10^1$

a/h	4		100	
Elasticity	3.01123	*Err.%*	1.51021	*Err.%*
LD_{111}	2.98058	(-1.02)	1.47242	(-2.50)
LD_{222}	3.00982	(-0.05)	1.51021	(0.00)
LD_{555}	3.01123	(0.00)	1.51021	(0.00)
ED_{111}	1.58218	(-47.5)	1.10845	(-26.6)
ED_{444}	2.79960	(-7.03)	1.50989	(-0.02)
ED_{555}	2.84978	(-5.36)	1.50996	(-0.02)
ED_{777}	2.86875	(-4.73)	1.50999	(-0.01)
EDZ_{111}	2.34412	(-22.2)	1.15866	(-23.3)
EDZ_{444}	2.97886	(-1.07)	1.51017	(0.00)
EDZ_{555}	2.98737	(-0.79)	1.51018	(0.00)
EDZ_{777}	2.99670	(-0.48)	1.51019	(-0.00)
$VAPAS_0$	1.5136	(-49.7)	1.50788	(-0.15)
$VAPAS$	3.0198	(0.28)	1.5102	(0.00)
$EHSAPT$	2.62602	(-12.80)	1.13191	(-25.05)

Table 3: Transverse displacement at
$z = z_{\text{bottom}}^{\text{upper skin}} = \frac{3}{10}h,\ x = a/2,\ y = b/2,\ \frac{E_{\text{lower skin}}}{E_{\text{core}}} \equiv FCSR = 10^5$

a/h	4		100	
Elasticity	1.31593×10^{-2}	Err.%	2.08948×10^{-3}	Err.%
LD_{111}	9.79008×10^{-3}	(-25.6)	1.96509×10^{-3}	(-5.95)
LD_{222}	1.31471×10^{-2}	(-0.09)	2.08948×10^{-3}	(0.00)
LD_{555}	1.31593×10^{-2}	(0.00)	2.08949×10^{-3}	(0.00)
ED_{111}	1.79831×10^{-4}	(-98.6)	1.19941×10^{-4}	(-94.3)
ED_{444}	1.16851×10^{-3}	(-91.1)	1.64835×10^{-4}	(-92.1)
ED_{555}	4.29224×10^{-3}	(-67.4)	1.73120×10^{-4}	(-91.7)
ED_{777}	1.08119×10^{-2}	(-17.8)	2.96304×10^{-4}	(-85.8)
EDZ_{111}	8.36735×10^{-4}	(-93.6)	1.63329×10^{-4}	(-92.2)
EDZ_{444}	1.26288×10^{-2}	(-4.03)	1.16305×10^{-3}	(-44.3)
EDZ_{555}	1.30409×10^{-2}	(-0.90)	1.78411×10^{-3}	(-14.6)
EDZ_{777}	1.31363×10^{-2}	(-0.17)	2.02060×10^{-3}	(-3.30)
$VAPAS_0$	1.6421×10^{-4}	(-98.7)	1.6314×10^{-4}	(-92.2)
$VAPAS$	1.49076	(>100)	2.4667×10^{-3}	(-18.0)
$EHSAPT$	1.29687×10^{-2}	(-1.45)	1.93859×10^{-3}	(-7.22)

3.1.2.4 Test Case 2

When results from test case 2 are compared with EHSAPT results again the pattern observed above is seen in Tables 4, 5. As the face to core ratio (FCSR) is increased thereby making the core more compliant and less stiff in comparison to the facesheets the results become more accurate.

Also, EHSAPT results are more accurate for a thicker plate where the a/h_{tot} ratio is small as seen in Tables 2, 3, 4 and 5.

Table 4: Transverse displacement at
$z = 0,\ x = a/2,\ y = b/2,\ \frac{E_{\text{lower skin}}}{E_{\text{core}}} \equiv FCSR = 7.3 \times 10^1$

a/h	2		4		10		100	
Elasticity	0.22733	Err%	0.198251	Err%	0.190084	Err%	0.188542	Err%
EDZ_{555}	0.246804	8.57	0.201527	1.65	0.188663	−0.75	0.186228	−1.23
LD_{222}	0.219334	−3.52	0.195992	−1.14	0.18971	−0.20	0.188538	−0.00
LD_{555}	0.227331	0	0.198251	0	0.190084	0	0.188542	0
$VAPAS$	0.191717	−15.67	0.192759	−2.77	0.189362	−0.38	0.188535	−0.00
$EHSAPT$	0.229035	0.75	0.20063	1.20	0.19292	1.49	0.203701	8.04

Table 5: Transverse displacement at
$z = 0,\ x = a/2,\ y = b/2,\ \frac{E_{\text{lower skin}}}{E_{\text{core}}} \equiv FCSR = 7.3 \times 10^8$

a/h	2		4		10		100	
Elasticity	1469.5	Err%	1370.58	Err%	1260.31	Err%	149.506	Err%
EDZ_{555}	1283.34	-12.67	1323.09	-3.47	1251.11	-0.73	149.464	-0.03
LD_{222}	1468.29	-0.08	1370.09	-0.04	1260.23	-0.01	149.507	0.00
LD_{555}	1469.5	0.00	1370.58	0.00	1260.31	0.00	149.507	0.00
$VAPAS$	412009	>100%	101187	>100%	16120.2	>100%	166.591	11.43
$EHSAPT$	1466.82	-0.18	1362.65	-0.58	1248.98	-0.90	142.709	-4.55

3.1.3 Comparison with FEM (ANSYS) for Unsymmetric Geometry and Loading

The case of a simply supported sandwich plate subjected to unsymmetric sinusoidal transverse loading on the top and bottom faces sheets respectively will be studied.

$$q^t(x,y) = q_0^t \sin\frac{\pi x}{a}\sin\frac{\pi y}{b}, \qquad 0 \le x \le a, \qquad 0 \le y \le b \tag{59a}$$

$$q^b(x,y) = q_0^b \sin\frac{\pi x}{a}\sin\frac{\pi y}{b}, \qquad 0 \le x \le a, \qquad 0 \le y \le b \tag{59b}$$

where $q_0^b = \frac{q_0^t}{2}$

A sandwich configuration consisting of unidirectional graphite/epoxy faces with moduli (in gigapascals) of $E_1^f = 181.0,\ E_2^f = E_3^f = 10.3,\ G_{12}^f = G_{31}^f = 7.17$, and $G_{23}^f = 5.96$ and Poisson's ratio of $\nu_{12}^f = 0.277,\ \nu_{31}^f = 0.016$ and $\nu_{32}^f = 0.4$. The core is made up of hexagonal glass/phenolic honeycomb with moduli (in gigapascals) of $E_1^c = E_2^c = 0.032,\ E_3^c = 0.300,\ G_{23}^c = G_{31}^c = 0.048,\ and\ G_{12}^c = 0.013$ and Poisson's ratio of $\nu_{12}^c = \nu_{31}^c = \nu_{32}^c = 0.250$.

The following unsymmetric geometric configuration is defined:

- $f^t = 2$ mm.
- $f^b = 1$ mm.
- The core thickness is $2c = 16$ mm.
- The total thickness of the plate is defined to be $h_{tot} = f^t + f^b + 2c$.

In the following results, the displacements are normalized with:

$$100 h_{tot} \frac{q_0^t}{E_1^f}$$

and the stresses with:

$$q_0^t \frac{a^2}{h_{tot}^2}$$

The transverse displacement profile from ANSYS is shown in Figure 3.1.3. It can be seen that the maximum displacement is obtained at the top face sheet at $x = a/2$, $y = b/2$ and $z = c + f^t$.

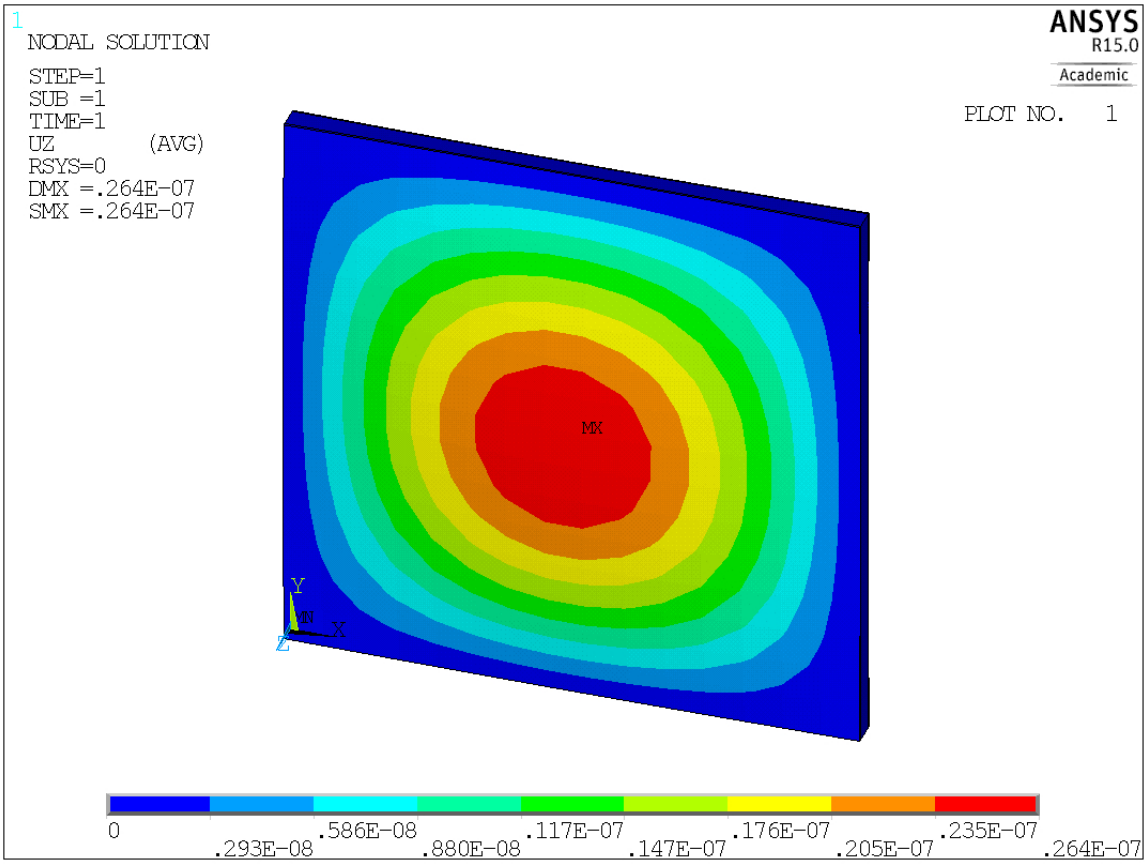

Figure 14: Ansys plot-Transverse displacement w^t, at the top face $z = c + f^t$

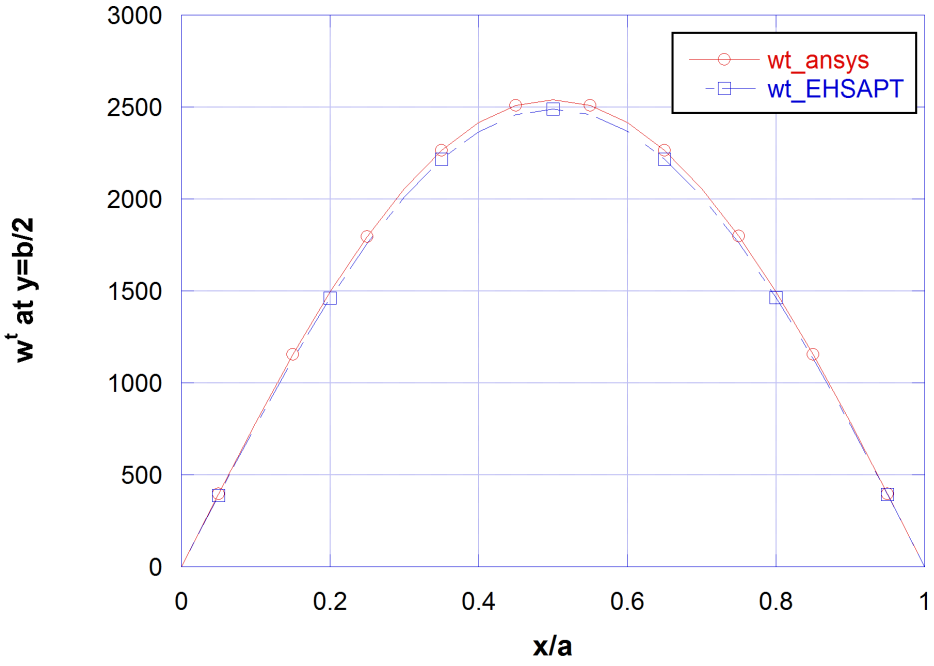

Figure 15: Comparison with ANSYS: Transverse displacement w^t, at the top face $z = c + f^t$ at $y = \frac{b}{2}$

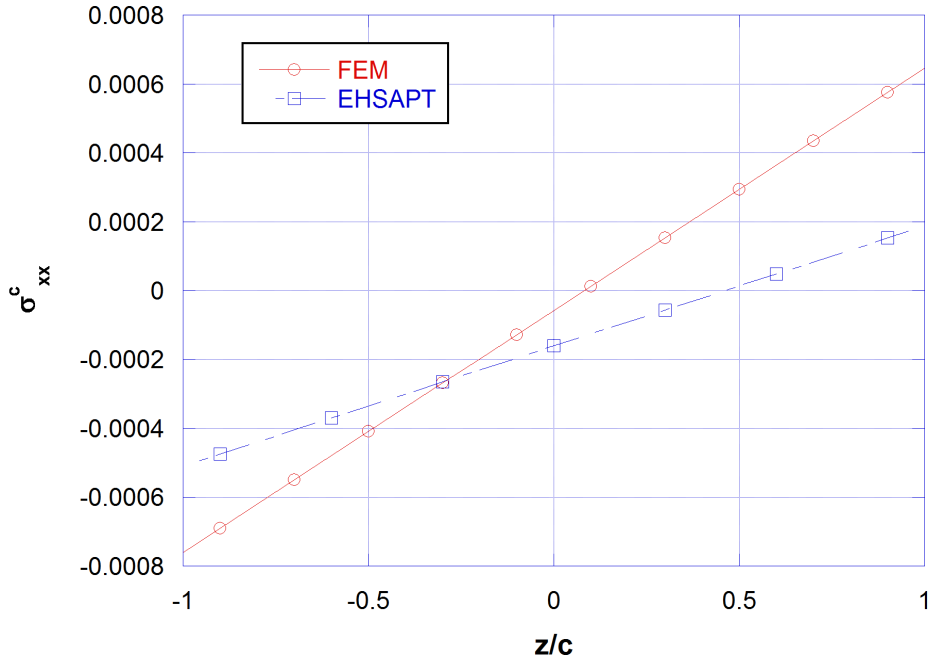

Figure 16: Comparison with ANSYS: Transverse normal stress σ^c_{xx} at $x = \frac{a}{2}$, $y = \frac{b}{2}$

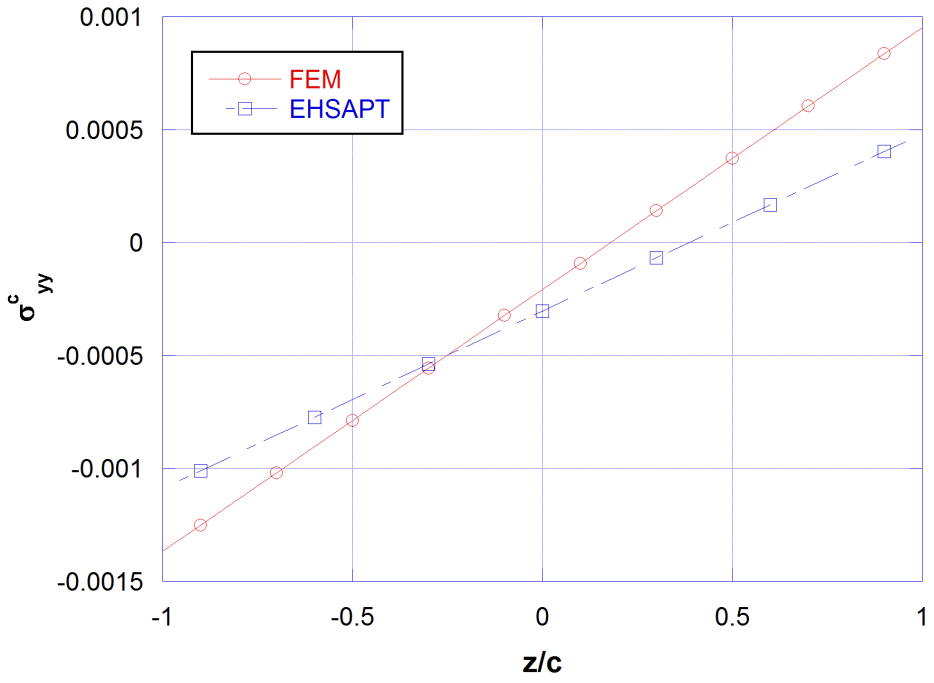

Figure 17: Comparison with ANSYS: Transverse normal stress σ^c_{yy} at $x = \frac{a}{2}$, $y = \frac{b}{2}$

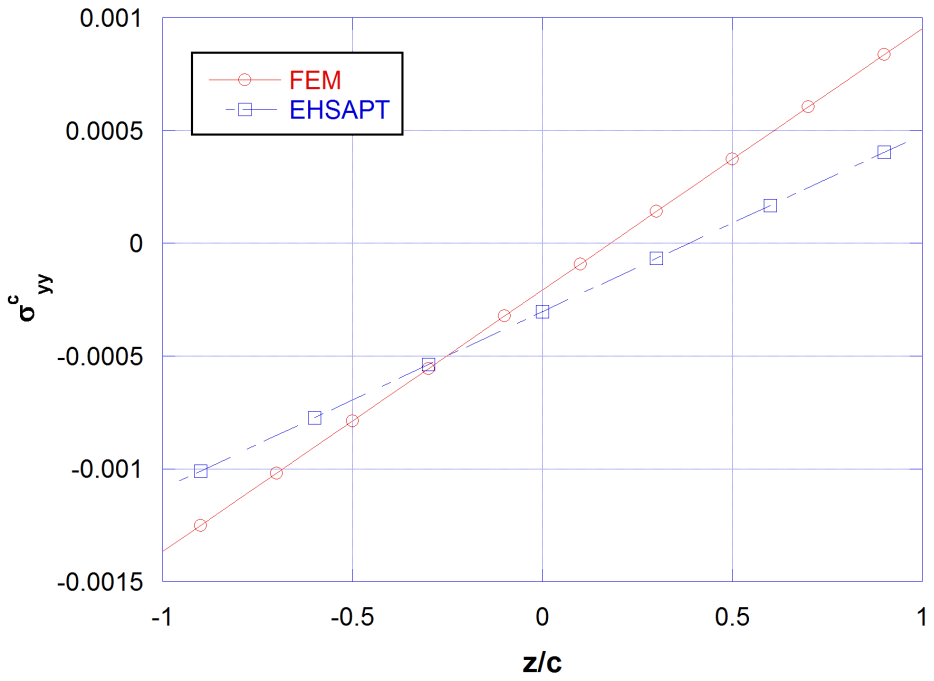

Figure 18: Comparison with ANSYS: Transverse normal stress σ^c_{zz} at $x = \frac{a}{2}$, $y = \frac{b}{2}$

3.2 Dynamic Model

3.2.1 Application of EHSAPT to a Simply Supported Sandwich Plate

We now consider the case of a simply supported rectangular plate. The following boundary conditions are applied: For $x = 0,\ a$

$$v_0^b = v_0^c \quad = v_0^t \quad = 0 \tag{60a}$$

$$w^b = w_0^c \quad = w^t \quad = 0 \tag{60b}$$

$$w^b{}_{,y} = \phi_0^c \quad = w^t{}_{,y} = 0 \tag{60c}$$

$$\tilde{N}_{xx}^b = \tilde{N}_{xx}^c \ = \tilde{N}_{xx}^t = 0 \tag{60d}$$

$$\tilde{M}_{xx}^b = \tilde{M}_{xx}^c = \tilde{M}_{xx}^t = 0 \tag{60e}$$

similar boundary conditions can be written for the other two boundaries of the plate at $y = 0$ and b

The displacements can be written in the following form;

$$u_0^t = U^T \cos\frac{m\pi x}{a}\sin\frac{n\pi y}{b}e^{i\omega t}, \quad u_0^c = U^C \cos\frac{m\pi x}{a}\sin\frac{n\pi y}{b}e^{i\omega t}, \quad u_0^b = U^B \cos\frac{m\pi x}{a}\sin\frac{n\pi y}{b}e^{i\omega t} \tag{61a}$$

$$v_0^t = V^T \sin\frac{m\pi x}{a}\cos\frac{n\pi y}{b}e^{i\omega t}, \quad v_0^c = V^C \sin\frac{m\pi x}{a}\cos\frac{n\pi y}{b}e^{i\omega t}, \quad v_0^b = V^B \sin\frac{m\pi x}{a}\cos\frac{n\pi y}{b}e^{i\omega t} \tag{61b}$$

$$w^t = W^T \sin\frac{m\pi x}{a}\sin\frac{n\pi y}{b}e^{i\omega t}, \quad w_0^c = W^C \sin\frac{m\pi x}{a}\sin\frac{n\pi y}{b}e^{i\omega t}, \quad w^b = W^B \sin\frac{m\pi x}{a}\sin\frac{n\pi y}{b}e^{i\omega t} \tag{61c}$$

$$\phi_0^c = \Phi\ \sin\frac{m\pi x}{a}\cos\frac{n\pi y}{b}e^{i\omega t}, \qquad \psi_0^c = \Psi\ \cos\frac{m\pi x}{a}\sin\frac{n\pi y}{b}e^{i\omega t} \tag{61d}$$

where $U^T,\ U^C,\ U^B,\ V^T,\ V^C,\ V^B,\ W^T,\ W^C,\ W^B,\ \Phi$ and Ψ are constants. Substituting equations Eqn. (61) into Eqn. (90) results in a system of eleven equations

which are arranged in matrix form to obtain the following:

$$([K]-\lambda[M])\begin{Bmatrix} u_0^b \\ u_0^c \\ u_0^t \\ v_0^b \\ v_0^c \\ v_0^t \\ w^b \\ w_0^c \\ w^t \\ \phi_0^c \\ \psi_0^c \end{Bmatrix} = 0, \qquad \text{where} \quad \lambda = \omega^2 \tag{62}$$

where $[K]$ and $[M]$ are the stiffness and mass matrices, respectively.

3.2.1.1 Comparison with Elasticity Solution

In this section the numerical results for several different geometric configurations are presented and a parametric study to analyze the free response of laminated composite plates is carried out. The results are compared to the elasticity solution provided by Noor [9]. In order to make the comparison a simply supported square laminated plate with the face sheets and core constructed from the same material is considered. Two different symmetric layouts with respect to the middle plane such that the fiber orientations of the laminas alternate between 0° and 90° with respect to the x-axis are considered and the results are compared with the elasticity solution for the given

configurations. The following material properties are used:

$$E_1/E_2 = 3,\ E_2 = E_3,\ G_{12} = G_{13} = 0.6E_2,\ G_{23} = 0.5E_2,\ \nu_{12} = \nu_{13} = \nu_{23} = 0.25$$

The assumed displacement functions (61) are substituted into the governing differential equations (90) and the resulting eigen system is solved. The fundamental natural frequencies ω are then evaluated such that

$$\lambda = (\omega b^2/h)\sqrt{\rho/E_2}$$

where ω is the circular frequency

Table 6: Non-dimensionalized fundamental frequencies $\lambda = (\omega b^2/h)\sqrt{\rho/E_2}$ for a simply supported square plate with $a/h = 5$

Lamination & No of Layers	Elasticity	EHSAPT
0/90/0	6.6185	6.56874
0/90/0/90/0	6.6468	6.6521

Table 6 shows that the results from EHSAPT closely match the elasticity solutions and provide the necessary basis to verify and validate our results. After this necessary validation we carry out a parametric study and analyze the effect of variation of geometric and material parameters on the fundamental natural frequency of the structure.

3.2.2 Parametric Study

The variation of the fundamental natural frequency with respect to the following geometric and material parameters is studied.

1. a/h: side-to-thickness ratio

2. t_c/t_f: thickness of the core to thickness of the face sheets ratio

3. a/b: aspect ratio

4. E_1^c/E_2^c: degree of orthotropy of the core

5. E_1^f/E_2^f: degree of orthotropy of the face sheets

3.2.2.1 5-Ply Symmetric Laminate with typical material properties

The material properties of individual layers in the face sheets and the core are considered to be typical of high fibrous composites.

$$E_1^{f,c}/E_2^{f,c} = \text{open},\ E_2^{f,c} = E_3^{f,c}\ G_{12}^{f,c} = G_{13}^{f,c} = 0.6E_2^{f,c},\ G_{23}^{f,c} = 0.5E_2^{f,c},\ \nu_{12}^{f,c} = \nu_{13}^{f,c} = \nu_{23}^{f,c} = 0.25$$

The face sheets are considered to be laminated plates and three different symmetric layouts of the composite sandwich laminate are considered.

- 0/90/core/90/0
- 0/60/core/60/0
- 0/45/core/45/0

Initially the variation of the normalized fundamental natural frequency with the side to thickness ratio for a simply supported square plate with $t_c/t_f = 10$, $E_1^f/E_2^f = 3$ and $E_1^c/E_2^c = 10$ is considered in Figure 19. It can be seen that as the side to thickness ratio increases the natural frequency also starts to increase for all three laminates considered. It can be seen that the highest fundamental natural frequency is achieved in the case of the 0/45/core/45/0 symmetric layout for any given a/h ratio.

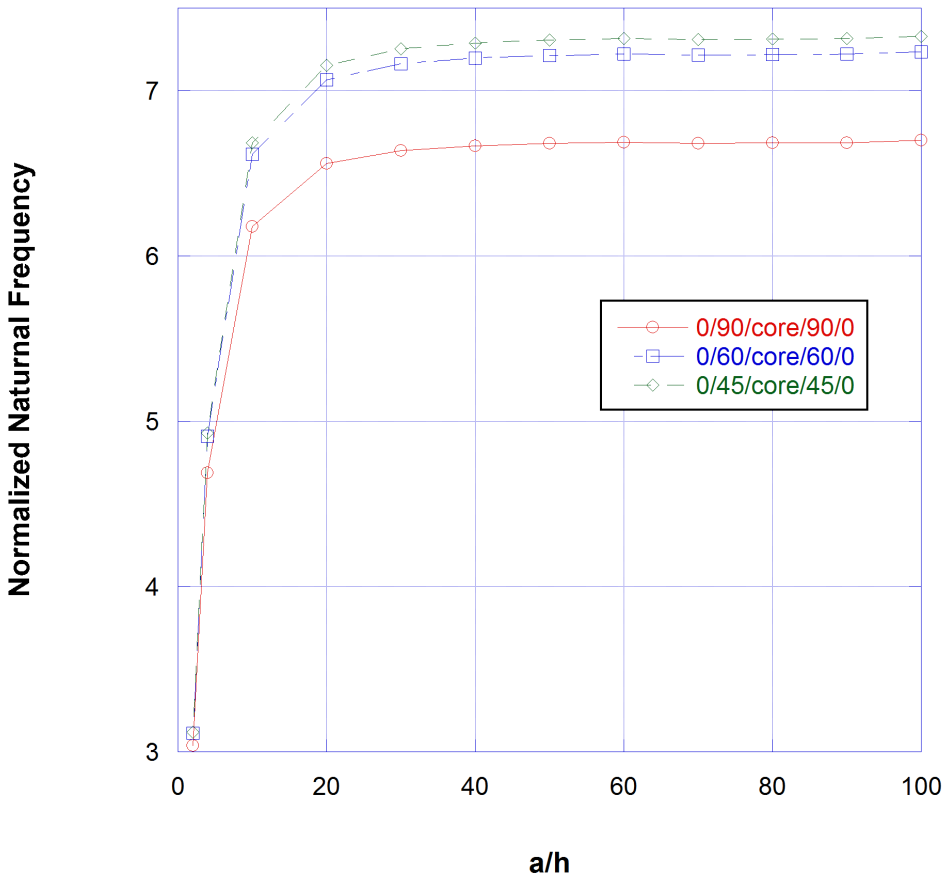

Figure 19: Normalized Fundamental Natural Frequency versus a/h ratio

Next the variation of the normalized fundamental natural frequency with the thickness of the core to thickness of the flange ratio for a simply supported square plate with $a/h = 10$, $E_1^f/E_2^f = 3$ and $E_1^c/E_2^c = 10$ is analyzed as seen in Figure 20. It can be seen that as the core thickness increases in relation to the thickness of the flange the fundamental natural frequency starts to decrease. Again it can be seen that the highest fundamental natural frequency is achieved in the case of the 0/45/core/45/0 symmetric layout for any given t_c/t_f ratio.

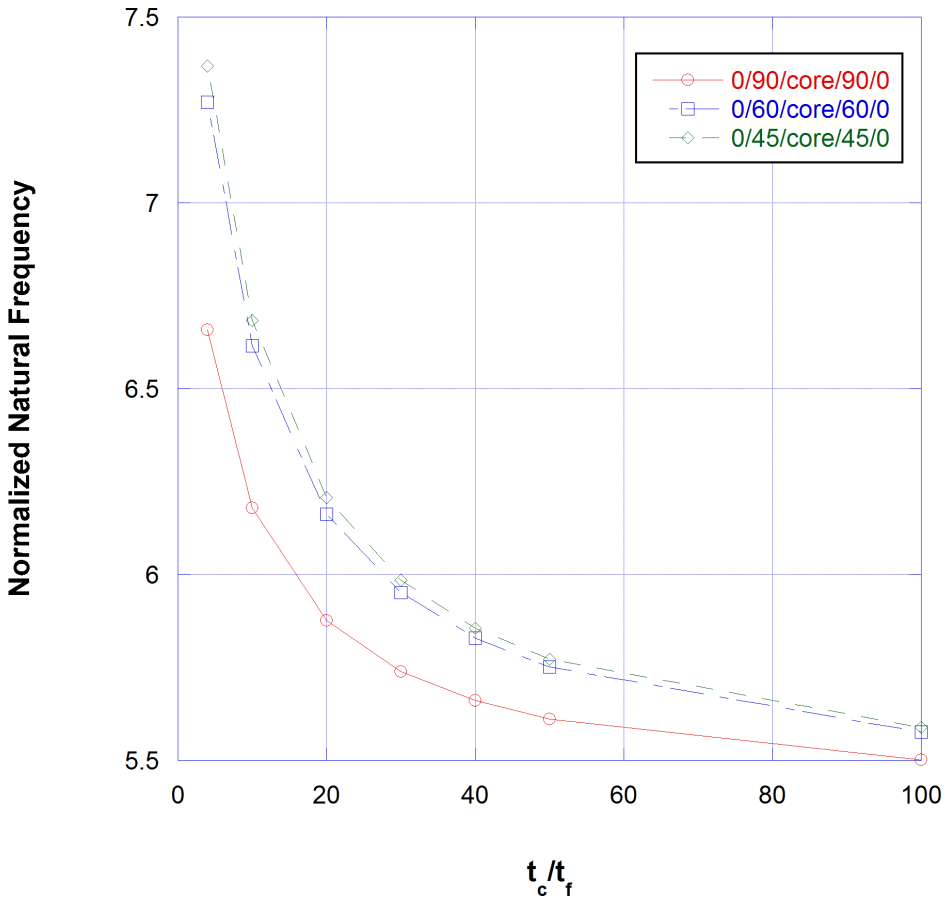

Figure 20: Normalized fundamental natural frequency versus t_c/t_f ratio

In the next case the variation of the fundamental natural frequency with the aspect ratio of the simply supported plate with $t_c/t_f = 10$, $a/h = 10$, $E_1^f/E_2^f = 3$ and $E_1^c/E_2^c = 10$ is considered in Figure 21. It can be seen that as the aspect ratio increases and the plate becomes narrower, its fundamental natural frequency starts to decrease. In this case the layout of the laminate does not seem to have a significant effect on the natural frequency of the laminate composite plate.

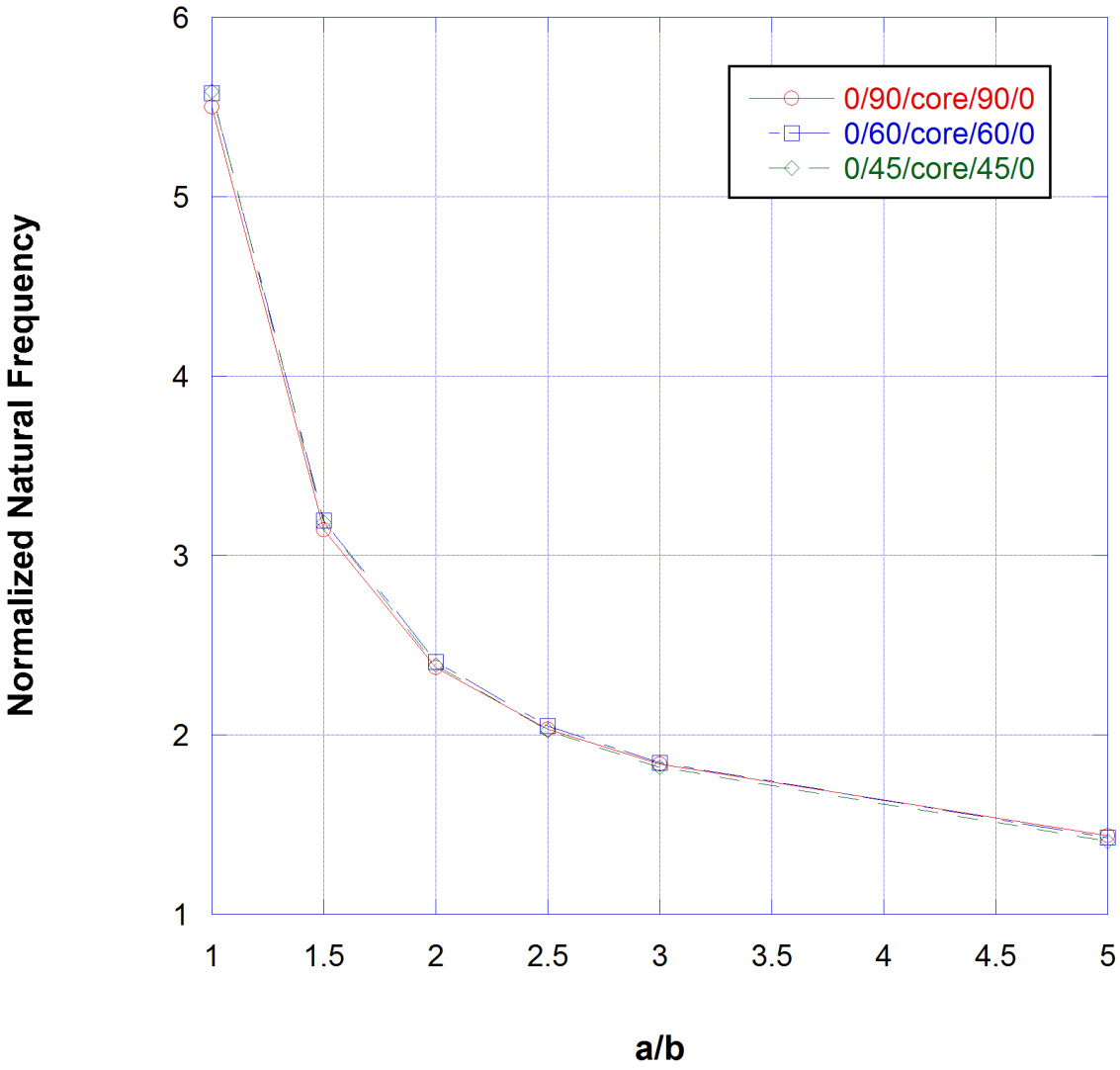

Figure 21: Normalized fundamental natural frequency versus aspect ratio a/b

The effect of variation of the degree of orthotropy of the core is now considered for a simply supported square laminated plate with $t_c/t_f = 10$, $a/h = 10$ and $E_1^f/E_2^f = 3$ as seen in Figure 22. It can be seen that as the degree of orthotropy of the core increases the fundamental natural frequency of the plate starts to decrease and the isotropic core provides the highest natural frequency for any laminated layout. Again the 0/45/core/45/0 layout seems to provide the highest fundamental natural frequency for any given E_1^c/E_2^c ratio.

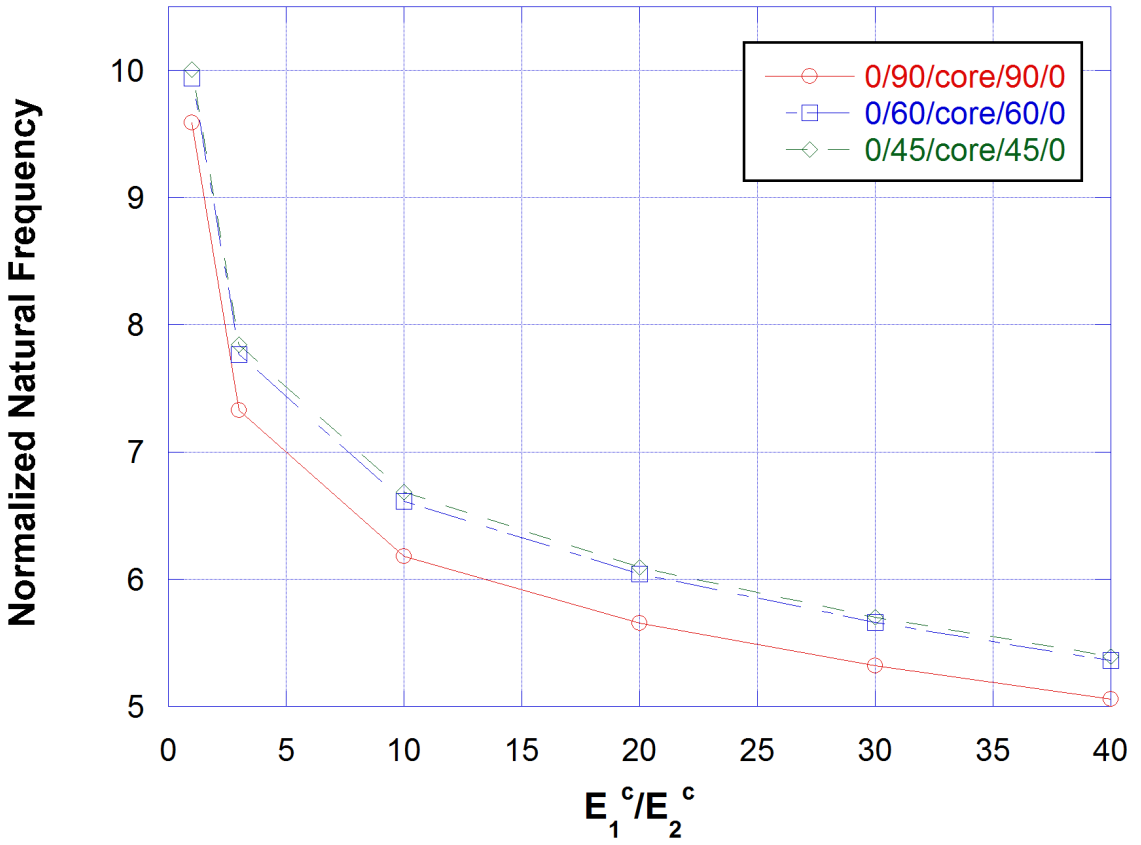

Figure 22: Normalized fundamental natural frequency versus variation in the E_1^c/E_2^c ratio

Finally the effect of variation of degree of orthotropy of the face sheets for a simply supported square plate with an isotropic core and $t_c/t_f = 10$ and $a/h = 10$ is considered Figure 23. It can be seen that as the ratio E_1^f/E_2^f increases the fundamental natural frequency of the plate also increases and hence it can be concluded that a combination of an isotropic core and highly orthotropic flanges provides the highest fundamental natural frequency.

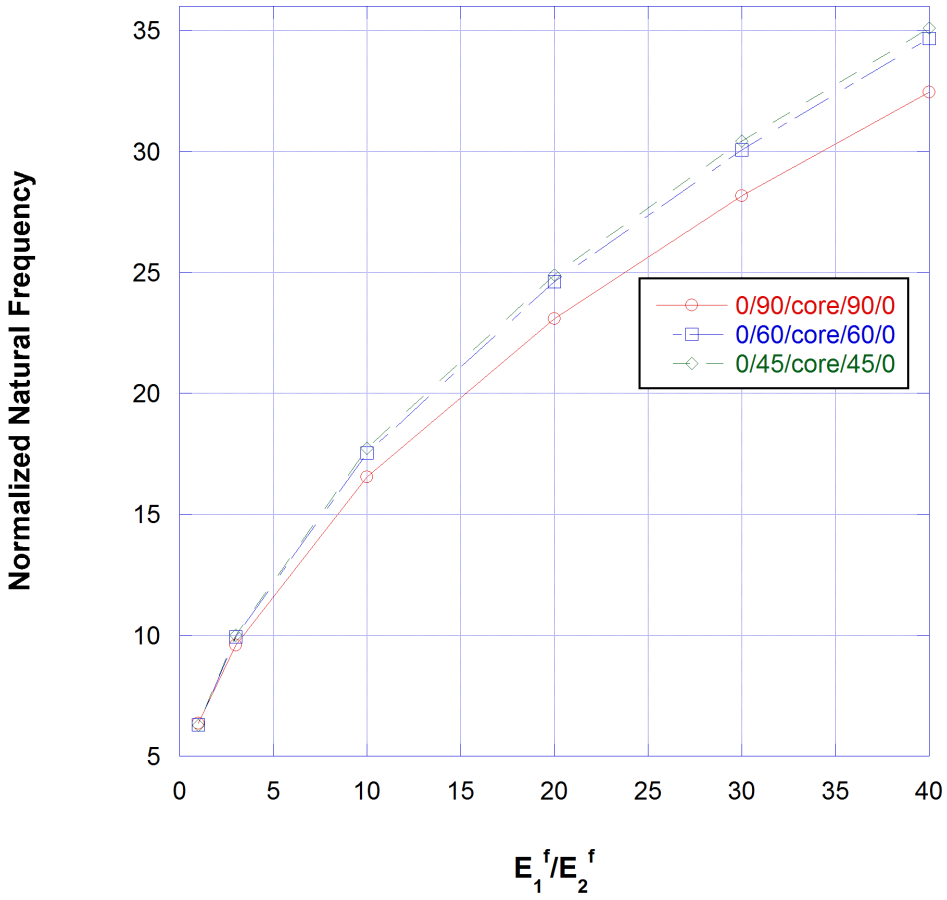

Figure 23: Normalized fundamental natural frequency versus variation in the E_1^f/E_2^f ratio

3.2.2.2 3-Ply Symmetric Graphite-Epoxy T300/934 Laminate

After having carried out a parametric study on a generic sandwich construction, we now consider an actual plate configuration and analyze the effect of variation of the parameters defined above on this configuration. A 3-Ply Laminated Graphite-Epoxy T300/934 with the following material properties is now analyzed.

Face Sheets

$$E_1 = 131 \text{ GPa}$$

$$E_2 = 10.34 \text{ GPa}, \ E_2 = E_3$$

$$G_{12} = 6.895 \text{ GPa},$$

$$G_{13} = 6.205 \text{ GPa},$$

$$G_{23} = 6.895 \text{ GPa},$$

$$\nu_{12} = 0.25, \ \nu_{13} = 0.22, \ \nu_{23} = 0.49$$

$$\rho = 1627 \text{ kg/m}^3$$

Core Properties (Isotropic)

$$E_1 = E_2 = E_3 = 2G = 6.89 \times 10^{-}3 \text{ GPa}$$

$$G_{12} = G_{13} = G_{23} = 3.45 \times 10^{-}3 \ \text{ GPa}$$

$$\nu_{12} = \nu_{13} = \nu_{23} = 0$$

$$\rho = 97 \ \text{ kg/m}^3$$

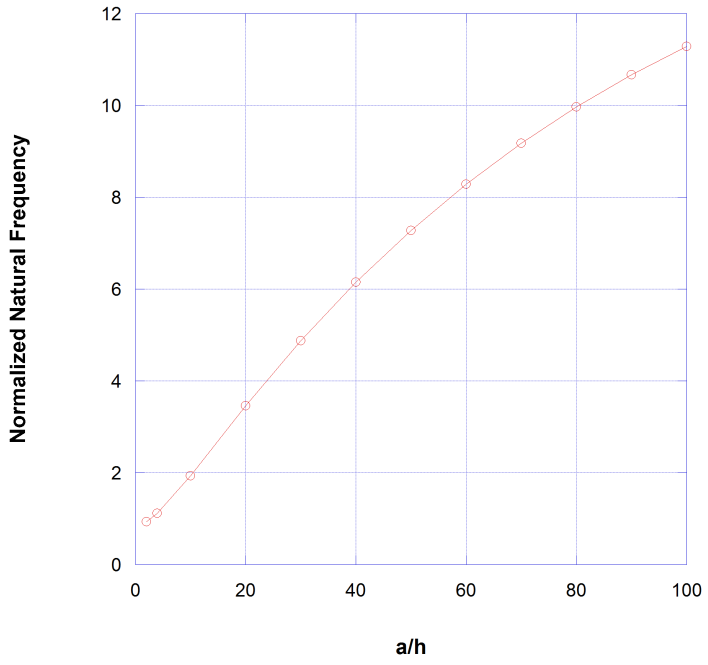

Figure 24: Normalized fundamental natural frequency versus side-to-thickness ratio (a/h) of a simply supported 3-ply square plate

The variation of the normalized fundamental natural frequency with the side to thickness ratio (a/h) for a simply supported square plate with $t_c/t_f = 10$ is considered as seen in Figure 24. It can be seen that similar behavior as observed in the case of the generic material properties above is seen here and the natural frequency increases as a/h_{tot} ratio increases.

Next the variation of the normalized fundamental natural frequency with the thickness of the core to thickness of the flange ratio for a simply supported square plate with $a/h_{tot} = 10$ is considered as shown in Figure 25. It can again be seen that as the core thickness increases in relation to the thickness of the flange the fundamental natural frequency starts to decrease.

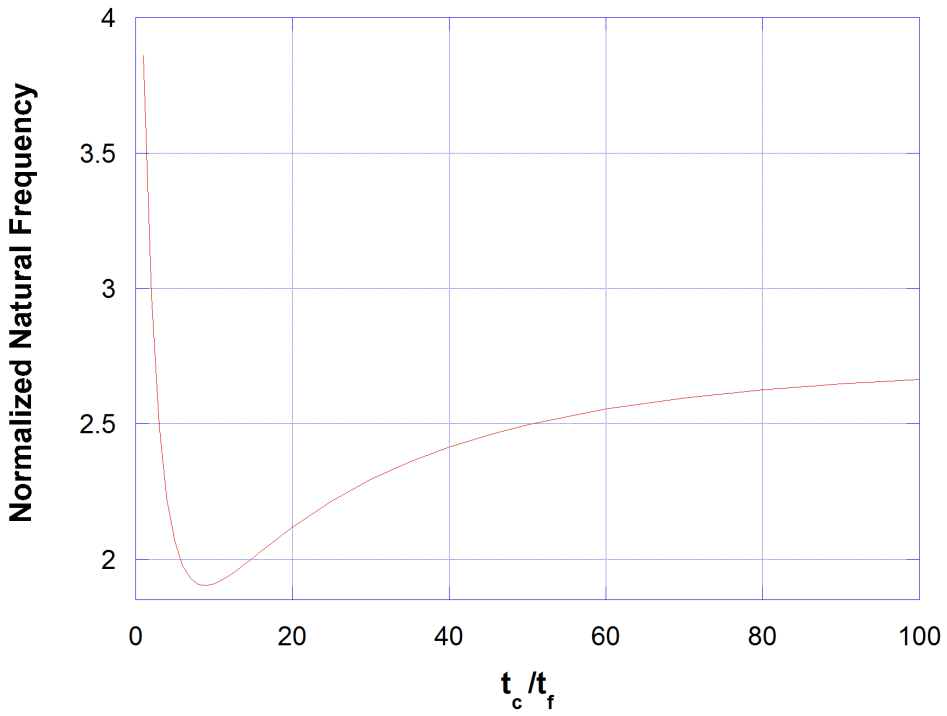

Figure 25: Normalized fundamental natural frequency versus thickness of core to thickness of face sheet $\frac{t_c}{t_f}$ for a simply supported 3-ply square plate

Finally the variation of the fundamental natural frequency with the aspect ratio

of the simply supported plate with $t_c/t_f = 10$ and $a/h = 10$ is considered as shown in Figure 26. It can be seen that as the aspect ratio increases the fundamental natural frequency starts to decrease. This result again matches the behavior as predicted by the study with generic material properties above.

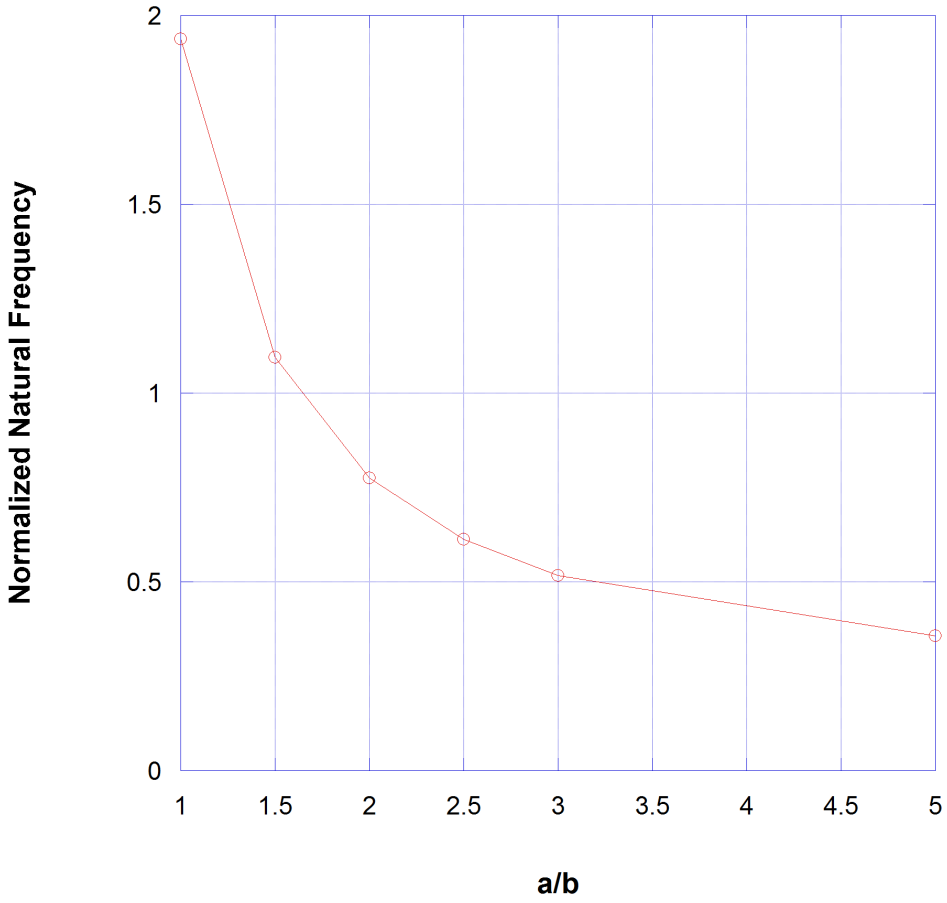

Figure 26: Normalized fundamental natural frequency versus aspect ratio (a/b) of a simply supported 3-ply plate

3.3 Nonlinear Static Analysis

We consider a sandwich configuration consisting of unidirectional graphite/epoxy faces with moduli (in GPa) of $E_1^f = 181.0$, $E_2^f = E_3^f = 10.3$, $G_{12}^f = G_{31}^f = 7.17$, and $G_{23}^f = 5.96$ and Poisson's ratio of $\nu_{12}^f = 0.277$, $\nu_{31}^f = 0.016$ and $\nu_{32}^f = 0.4$. The

core is made up of hexagonal glass/phenolic honeycomb with moduli (in GPa) of $E_1^c = E_2^c = 0.032,\ E_3^c = 0.300,\ G_{23}^c = G_{31}^c = 0.048,$ and $G_{12}^c = 0.013$ and Poisson's ratio of $\nu_{12}^c = \nu_{31}^c = \nu_{32}^c = 0.250$. The two face sheets are identical with a thickness of $f = 2$ mm. The core thickness is $2c = 16$ mm. The total thickness of the plate is defined to be $h_{tot} = 2f + 2c$ and we consider a square plate with $a = b = 20h_{tot}$, respectively.

In the following results, the applied load has been normalized with $\frac{E_1^t h_{tot}^4}{a^4}$, the stresses have been normalized with $\frac{E_1^c h_{tot}^2}{a^2}$ and the displacements have been normalized with h_{tot}. We consider four sets of boundary conditions

1. Simply Supported with moveable edges.

2. Simply Supported with fixed edges.

3. Clamped with moveable edges.

4. Clamped with fixed edges.

For movable (stress-free) boundary conditions the supported edges are free to move along the normal direction to the boundary whereas the out-of-plane displacement is fixed. However, for immovable boundary condition, the plate is prevented from any in-plane displacement along the normal and tangential directions to the edges and also any out-of-plane displacement is prevented.

In all cases considered the results are computed for two different sets of scenarios. First the total strain energy is computed with the strain-displacement relations for the core to be nonlinear and then in the second case the strain-displacement relations

are considered to be linear and a comparison is made between the two sets of results to appreciate the difference in computed values versus the computational effort.

3.3.1 Simply Supported Case with Moveable Edges

We first consider the case of a simply supported plate with moveable edges, the edges are free to move along the normal direction to the boundary but the out of plane displacement is fixed. The geometric boundary conditions for the edges $x = 0$, a are as follows;

$$\begin{aligned} v_0^b = v_0^c = v_0^t = 0 \\ w^b = w_0^c = w^t = 0 \\ w^b{}_{,y} = \phi_0^c = w^t{}_{,y} = 0 \end{aligned} \tag{63}$$

Similarly, for $y = 0$, b the geometric boundary conditions are as follows;

$$\begin{aligned} u_0^b = u_0^c = u_0^t = 0 \\ w^b = w_0^c = w^t = 0 \\ w^b{}_{,x} = \psi_0^c = w^t{}_{,x} = 0 \end{aligned} \tag{64}$$

These boundary conditions can be satisfied by selecting the following assumed shape functions. It should be noted that the shape functions selected here also satisfy the natural boundary conditions of the problem. While this is not a requirement for the solution process, it generally results in a more accurate and rapidly converging solution.

$$u_0^t = \sum_{m=1}^{M}\sum_{n=1}^{N} U_{mn}^T \cos\frac{m\pi x}{a}\sin\frac{n\pi y}{b}, \qquad u_0^c = \sum_{m=1}^{M}\sum_{n=1}^{N} U_{mn}^C \cos\frac{m\pi x}{a}\sin\frac{n\pi y}{b},$$

$$u_0^b = \sum_{m=1}^{M}\sum_{n=1}^{N} U_{mn}^B \cos\frac{m\pi x}{a}\sin\frac{n\pi y}{b}, \qquad v_0^t = \sum_{m=1}^{M}\sum_{n=1}^{N} V_{mn}^T \sin\frac{m\pi x}{a}\cos\frac{n\pi y}{b},$$

$$
\begin{aligned}
v_0^c &= \sum_{m=1}^{M}\sum_{n=1}^{N} V_{mn}^C \sin\frac{m\pi x}{a}\cos\frac{n\pi y}{b}, & v_0^b &= \sum_{m=1}^{M}\sum_{n=1}^{N} V_{mn}^B \sin\frac{m\pi x}{a}\cos\frac{n\pi y}{b} \\
w^t &= \sum_{m=1}^{M}\sum_{n=1}^{N} W_{mn}^T \sin\frac{m\pi x}{a}\sin\frac{n\pi y}{b}, & w_0^c &= \sum_{m=1}^{M}\sum_{n=1}^{N} W_{mn}^C \sin\frac{m\pi x}{a}\sin\frac{n\pi y}{b}, \\
w^b &= \sum_{m=1}^{M}\sum_{n=1}^{N} W_{mn}^B \sin\frac{m\pi x}{a}\sin\frac{n\pi y}{b}, & \phi_0^c &= \sum_{m=1}^{M}\sum_{n=1}^{N} \Phi_{mn} \sin\frac{m\pi x}{a}\cos\frac{n\pi y}{b}, \\
\psi_0^c &= \sum_{m=1}^{M}\sum_{n=1}^{N} \Psi_{mn} \cos\frac{m\pi x}{a}\sin\frac{n\pi y}{b} & & \qquad (65)
\end{aligned}
$$

The nonlinear strain displacement relations (30) and the stress strain relations (31) are substituted into the total potential energy Equation (34), and integration is carried out with respect to z, the thickness coordinate. The assumed shape functions equations (65) are then substituted into the resulting equation and integrations with respect to the inplane coordinates x and y are carried out. This results in an equation in terms of the unknown coefficients U_{mn}^T, U_{mn}^C, U_{mn}^B, V_{mn}^T, V_{mn}^C, V_{mn}^T, W_{mn}^T, W_{mn}^C, W_{mn}^B, Φ_{mn}, Ψ_{mn}. The resulting equation is then differentiated with respect to the unknown coefficients equation (20b) to minimize the energy functional $\Pi(U_{ij})$. This results in $M \times N$ nonlinear equations for the $M \times N$ unknown coefficients. The resulting simultaneous nonlinear equations are then solved using the Newton-Raphson method where the initial guess is taken to be the result from the linear solution for the simply supported case with moveable edges.

We first consider the case where both the facesheets and the core are considered to be nonlinear. It can be seen that as the applied load q_0 increases, the maximum deflection w^t at the center point on the surface of the top facesheet of the plate is no more linear Figure 27. It can be seen that the linear theory results in predicting much higher displacements.

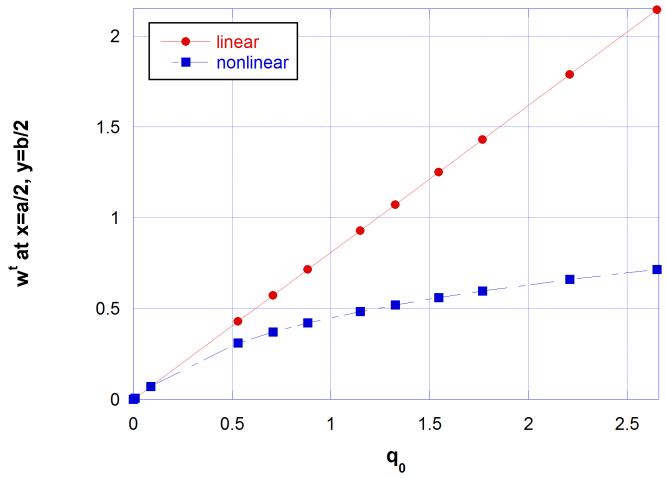

Figure 27: w^t for a simply supported square plate with moveable edges : linear vs nonlinear

Next we consider the case where the strain-displacement relations for the core are linear and the non-linear terms in the strain-displacement relations were dropped while computing the total potential energy in the Ritz Method. Figure 28 shows that the response is virtually identical and the effect of including the nonlinear terms in the strain-displacement terms in the core is not significant.

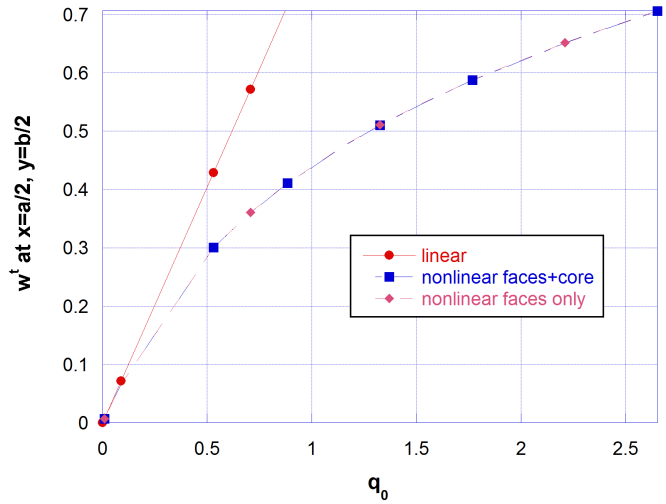

Figure 28: w^t for a simply supported plate with moveable edges: linear vs all nonlinear vs only faces nonlinear

The same results are presented in tabular form below in Table 7 to help appreciate the effect of inclusion of the nonlinear terms in the core.

Table 7: w^t at $x = \frac{a}{2}$ and $y = \frac{b}{2}$ for a simply supported square plate with moveable edges-all nonlinear vs only facesheets nonlinear

q_0	All Nonlinear	Only Facesheets Nonlinear
8.83978×10^{-7}	7.14773×10^{-7}	7.14773×10^{-7}
0.00883978	0.00714622	0.00714624
0.0883978	0.070117	0.0701207
0.530387	0.310883	0.310995
0.707182	0.371155	0.371309
0.883978	0.421338	0.42153
1.14917	0.484177	0.484417
1.32597	0.520252	0.520521
1.54696	0.560601	0.560902
1.76796	0.596855	0.597186
2.20994	0.660301	0.660685
2.65193	0.71498	0.71541

It can be seen that with the inclusion of nonlinear effects in the core the overall displacement is lower than the displacement if the nonlinear effects are not included.

3.3.1.1 Convergence Study

As with any approximate method the number of terms included in the approximate solution is expected to have a significant effect on the accuracy of the result. A convergence study is therefore carried out to study the effect of increasing the number of unknown coefficients in the assumed solution for the Ritz method. As the number of terms is increased rapid convergence is observed as shown in Figure 29 and 30. The results are also presented in tabular form below in Table 8.

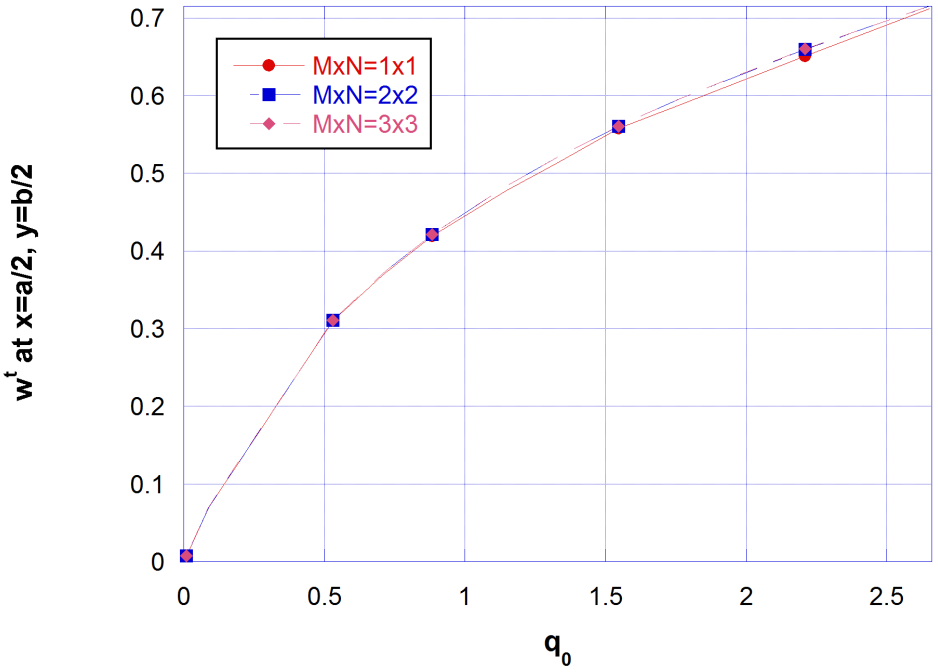

Figure 29: Convergence study for Ritz Method simply supported square plate with moveable edges

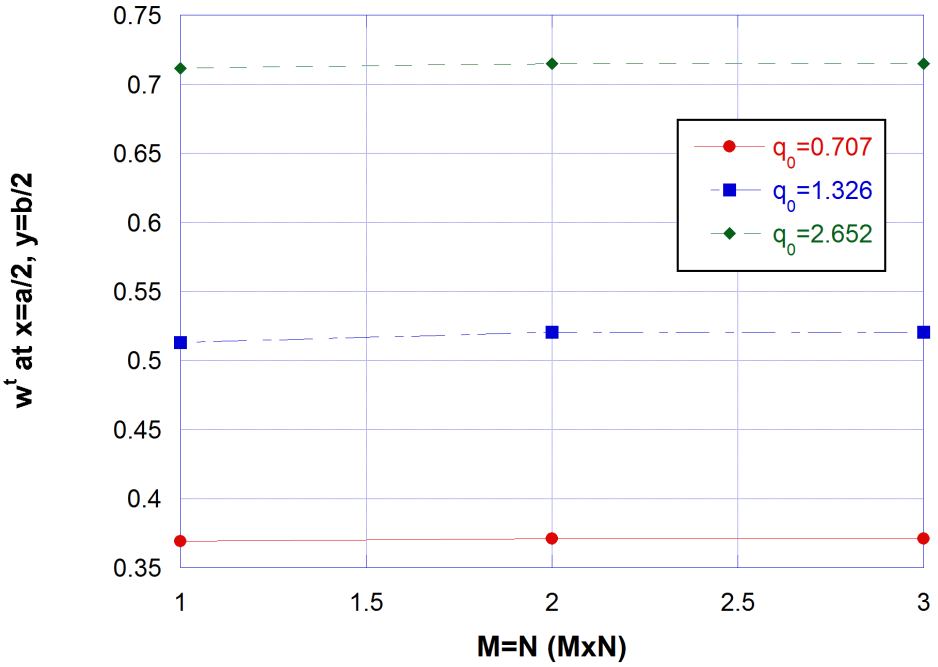

Figure 30: Convergence study for Ritz Method simply supported square plate with moveable edges-selective loads

Table 8: Convergence study for Ritz Method for a simply supported square plate with moveable edges

q_0	$M \times N = 1 \times 1$	$M \times N = 2 \times 2$	$M \times N = 3 \times 3$
8.83978×10^{-7}	6.88796×10^{-7}	7.14768×10^{-7}	7.14773×10^{-7}
0.00883978	0.006987	0.007138	0.00714622
0.0883978	0.069967	0.070098	0.070117
0.530387	0.309798	0.310859	0.310883
0.707182	0.368979	0.371148	0.371155
0.883978	0.419376	0.421335	0.421338
1.14917	0.477987	0.484169	0.484177
1.32597	0.512965	0.520251	0.520252
1.54696	0.557632	0.560587	0.560601
1.76796	0.588754	0.596645	0.596855
2.20994	0.65081	0.659871	0.660301
2.65193	0.71167	0.71488	0.71498

The rapid convergence can be attributed to the fact that the assumed approximate solution equations (65) not only satisfy the geometric boundary conditions of the problem, but also the natural boundary conditions.

3.3.1.2 Stress Analysis (Simply Supported with Moveable Edges)

The distribution of the axial stresses σ_{xx} and σ_{yy} in the core as a function of z at the midspan location, $x = \frac{a}{2}$ and $y = \frac{b}{2}$ (where the bending moment is maximum) is plotted in Figures 32 and 44 and Figures 34 and 46. Note that for both the linear solution and the nonlinear solution, there is no symmetry with regard to the mid-plane ($z = 0$).

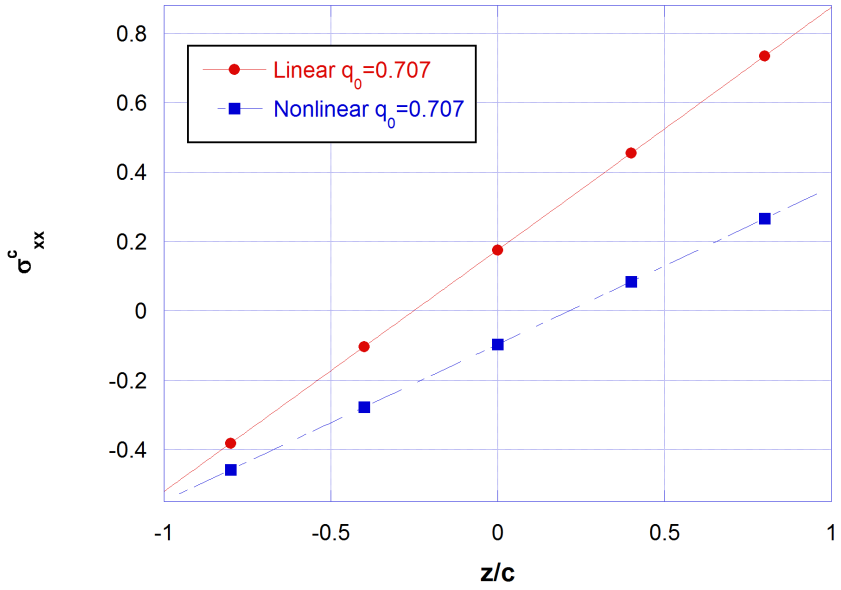

Figure 31: Through-thickness distribution in the core of the in-plane stress, σ_{xx}, at $x = a/2$ and $y = b/2$-linear vs nonlinear, $\hat{q}_0 = 0.707$

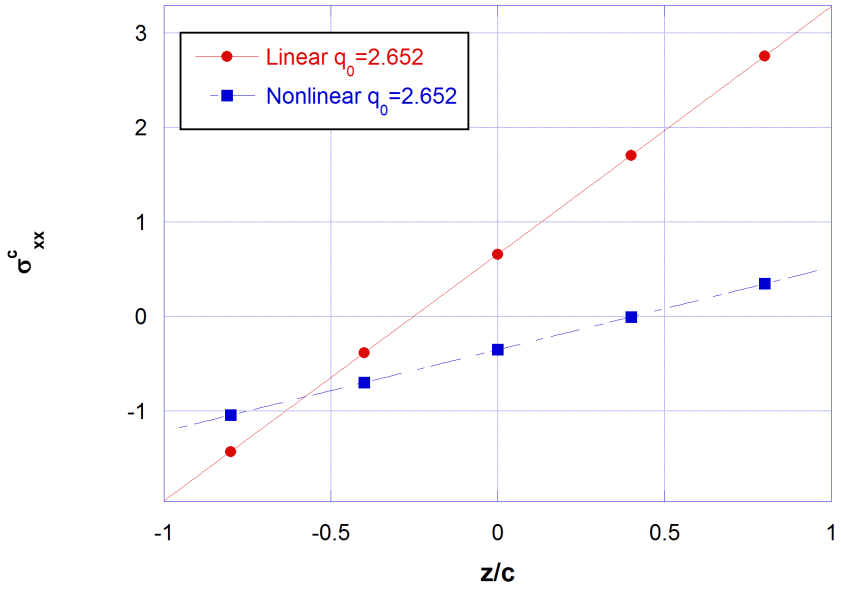

Figure 32: Through-thickness distribution in the core of the in-plane stress, σ_{xx}, at $x = a/2$ and $y = b/2$-linear vs nonlinear, $\hat{q}_0 = 2.652$

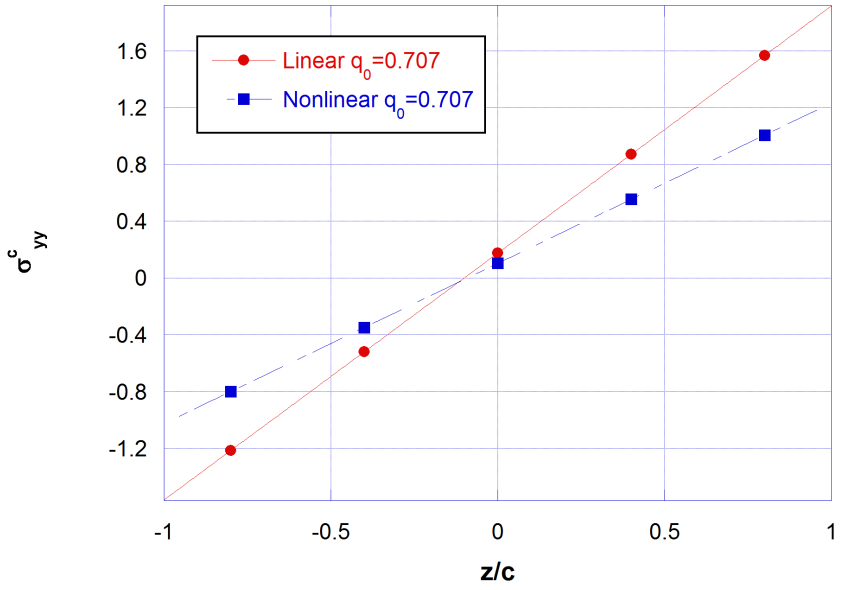

Figure 33: Through-thickness distribution in the core of the in-plane stress, σ_{yy}, at $x = a/2$ and $y = b/2$-linear vs nonlinear, $\hat{q}_0 = 0.707$

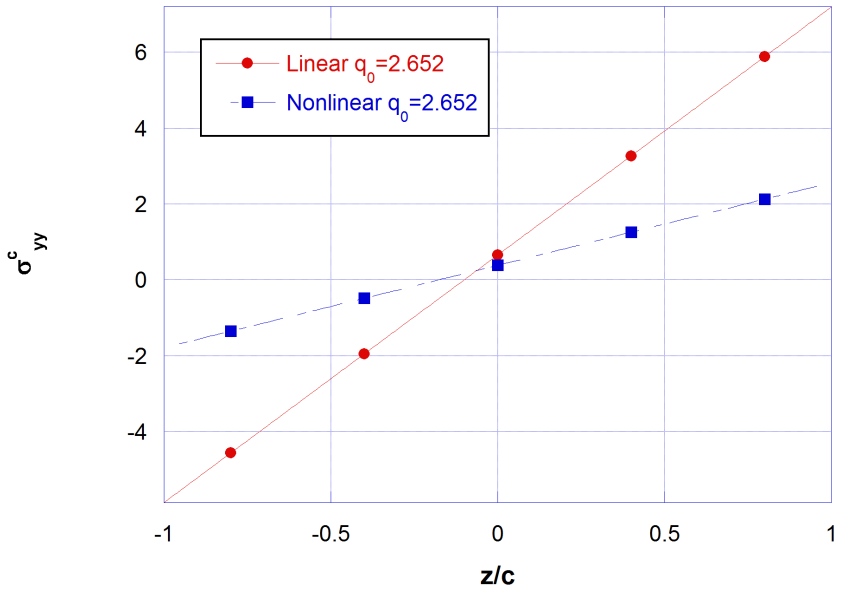

Figure 34: Through-thickness distribution in the core of the in-plane stress, σ_{yy}, at $x = a/2$ and $y = b/2$-linear vs nonlinear, $\hat{q}_0 = 2.652$

The through-thickness distribution of the transverse normal stress in the core, σ_{zz}, at the midspan location, $x = a/2$ and $y = b/2$, is shown in Figure 35.

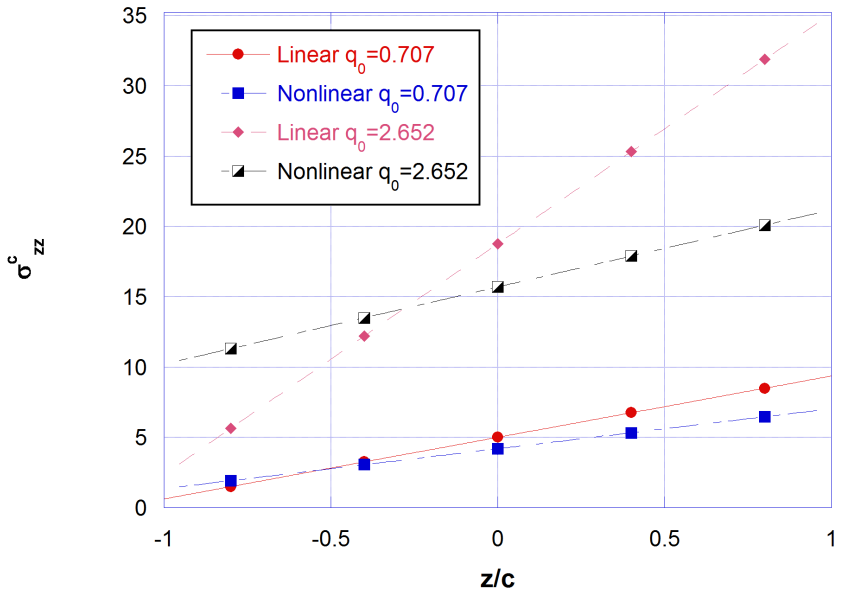

Figure 35: Through-thickness distribution in the core of the transverse normal stress, σ_{zz}, at $x = a/2$ and $y = b/2$-linear vs nonlinear

It should be noted that as expected the stress predicted by the nonlinear theory is lesser in magnitude as compared to the predictions of the linear theory as the displacement predicted by the nonlinear theory was also smaller in magnitude.

3.3.2 Simply Supported Plate with Fixed Edges

We now consider the case of a simply supported plate with fixed edges, the in-plane displacement along the edges is restricted from movement along both the tangential and normal directions to the edge and also the out of plane displacement is fixed.

The geometric boundary conditions for the boundaries $x = 0$, a are as follows:

$$\begin{aligned} u_0^b &= u_0^c = u_0^t = 0 \\ v_0^b &= v_0^c = v_0^t = 0 \\ w^b &= w_0^c = w^t = 0 \\ w^b{}_{,y} &= \phi_0^c = w^t{}_{,y} = 0 \end{aligned} \tag{66}$$

similarly, for $y = 0$, b the geometric boundary conditions are as follows:

$$\begin{aligned} u_0^b &= u_0^c = u_0^t = 0 \\ v_0^b &= v_0^c = v_0^t = 0 \\ w^b &= w_0^c = w^t = 0 \\ w^b{}_{,x} &= \psi_0^c = w^t{}_{,x} = 0 \end{aligned} \tag{67}$$

These boundary conditions can be satisfied by selecting the following assumed shape functions

$$\begin{aligned} u_0^t &= \sum_{m=1}^{M}\sum_{n=1}^{N} U_{mn}^T \sin\frac{m\pi x}{a}\sin\frac{n\pi y}{b}, & u_0^c &= \sum_{m=1}^{M}\sum_{n=1}^{N} U_{mn}^C \sin\frac{m\pi x}{a}\sin\frac{n\pi y}{b}, \\ u_0^b &= \sum_{m=1}^{M}\sum_{n=1}^{N} U_{mn}^B \sin\frac{m\pi x}{a}\sin\frac{n\pi y}{b}, & v_0^t &= \sum_{m=1}^{M}\sum_{n=1}^{N} V_{mn}^T \sin\frac{m\pi x}{a}\sin\frac{n\pi y}{b}, \\ v_0^c &= \sum_{m=1}^{M}\sum_{n=1}^{N} V_{mn}^C \sin\frac{m\pi x}{a}\sin\frac{n\pi y}{b}, & v_0^b &= \sum_{m=1}^{M}\sum_{n=1}^{N} V_{mn}^B \sin\frac{m\pi x}{a}\sin\frac{n\pi y}{b} \\ w^t &= \sum_{m=1}^{M}\sum_{n=1}^{N} W_{mn}^T \sin\frac{m\pi x}{a}\sin\frac{n\pi y}{b}, & w_0^c &= \sum_{m=1}^{M}\sum_{n=1}^{N} W_{mn}^C \sin\frac{m\pi x}{a}\sin\frac{n\pi y}{b}, \\ w^b &= \sum_{m=1}^{M}\sum_{n=1}^{N} W_{mn}^B \sin\frac{m\pi x}{a}\sin\frac{n\pi y}{b}, & \phi_0^c &= \sum_{m=1}^{M}\sum_{n=1}^{N} \Phi_{mn} \sin\frac{m\pi x}{a}\cos\frac{n\pi y}{b}, \\ \psi_0^c &= \sum_{m=1}^{M}\sum_{n=1}^{N} \Psi_{mn} \cos\frac{m\pi x}{a}\sin\frac{n\pi y}{b} \end{aligned} \tag{68}$$

The nonlinear strain displacement relations (30) and the stress strain relations (31) are substituted in the total potential energy equation (34) and integration is carried out with respect to z, the thickness coordinate. The assumed shape functions equations (68) are then substituted into the resulting equation and integrations with respect to the inplane coordinates x and y are carried out. This results in an equation in terms of the unknown coefficients U^T_{mn}, U^C_{mn}, U^B_{mn}, V^T_{mn}, V^C_{mn}, V^T_{mn}, W^T_{mn}, W^C_{mn}, W^B_{mn}, Φ_{mn}, Ψ_{mn}. The resulting equation is then differentiated with respect to the unknown coefficients, equation (20b), to minimize the energy functional $\Pi(U_{ij})$. This results in $M \times N$ nonlinear equations for the $M \times N$ unknown coefficients. The resulting simultaneous nonlinear equations are then solved using the Newton-Raphson method where the solutions from the nonlinear simply supported with free edges case serves as the initial guess in the Newton-Raphson method.

First consider the case where both the facesheets and the core are assumed to be nonlinear. It can be seen in Figure 36 that as the applied load q_0 increases the maximum deflection w^t at the center point on the surface of the top facesheet of the plate is no more linear and the linear theory results in predicting much higher displacements.

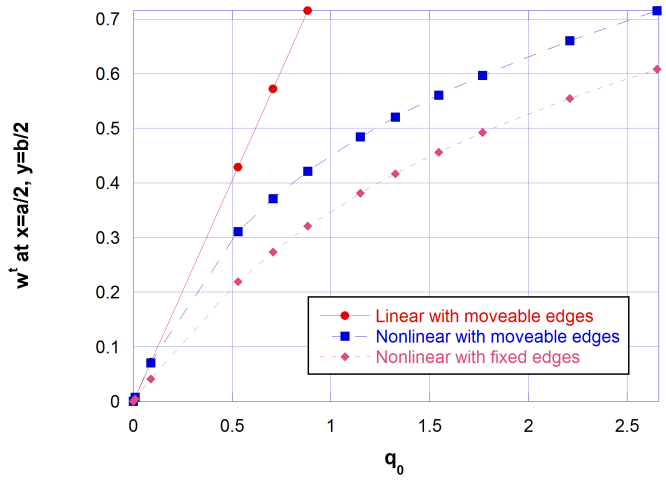

Figure 36: w^t for a simply supported square plate with fixed edges-simply supported linear vs simply supported with moveable edges vs simply supported with fixed edges

It can be seen in Figure 36 that the maximum deflection at $x = \frac{a}{2}$ and $y = \frac{b}{2}$ decreases as the simply supported edges are prevented from moving in the normal direction to the edge.

Consider again the case where only the facesheets are assumed to be nonlinear and the core is linear. The results are virtually identical as shown in Figure 37 and Table 9.

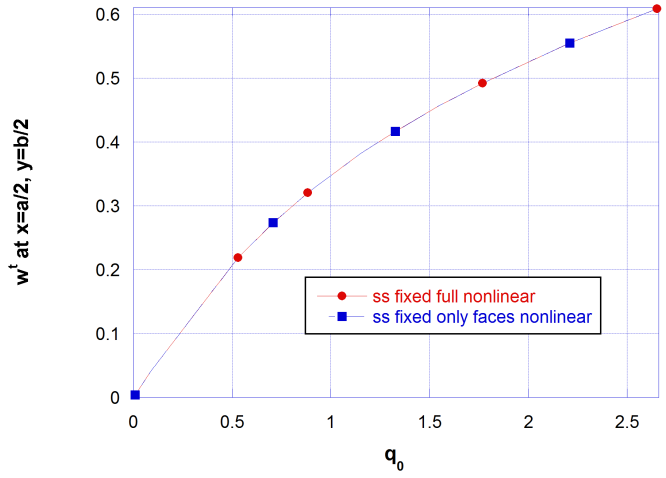

Figure 37: w^t for a simply supported square plate with fixed edges-full nonlinear vs only faces nonlinear

Table 9: w^t at $x = \frac{a}{2}$ and $y = \frac{b}{2}$ for a simply supported square plate with fixed edges-all nonlinear vs only facesheets nonlinear

q_0	All Nonlinear	Only Facesheets Nonlinear
8.84×10^{-7}	4.14×10^{-7}	4.14×10^{-7}
8.83978×10^{-3}	4.13667×10^{-3}	4.13668×10^{-3}
0.0883978	0.041171	0.041172
0.530387	0.218676	0.218723
0.707182	0.273309	0.273386
0.883978	0.320647	0.320753
1.14917	0.381358	0.381506
1.32597	0.416629	0.416803
1.54696	0.456266	0.456469
1.76796	0.491963	0.492194
2.20994	0.55446	0.554741
2.65193	0.608238	0.608563

It can be seen that with the inclusion of nonlinear effects in the core the overall displacement is lower than the displacement if the nonlinear effects are not included.

3.3.3 Clamped with Moveable Edges

We now consider the case of a clamped plate with moveable edges, the edges are free to move along the normal direction to the boundary but the out of plane displacement and rotation of the edge is fixed. The geometric boundary conditions for the edges $x = 0, a$ are as follows:

$$\begin{aligned} v_0^b = v_0^c = v_0^t = 0 \\ w^b = w_0^c = w^t = 0 \\ {w^b}_{,y} = \phi_0^c = {w^t}_{,y} = 0 \\ {w^b}_{,x} = \psi_0^c = {w^t}_{,x} = 0 \end{aligned} \tag{69}$$

similarly, for $y = 0,\ b$ the geometric boundary conditions are as follows;

$$\begin{aligned} u_0^b &= u_0^c = u_0^t = 0 \\ w^b &= w_0^c = w^t = 0 \\ w^b{}_{,x} &= \psi_0^c = w^t{}_{,x} = 0 \\ w^b{}_{,y} &= \phi_0^c = w^t{}_{,y} = 0 \end{aligned} \tag{70}$$

These boundary conditions can be satisfied by selecting the following assumed shape functions

$$\begin{aligned} u_0^t &= \sum_{m=1}^{M}\sum_{n=1}^{N} U_{mn}^T \cos\frac{m\pi x}{a}\sin\frac{n\pi y}{b}, \qquad u_0^c = \sum_{m=1}^{M}\sum_{n=1}^{N} U_{mn}^C \cos\frac{m\pi x}{a}\sin\frac{n\pi y}{b} \\ u_0^b &= \sum_{m=1}^{M}\sum_{n=1}^{N} U_{mn}^B \cos\frac{m\pi x}{a}\sin\frac{n\pi y}{b}, \qquad v_0^t = \sum_{m=1}^{M}\sum_{n=1}^{N} V_{mn}^T \sin\frac{m\pi x}{a}\cos\frac{n\pi y}{b} \\ v_0^c &= \sum_{m=1}^{M}\sum_{n=1}^{N} V_{mn}^C \sin\frac{m\pi x}{a}\cos\frac{n\pi y}{b}, \qquad v_0^b = \sum_{m=1}^{M}\sum_{n=1}^{N} V_{mn}^B \sin\frac{m\pi x}{a}\cos\frac{n\pi y}{b} \\ w^t &= \sum_{m=1}^{M}\sum_{n=1}^{N} W_{mn}^T \left[1-\cos\left(\frac{2\pi x}{a}\right)\right]\left[1-\cos\left(\frac{2\pi y}{b}\right)\right] \\ w_0^c &= \sum_{m=1}^{M}\sum_{n=1}^{N} W_{mn}^C \left[1-\cos\left(\frac{2\pi x}{a}\right)\right]\left[1-\cos\left(\frac{2\pi y}{b}\right)\right] \\ w^b &= \sum_{m=1}^{M}\sum_{n=1}^{N} W_{mn}^B \left[1-\cos\left(\frac{2\pi x}{a}\right)\right]\left[1-\cos\left(\frac{2\pi y}{b}\right)\right] \\ \phi_0^c &= \sum_{m=1}^{M}\sum_{n=1}^{N} \Phi_{mn} \left[1-\cos\left(\frac{2\pi x}{a}\right)\right]\sin\left(\frac{2\pi y}{b}\right) \\ \psi_0^c &= \sum_{m=1}^{M}\sum_{n=1}^{N} \Psi_{mn} \left[1-\cos\left(\frac{2\pi y}{b}\right)\right]\sin\left(\frac{2\pi x}{a}\right) \end{aligned} \tag{71}$$

The nonlinear strain relations (30) and the stress strain relations (31) are substituted into the equations for the total potential energy equation (34) and integration is carried out with respect to z, the thickness coordinate. The assumed shape functions equations (71) are then substituted into the resulting equation and integrations

with respect to the inplane coordinates x and y is carried out. This results in an equation in terms of the unknown coefficients U^T_{mn}, U^C_{mn}, U^B_{mn}, V^T_{mn}, V^C_{mn}, V^T_{mn}, W^T_{mn}, W^C_{mn}, W^B_{mn}, Φ_{mn}, Ψ_{mn}. The resulting equation is then differentiated with respect to the unknown coefficients, equation (20b), to minimize the functional $\Pi(U_{ij})$. This results in $M \times N$ nonlinear equations for the $M \times N$ unknown coefficients. The resulting simultaneous nonlinear equations are then solved using the Newton-Raphson method where the initial guess is taken to be the results from the simply supported with fixed edges case. First consider the case where both the facesheets and the core are assumed to be nonlinear.

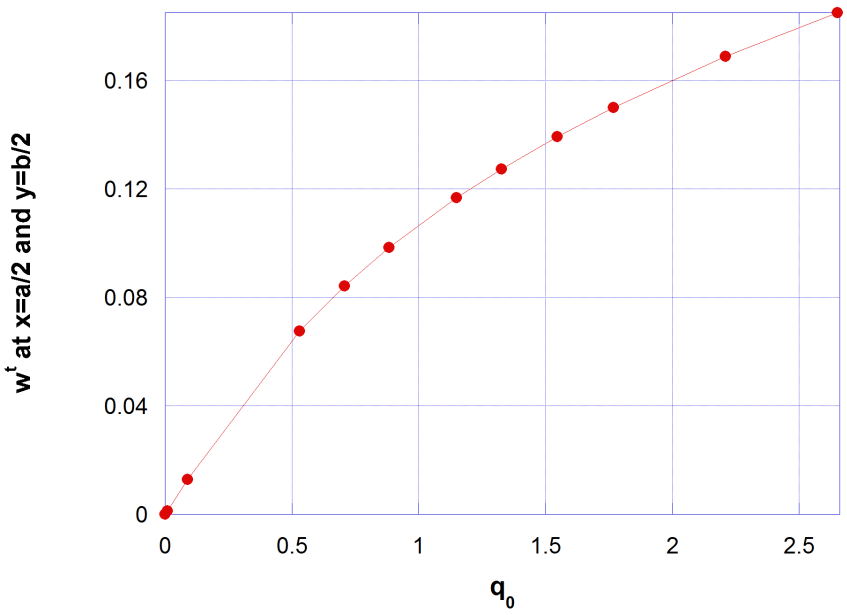

Figure 38: Nonlinear transverse displacement w^t for a clamped square plate with moveable edges

The result from the clamped moveable edges case is compared to the simply supported with moveable edges case and the simply supported with fixed edges case in Figure 39. It can be seen that the clamped with moveable edges case results in the

least displacement as compared to the other two cases considered.

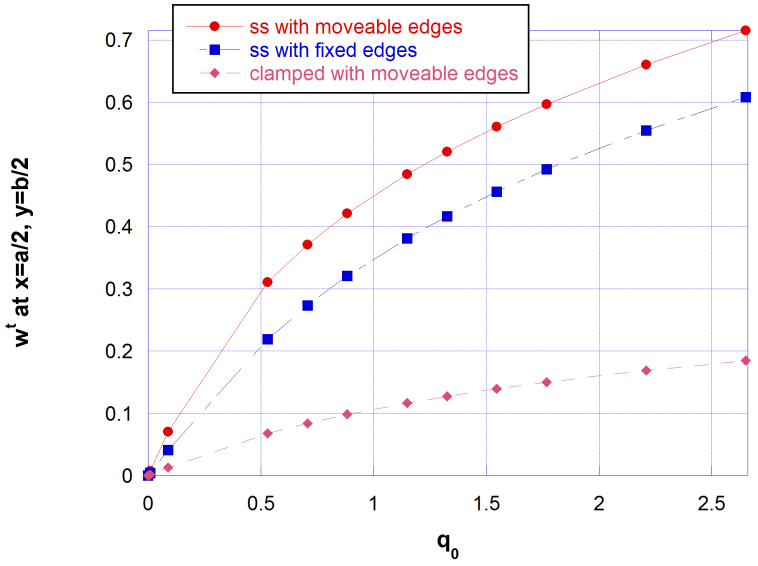

Figure 39: Nonlinear transverse displacement w^t-simply supported with moveable edges vs simply supported with fixed edges vs clamped with moveable edges

Consider again the case where only the facesheets are assumed to be nonlinear and the core is considered to be linear the results are again virtually identical as shown in Figure 40 and Table 9.

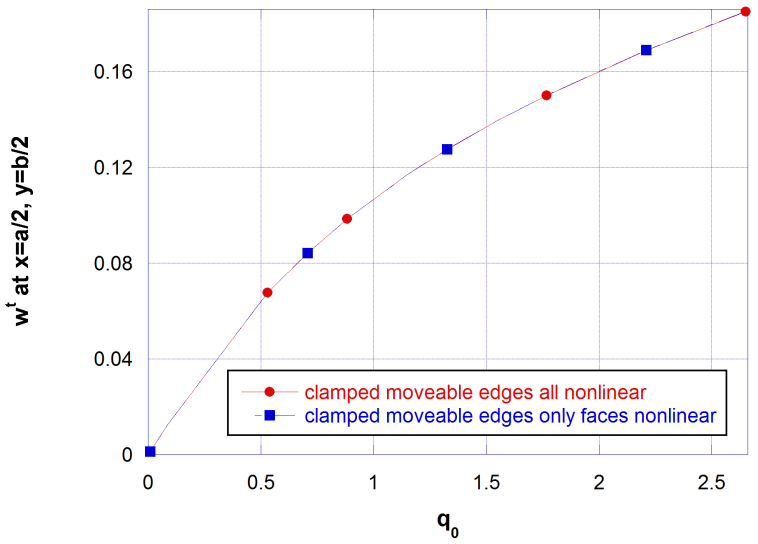

Figure 40: w^t for a clamped plate with moveable edges-full nonlinear vs only facesheets nonlinear

The same result is presented in tabular form in Table 10.

Table 10: w^t at $x = \frac{a}{2}$ and $y = \frac{b}{2}$ for a clamped square plate with moveable edges-all nonlinear vs only facesheets nonlinear

q_0	All Nonlinear	Only Facesheets Nonlinear
8.84×10^{-7}	1.29×10^{-7}	1.29×10^{-7}
0.00884	0.001292	0.001292
0.088398	0.012848	0.012849
0.530387	0.067577	0.067596
0.707182	0.084173	0.084203
0.883978	0.098491	0.098531
1.14917	0.116797	0.116852
1.32597	0.127413	0.127477
1.54696	0.139333	0.139407
1.76796	0.150061	0.150145
2.20994	0.168835	0.168937
2.65193	0.184986	0.185103

It can again be seen that the inclusion of the nonlinear strains in the core causes the overall displacement to be lower than the displacement if the nonlinear effects are not included.

3.3.4 Fully Clamped with Fixed Edges

Consider now the case of a fully clamped plate with immoveable and fixed edges in which the in-plane displacement along the edges is restricted from movement both tangential and normal to the edge, and also with out of plane displacement fixed and with no rotation on the edges allowed. The geometric boundary conditions for the

boundaries $x = 0$, a are as follows:

$$\begin{aligned} u_0^b &= u_0^c = u_0^t = 0 \\ v_0^b &= v_0^c = v_0^t = 0 \\ w^b &= w_0^c = w^t = 0 \\ w^b{}_{,y} &= \phi_0^c = w^t{}_{,y} = 0 \\ w^b{}_{,x} &= \psi_0^c = w^t{}_{,x} = 0 \end{aligned} \tag{72}$$

Similarly, for $y = 0$, b the geometric boundary conditions are as follows:

$$\begin{aligned} u_0^b &= u_0^c = u_0^t = 0 \\ v_0^b &= v_0^c = v_0^t = 0 \\ w^b &= w_0^c = w^t = 0 \\ w^b{}_{,x} &= \psi_0^c = w^t{}_{,x} = 0 \\ w^b{}_{,y} &= \phi_0^c = w^t{}_{,y} = 0 \end{aligned} \tag{73}$$

These boundary conditions can be satisfied by selecting the following assumed shape functions

$$\begin{aligned} u_0^t &= \sum_{m=1}^{M}\sum_{n=1}^{N} U_{mn}^T \sin\frac{m\pi x}{a}\sin\frac{n\pi y}{b}, & u_0^c &= \sum_{m=1}^{M}\sum_{n=1}^{N} U_{mn}^C \sin\frac{m\pi x}{a}\sin\frac{n\pi y}{b} \\ u_0^b &= \sum_{m=1}^{M}\sum_{n=1}^{N} U_{mn}^B \sin\frac{m\pi x}{a}\sin\frac{n\pi y}{b}, & v_0^t &= \sum_{m=1}^{M}\sum_{n=1}^{N} V_{mn}^T \sin\frac{m\pi x}{a}\sin\frac{n\pi y}{b} \\ v_0^c &= \sum_{m=1}^{M}\sum_{n=1}^{N} V_{mn}^C \sin\frac{m\pi x}{a}\sin\frac{n\pi y}{b}, & v_0^b &= \sum_{m=1}^{M}\sum_{n=1}^{N} V_{mn}^B \sin\frac{m\pi x}{a}\sin\frac{n\pi y}{b} \end{aligned}$$

$$
\begin{aligned}
w^t &= \sum_{m=1}^{M}\sum_{n=1}^{N} W_{mn}^{T}\left[1-\cos\left(\frac{2\pi x}{a}\right)\right]\left[1-\cos\left(\frac{2\pi y}{b}\right)\right] \\
w_0^c &= \sum_{m=1}^{M}\sum_{n=1}^{N} W_{mn}^{C}\left[1-\cos\left(\frac{2\pi x}{a}\right)\right]\left[1-\cos\left(\frac{2\pi y}{b}\right)\right] \\
w^b &= \sum_{m=1}^{M}\sum_{n=1}^{N} W_{mn}^{B}\left[1-\cos\left(\frac{2\pi x}{a}\right)\right]\left[1-\cos\left(\frac{2\pi y}{b}\right)\right] \\
\phi_0^c &= \sum_{m=1}^{M}\sum_{n=1}^{N} \Phi_{mn}\ \left[1-\cos\left(\frac{2\pi x}{a}\right)\right]\sin\left(\frac{2\pi y}{b}\right) \\
\psi_0^c &= \sum_{m=1}^{M}\sum_{n=1}^{N} \Psi_{mn}\ \left[1-\cos\left(\frac{2\pi y}{b}\right)\right]\sin\left(\frac{2\pi x}{a}\right)
\end{aligned}
\tag{74}
$$

The nonlinear strain relations (30) and the stress strain relations (31) are substituted into the total potential energy equation (34), and integration is carried out with respect to z, the thickness coordinate. The assumed shape functions equations (**??**) are then substituted into the resulting equation and integrations with respect to the inplane coordinates x and y are carried out. This results in an equation in terms of the unknown coefficients U_{mn}^{T}, U_{mn}^{C}, U_{mn}^{B}, V_{mn}^{T}, V_{mn}^{C}, V_{mn}^{T}, W_{mn}^{T}, W_{mn}^{C}, W_{mn}^{B}, Φ_{mn}, Ψ_{mn}. The resulting equation is then differentiated with respect to the unknown coefficients, equation (20b), to minimize the functional $\Pi(U_{ij})$. This results in $M \times N$ nonlinear equations for the $M \times N$ unknown coefficients. The resulting simultaneous nonlinear equations are then solved using the Newton-Raphson method where the initial guess is taken to be the result from the clamped with moveable edges case. We first consider the case where both the facesheets and the core are considered to be nonlinear as shown in Figure 41.

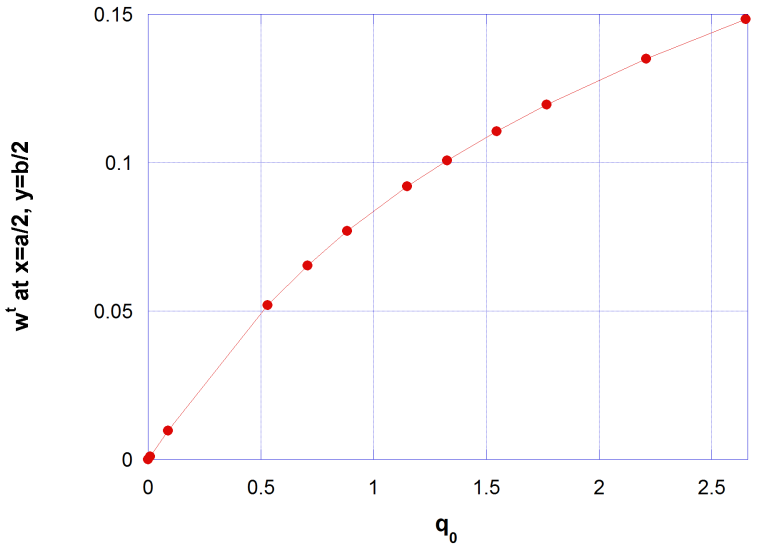

Figure 41: Nonlinear transverse displacement w^t for a fully clamped square plate with fixed edges

The result for the clamped with fixed edges case is now compared with the simply supported with moveable edges, simply supported with fixed edges and the clamped with moveable edges cases, as shown in Figure 42.

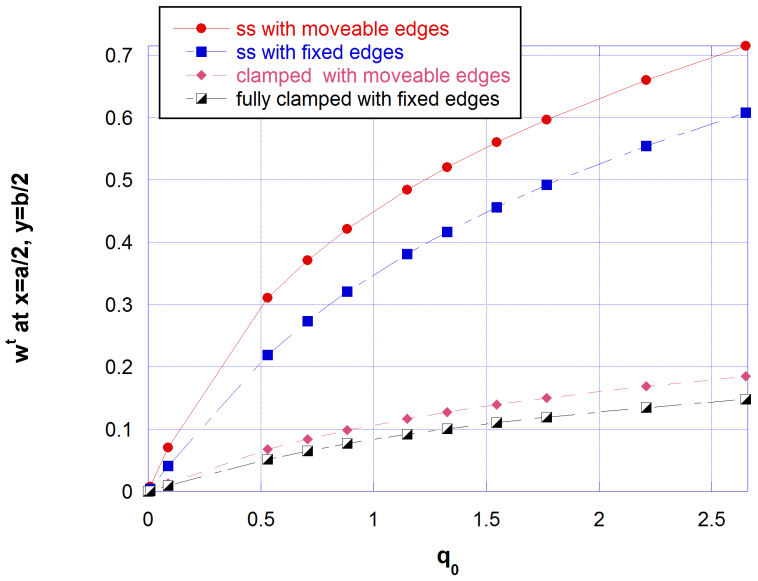

Figure 42: Nonlinear transverse displacement w^t for a square plate: fully clamped with fixed edges vs simply supported with moveable edges vs simply supported with fixed edges vs clamped with moveable edges

It can be seen in Figure 42 that the maximum deflection at $x = \frac{a}{2}$ and $y = \frac{b}{2}$ decreases as the boundary conditions for the plate are changed from simply supported with moveable edges to the simply supported with fixed edges and then from clamped with moveable edges to clamped with fixed edges cases.

Consider again the case where only the facesheets are assumed to be nonlinear and the core is considered to be linear. The results are virtually identical as shown in Figure 43 and Table 11.

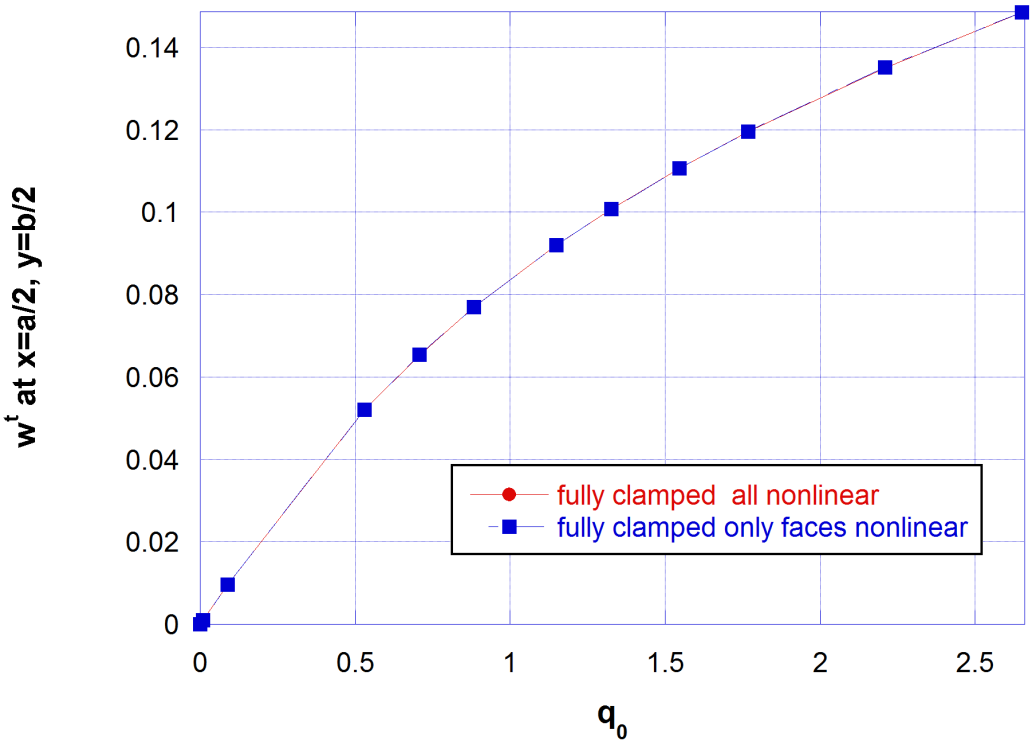

Figure 43: w^t for a fully clamped square plate with fixed edges-fully nonlinear vs only faces nonlinear

The same result is presented in tabular form below in Table 11:

Table 11: w^t at $x = \frac{a}{2}$ and $y = \frac{b}{2}$ for a clamped square plate with fixed edges-all nonlinear vs only facesheets nonlinear

q_0	All Nonlinear	Only Facesheets Nonlinear
8.84×10^{-7}	9.70×10^{-8}	9.70×10^{-8}
0.00884	0.000969759	0.000969761
0.088398	0.0096583	0.00965858
0.530387	0.0520164	0.0520295
0.707182	0.065352	0.0653733
0.883978	0.0769907	0.0770203
1.14917	0.0919965	0.0920381
1.32597	0.100742	0.100791
1.54696	0.110587	0.110645
1.76796	0.119463	0.119529
2.20994	0.135017	0.135098
2.65193	0.148409	0.148504

3.3.5 Stress Analysis Results (All Boundary Conditions Comparison)

The distribution of the normal stresses through the thickness of the core for all four load cases considered are presented below:

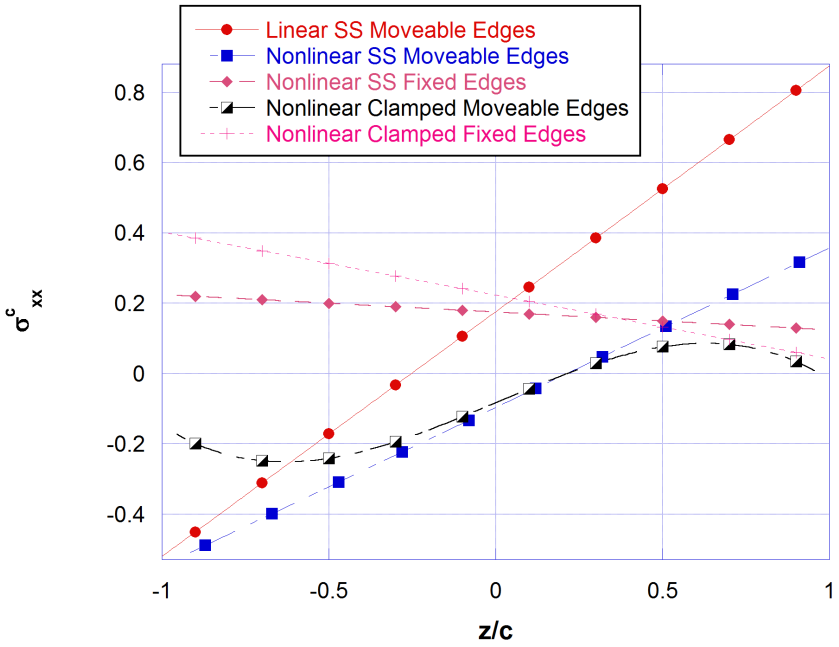

Figure 44: Through the thickness distribution of $\hat{\sigma}^c_{xx}$ for $\hat{q}_0 = 0.707$

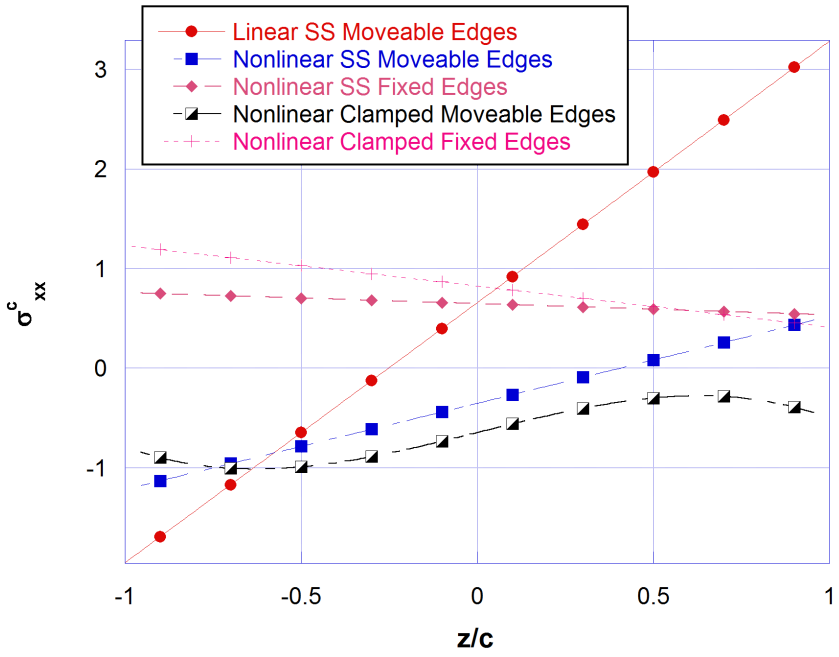

Figure 45: Through the thickness distribution of $\hat{\sigma}^c_{xx}$ for $\hat{q}_0 = 2.562$

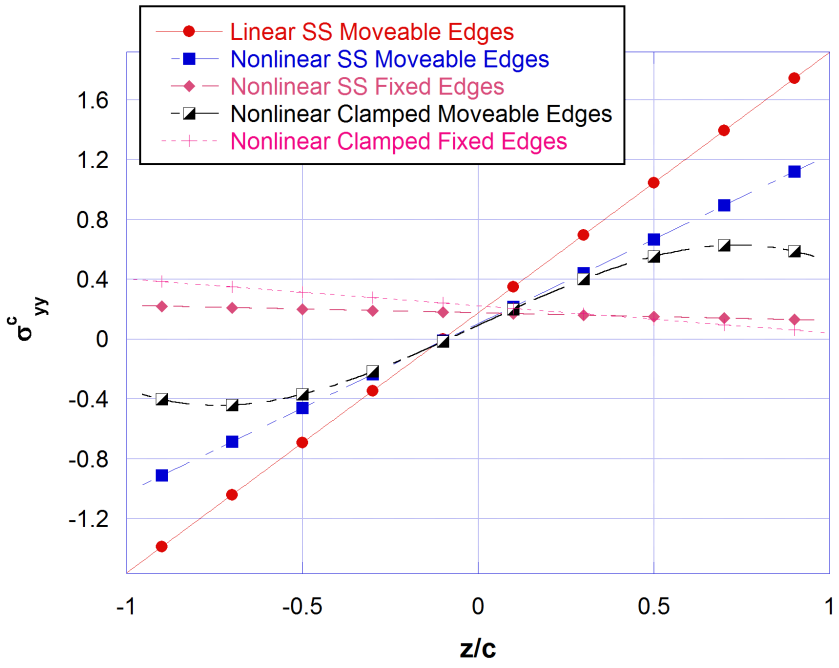

Figure 46: Through the thickness distribution of $\hat{\sigma}^c_{yy}$ for $\hat{q}_0 = 0.707$

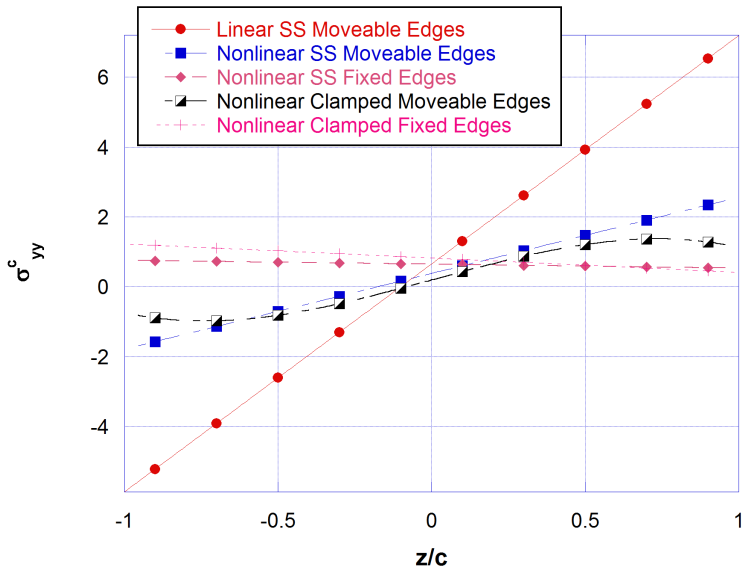

Figure 47: Through the thickness distribution of $\hat{\sigma}^c_{yy}$ for $\hat{q}_0 = 2.562$

It can be seen in Figures 44,45,46 and 47 that the fixed edges cases produce a different profile as compared to the moveable edges case.

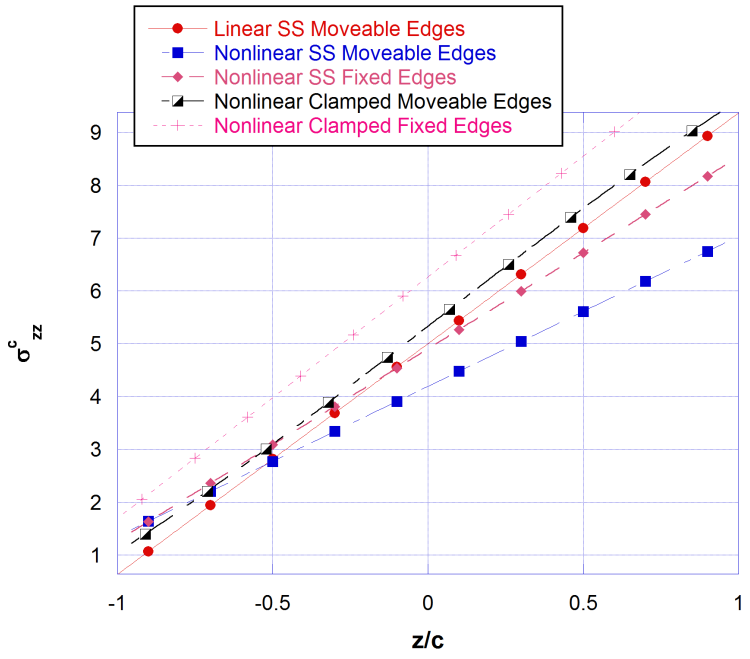

Figure 48: Through the thickness distribution of $\hat{\sigma}^c_{zz}$ for $\hat{q}_0 = 0.707$

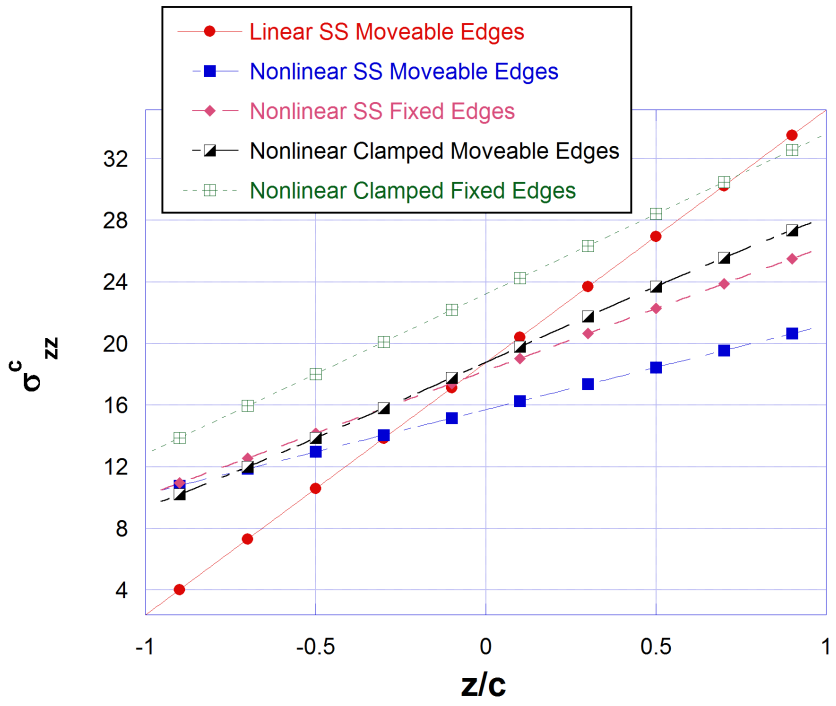

Figure 49: Through the thickness distribution of $\hat{\sigma}^c_{zz}$ for $\hat{q}_0 = 2.562$

It can be seen in Figures 48 and 49 that the clamped with fixed edges case results in the highest stress for the same load level for all four boundary condition cases.

Chapter IV

CONCLUSIONS AND FUTURE WORK

4.1 Conclusions

The Extended High-Order Sandwich Panel Theory (EHSAPT) was presented for laminated sandwich plates that allows for the transverse shear distribution in the core to acquire the proper distribution as the core stiffness increases as a result of non-negligible axial stresses in the core. Thus, this theory is valid for both soft and stiff cores with thin facesheets. The theory assumes a transverse displacement in the core that varies as a second-order equation in the transverse coordinate z, and an axial displacement field that is third order in z. The novelty of EHSAPT is that it allows for five generalized displacement variables in the core (the transverse and the two axial displacements at the centroid of the core and two rotations at the mid-plane of the core) and that it has been formulated for a sandwich panel with a general layout and no restrictions are imposed on the geometric configuration of the plate. Results were presented for a wide variety of configurations in terms of aspect ratios, etc. The major assumptions of the theory are as follows:

1. The face sheets satisfy the Euler-Bernoulli assumptions and their thicknesses are small compared to the overall thickness of the sandwich plate. The two facesheets (i.e., the top and bottom facesheets) can be constructed from different materials and can have different thicknesses. In addition, the free vibration

model was developed to allow for the facesheets to be laminated plates with different layups for the top and bottom facesheets. Additionally, the top and bottom facesheets can have different number of laminas with varying angles and the thicknesses of the individual laminas can also be varied.

2. The core is compressible in the transverse and axial directions(transverse displacement is 2nd order in z and in plane displacement is 3rd order in z).

3. The facesheets and core are considered to be perfectly bonded at their interfaces.

4. The facesheets and core material do not exhibit bending-twist coupling.

Validation of the present theory was performed using both static loading and a free vibration analysis and in both cases the results were then compared to existing elasticity solutions. In the study of a static half-sine load applied to the top face sheet of a simply supported sandwich plate, EHSAPT was found to be very close to the elasticity solution both in terms of displacements, stresses and strains.

The free vibration analysis of a simply supported sandwich plate was then carried out. The existing elasticity solution by Noor [9] provides a benchmark against which the theory is compared. After establishing the validity of EHSAPT for dynamic analysis, a parametric study is carried out to analyze the effect of variation of several material and geometric parameters on the fundamental natural frequency of a laminated sandwich plate.

A nonlinear static analysis of the sandwich plate was then carried out using variational techniques and the Ritz method. The kinematics were developed for a sandwich

plate undergoing small strains and moderate rotations. Employing the Ritz method, the total potential energy of the system was developed. Four different cases and combinations of boundary conditions were studied and approximate and assumed solutions satisfying the geometric boundary conditions were developed. The total potential energy was then evaluated and employing the Principle of Minimum Total Potential Energy, minimized with respect to the unknown coefficients in the assumed solution. This resulted in nonlinear simultaneous algebraic equations for the unknown coefficients in the approximate solution. The simultaneous nonlinear equations were then solved using the Newton-Raphson method. The initial guess for the approximate solution were chosen to be the analytical result from the linear solution.

A convergence study was then carried out to study the effect of variation of the number of terms in the assumed solution. The convergence study indicated that $M \times N = 3 \times 3$ produced a sufficiently converged result and further increase in the number of terms did not have a significant effect on the result. Rapid convergence was observed and attributed to the fact that the assumed solution not only satisfies the basic requirement of the Ritz method where it satisfies the geometric boundary conditions of the problem but in addition it also satisfies the natural boundary conditions of the problem.

A study was then carried out to analyze the effect of inclusion of nonlinear effects in the core where the results were computed considering only the facesheets with nonlinear strains and the core was considered to remain in the linear range. The results were then compared to the already calculated all nonlinear analysis. It was found out that the additional computational effort did not have a significant effect on

the overall results. It was however found out that including the nonlinear terms in the kinematics of the core caused the overall deformation of the plate to be slightly lower than the linear core.

A stress analysis was also carried out where the stresses predicted by the linear theory are compared against the nonlinear results and it is found that the magnitude of stresses is much lower when the nonlinear effects are taken into consideration.

After calculating and comparing the results for the simply supported case, three more cases for different sets of boundary conditions were considered. In all cases the results were also computed for the nonlinear faces and linear core combination and the overall effect was found to be not too significant. However, as highlighted above it is pertinent to mention that inclusion of the nonlinear effects in the core in all cases resulted in lowering the overall displacement.

During all calculations the following four sets of boundary conditions were considered

1. Simply Supported with moveable edges (Stress Free).

2. Simply Supported with fixed edges.

3. Clamped with moveable edges.

4. Clamped with fixed edges (Stress Free).

After calculation of the results from the simply supported with moveable edges case, the solution for each previous case served as an initial starting guess for the next case considered in the Newton-Raphson method for the solution of simultaneous

nonlinear equations. Since EHSAPT allows for analysis of plates with variable aspect ratios a further case where it was assumed that the depth of the plate was half the width was also considered in Appendix E. The results were again presented for various geometric configurations and were compared to the square plate.

4.2 Future Work

In most approximate solution procedures, infinite degree of freedom problems are reduced to finite degree of freedom problems. Three main approaches are used to achieve this type of dimensional reduction. In the first approach, the solution is sought at a finite number of discrete points of the structure; this approach is essentially a discretization procedure, because it transforms the original problem, expressed in terms of continuous, infinite degree of freedom functions, into a discrete problem involving the values of these functions at a finite number of points. The derivatives appearing in the governing equations are then approximated using finite difference techniques. The original equations are transformed into a set of algebraic equations that is easily solved.

In the second approach, the solution of the problem is approximated by a finite sum of continuous functions, each weighted by an unknown coefficient. The solution of the problem then reduces to the determination of the unknown coefficients.

Finally, the last approach, called the finite element method, combines aspects of the previous two. In this widely used approach, the solution domain is first divided into a finite number of sub-domains called finite elements. Within each element, the solution is then approximated by a finite number of continuous functions, based on

the value of these functions at discrete points, often called nodes, associated with the element. The main advantage of this two-step approximation process is that many aspects of the solution procedure can be carried out at the element level, i.e., by considering one single element at a time, independently of all others. The continuity of the solution across elements can be guaranteed by the fact that neighboring elements share common nodes. Here again, energy based methods and techniques provide a systematic way of obtaining algebraic equations for the unknown values of the solution at the nodes.

It is proposed that EHSAPT for plates be extended to the Finite Element Method (FEM). In addition, EHSAPT can also be further extended to solve a number of other structural analysis problems such as: thermal loading, effect of delamination, wrinkling, study of inter-laminar stresses in case of free edge problems and dynamic stability.

Appendix A

STATIC MODEL - STRESS RESULTANTS

$$\left\{N^t\right\} = \begin{Bmatrix} N^t_{xx} \\ N^t_{yy} \\ N^t_{xy} \end{Bmatrix} = \int_c^{c+f} \left\{\sigma^t\right\} dz, \qquad \textit{for the top face sheet} \tag{75a}$$

$$\left\{N^b\right\} = \begin{Bmatrix} N^b_{xx} \\ N^b_{yy} \\ N^b_{xy} \end{Bmatrix} = \int_{-c-f}^{-c} \left\{\sigma^b\right\} dz, \qquad \textit{for the bottom face sheet} \tag{75b}$$

Similarly

$$\left\{M^t\right\} = \begin{Bmatrix} M^t_{xx} \\ M^t_{yy} \\ M^t_{xy} \end{Bmatrix} = \int_c^{c+f} \left\{\sigma^t\right\} (z - c - \frac{f^t}{2})\, dz, \qquad \textit{for the top face sheet} \tag{75c}$$

$$\left\{M^b\right\} = \begin{Bmatrix} M^b_{xx} \\ M^b_{yy} \\ M^b_{xy} \end{Bmatrix} = \int_{-c-f}^{-c} \left\{\sigma^b\right\} (z + c + \frac{f^b}{2})\, dz, \qquad \textit{for the bottom face sheet}$$

(75d)

For the core the following resultants are defined

$$\left\{N^c\right\} = \begin{Bmatrix} N^c_{xx} \\ N^c_{yy} \\ N^c_{zz} \\ N^c_{yz} \\ N^c_{xz} \\ N^c_{xy} \end{Bmatrix} = \int_{-c}^{c} \left\{\sigma^c\right\} dz, \qquad \textit{for the core} \tag{76a}$$

Similarly, the following resultants are also defined for the core

$$\begin{Bmatrix} M^c_{xx_1} \\ M^c_{yy_1} \\ M^c_{zz_1} \\ M^c_{xy_1} \\ M^c_{yz_1} \\ M^c_{xz_1} \end{Bmatrix} = \int_{-c}^{c} \begin{Bmatrix} \sigma^c_{xx} \\ \sigma^c_{yy} \\ \sigma^c_{zz} \\ \sigma^c_{xy} \\ \sigma^c_{yz} \\ \sigma^c_{xz} \end{Bmatrix} z \; dz, \quad \begin{Bmatrix} M^c_{xx_2} \\ M^c_{yy_2} \\ M^c_{xy_2} \\ M^c_{yz_2} \\ M^c_{xz_2} \end{Bmatrix} = \int_{-c}^{c} \begin{Bmatrix} \sigma^c_{xx} \\ \sigma^c_{yy} \\ \sigma^c_{xy} \\ \sigma^c_{yz} \\ \sigma^c_{xz} \end{Bmatrix} z^2 \; dz, \quad \begin{Bmatrix} M^c_{xx_3} \\ M^c_{yy_3} \\ M^c_{xy_3} \end{Bmatrix} = \int_{-c}^{c} \begin{Bmatrix} \sigma^c_{xx} \\ \sigma^c_{yy} \\ \sigma^c_{xy} \end{Bmatrix} z^3 dz \tag{76b}$$

After evaluation, the following values are obtained where only the linear terms have been retained

$$N^t_{xx} = f^t C^t_{16} u^t_{0,y} + f^t C^t_{12} v^t_{0,y} + f^t C^t_{11} u^t_{0,x} + f^t C^t_{16} v^t_{0,x} \tag{77a}$$

$$N^t_{yy} = f^t C^t_{26} u^t_{0,y} + f^t C^t_{22} v^t_{0,y} + f^t C^t_{12} u^t_{0,x} + f^t C^t_{26} v^t_{0,x} \tag{77b}$$

$$N^t_{xy} = f^t C^t_{66} u^t_{0,y} + f^t C^t_{26} v^t_{0,y} + f^t C^t_{16} u^t_{0,x} + f^t C^t_{66} v^t_{0,x} \tag{77c}$$

$$N^b_{xx} = f^b C^b_{16} u^b_{0,y} + f^b C^b_{12} v^b_{0,y} + f^b C^b_{11} u^b_{0,x} + f^b C^b_{16} v^b_{0,x} \tag{77d}$$

$$N^b_{yy} = f^b C^b_{26} u^b_{0,y} + f^b C^b_{22} v^b_{0,y} + f^b C^b_{12} u^b_{0,x} + f^b C^b_{26} v^b_{0,x} \tag{77e}$$

$$N^b_{xy} = f^b C^b_{66} u^b_{0,y} + f^b C^b_{26} v^b_{0,y} + f^b C^b_{16} u^b_{0,x} + f^b C^b_{66} v^b_{0,x} \tag{77f}$$

$$M^t_{xx} = -\frac{1}{12} f^{t^3} C^t_{12} w^t{}_{,yy} - \frac{1}{6} f^{t^3} C^t_{16} w^t{}_{,xy} - \frac{1}{12} f^{t^3} C^t_{11} w^t{}_{,xx} \tag{77g}$$

$$M^t_{yy} = -\frac{1}{12} f^{t^3} C^t_{22} w^t{}_{,yy} - \frac{1}{6} f^{t^3} C^t_{26} w^t{}_{,xy} - \frac{1}{12} f^{t^3} C^t_{12} w^t{}_{,xx} \tag{77h}$$

$$M^t_{xy} = -\frac{1}{12} f^{t^3} C^t_{26} w^t{}_{,yy} - \frac{1}{6} f^{t^3} C^t_{66} w^t{}_{,xy} - \frac{1}{12} f^{t^3} C^t_{16} w^t{}_{,xx} \tag{77i}$$

$$M^b_{xx} = -\frac{1}{12} f^{b^3} C^b_{12} w^b{}_{,yy} - \frac{1}{6} f^{b^3} C^b_{16} w^b{}_{,xy} - \frac{1}{12} f^{b^3} C^b_{11} w^b{}_{,xx} \tag{77j}$$

$$M^b_{yy} = -\frac{1}{12} f^{b^3} C^b_{22} w^b{}_{,yy} - \frac{1}{6} f^{b^3} C^b_{26} w^b{}_{,xy} - \frac{1}{12} f^{b^3} C^b_{12} w^b{}_{,xx} \tag{77k}$$

$$M^b_{xy} = -\frac{1}{12} f^{b^3} C^b_{26} w^b{}_{,yy} - \frac{1}{6} f^{b^3} C^b_{66} w^b{}_{,xy} - \frac{1}{12} f^{b^3} C^b_{16} w^b{}_{,xx} \tag{77l}$$

Similarly, for the core;

$$\begin{aligned} N^c_{xx} = &- C^c_{13} w^b + C^c_{13} w^t + \frac{1}{3} c C^c_{12} v^b_{0,y} + \frac{4}{3} c C^c_{12} v^c_{0,y} + \frac{1}{3} c C^c_{12} v^t_{0,y} - \frac{1}{6} c f^b C^c_{12} w^b{}_{,yy} \\ &+ \frac{1}{6} c f^t C^c_{12} w^t{}_{,yy} + \frac{1}{3} c C^c_{11} u^b_{0,x} + \frac{4}{3} c C^c_{11} u^c_{0,x} + \frac{1}{3} c C^c_{11} u^t_{0,x} - \frac{1}{6} c f^b C^c_{11} w^b{}_{,xx} \\ &+ \frac{1}{6} c f^t C^c_{11} w^t{}_{,xx} \end{aligned} \tag{78a}$$

$$\begin{aligned} N^c_{yy} = &- C^c_{23} w^b + C^c_{23} w^t + \frac{1}{3} c C^c_{22} v^b_{0,y} + \frac{4}{3} c C^c_{22} v^c_{0,y} + \frac{1}{3} c C^c_{22} v^t_{0,y} - \frac{1}{6} c f^b C^c_{22} w^b{}_{,yy} \\ &+ \frac{1}{6} c f^t C^c_{22} w^t{}_{,yy} + \frac{1}{3} c C^c_{12} u^b_{0,x} + \frac{4}{3} c C^c_{12} u^c_{0,x} + \frac{1}{3} c C^c_{12} u^t_{0,x} - \frac{1}{6} c f^b C^c_{12} w^b{}_{,xx} \\ &+ \frac{1}{6} c f^t C^c_{12} w^t{}_{,xx} \end{aligned} \tag{78b}$$

$$\begin{aligned} N^c_{zz} = &- C^c_{33} w^b + C^c_{33} w^t + \frac{1}{3} c C^c_{23} v^b_{0,y} + \frac{4}{3} c C^c_{23} v^c_{0,y} + \frac{1}{3} c C^c_{23} v^t_{0,y} - \frac{1}{6} c f^b C^c_{23} w^b{}_{,yy} \\ &+ \frac{1}{6} c f^t C^c_{23} w^t{}_{,yy} + \frac{1}{3} c C^c_{13} u^b_{0,x} + \frac{4}{3} c C^c_{13} u^c_{0,x} + \frac{1}{3} c C^c_{13} u^t_{0,x} - \frac{1}{6} c f^b C^c_{13} w^b{}_{,xx} \\ &+ \frac{1}{6} c f^t C^c_{13} w^t{}_{,xx} \end{aligned} \tag{78c}$$

$$N^c_{xy} = \frac{1}{3}cC^c_{66}u^b_{0,y} + \frac{4}{3}cC^c_{66}u^c_{0,y} + \frac{1}{3}cC^c_{66}u^t_{0,y} + \frac{1}{3}cC^c_{66}v^b_{0,x} + \frac{4}{3}cC^c_{66}v^c_{0,x} + \frac{1}{3}cC^c_{66}v^t_{0,x} - \frac{1}{3}cf^bC^c_{66}w^b{}_{,xy} + \frac{1}{3}cf^tC^c_{66}w^t{}_{,xy} \tag{78d}$$

$$N^c_{yz} = - C^c_{44}v^b_0 + C^c_{44}v^t_0 + \frac{4}{3}cC^c_{44}w^c_{0,y} + \frac{1}{3}cC^c_{44}w^b{}_{,y} + \frac{1}{2}f^bC^c_{44}w^b{}_{,y} + \frac{1}{3}cC^c_{44}w^t{}_{,y} + \frac{1}{2}f^tC^c_{44}w^t{}_{,y} \tag{78e}$$

$$N^c_{xz} = - C^c_{55}u^b_0 + C^c_{55}u^t_0 + \frac{4}{3}cC^c_{55}w^c_{0,x} + \frac{1}{3}cC^c_{55}w^b{}_{,x} + \frac{1}{2}f^bC^c_{55}w^b{}_{,x} + \frac{1}{3}cC^c_{55}w^t{}_{,x} + \frac{1}{2}f^tC^c_{55}w^t{}_{,x} \tag{78f}$$

$$M^c_{xx_1} = \frac{1}{30}c\Big[20C^c_{13}\Big(- 2w^c_0 + w^b + w^t\Big) + c\Big[C^c_{12}\Big(- 6v^b_{0,y} + 6v^t_{0,y} - 8c\phi^c_{0,y} + 3f^b (w^b{}_{,yy} + 3f^tw^t{}_{,yy})\Big) + C^c_{11}\Big(- 6u^b_{0,x} + 6u^t_{0,x} + 8c\psi^c_{0,x} + 3f^b(w^b{}_{,xx} + 3f^tw^t{}_{,xx})\Big)\Big]\Big] \tag{78g}$$

$$M^c_{xx_2} = \frac{1}{30}c^2\Big[- 10C^c_{13}\Big(w^b - w^t\Big) + c\Big[C^c_{12}\Big(6v^b_{0,y} + 8v^c_{0,y} + 6v^t_{0,y} - 3f^bw^b{}_{,yy} + 3f^tw^t{}_{,yy}\Big) + C^c_{11}\Big(6u^b_{0,x} + 8u^c_{0,x} + 6u^t_{0,x} + 3f^bw^b{}_{,xx} + 3f^tw^t{}_{,xx}\Big)\Big]\Big] \tag{78h}$$

$$M^c_{xx_3} = \frac{1}{70}c^3\Big[28C^c_{13}(-2w^c_0 + w^b + w^t) + c\Big[C^c_{12}\Big(- 10v^b_{0,y} + 10v^t_{0,y} - 8c\phi^c_{0,y} + 5(f^bw^b{}_{,yy} + f^tw^t{}_{,yy})\Big) + C^c_{11}\Big(- 10u^b_{0,x} + 10u^t_{0,x} + 8c\psi^c_{0,x} + 5(f^bw^b{}_{,xx} + f^tw^t{}_{,xx})\Big)\Big]\Big] \tag{78i}$$

$$M^c_{yy_1} = \frac{1}{30}c\Big[20C^c_{23}\Big(- 2w^c_0 + w^b + w^t\Big) + c\Big[C^c_{22}\Big(- 6v^b_{0,y} + 6v^t_{0,y} - 8c\phi^c_{0,y} + 3(f^bw^b{}_{,yy} + f^tw^t{}_{,yy})\Big) + C^c_{12}\Big(- 6u^b_{0,x} + 6u^t_{0,x} + 8c\psi^c_{0,x} + 3(f^bw^b{}_{,xx} + f^tw^t{}_{,xx})\Big)\Big]\Big] \tag{78j}$$

$$M^c_{yy_2} = \frac{1}{30}c^2\Big[- 10C^c_{23}\Big(w^b - w^t\Big) + c\Big[C^c_{22}\Big(6v^b_{0,y} + 8v^c_{0,y} + 6v^t_{0,y} - 3f^bw^b{}_{,yy} + 3f^tw^t{}_{,yy}\Big) + C^c_{12}\Big(6u^b_{0,x} + 8u^c_{0,x} + 6u^t_{0,x} - 3f^bw^b{}_{,xx} + 3f^tw^t{}_{,xx}\Big)\Big]\Big] \tag{78k}$$

$$M^c_{yy_3} = \frac{1}{70}c^3\Big[28C^c_{23}\Big(-2w^c_0+w^b+w^t\Big)+c\Big[C^c_{22}\Big(-10v^b_{0,y}+10v^t_{0,y}-8c\phi^c_{0,y} + 5(f^b w^b{}_{,yy}+f^t w^t{}_{,yy})\Big)+C^c_{12}\Big(-10u^b_{0,x}+10u^t_{0,x}+8c\psi^c_{0,x}+5(f^b w^b{}_{,xx}+f^t w^t{}_{,xx})\Big)\Big]\Big] \tag{78l}$$

$$M^c_{zz_1} = \frac{1}{30}c\Big[20C^c_{33}\Big(-2w^c_0+w^b+w^t\Big)+c\Big[C^c_{23}\Big(-6v^b_{0,y}+6v^t_{0,y}-8c\phi^c_{0,y} + 3(f^b w^b{}_{,yy}+f^t w^t{}_{,yy})\Big)+C^c_{13}\Big(-6u^b_{0,x}+6u^t_{0,x}+8c\psi^c_{0,x}+3(f^b w^b{}_{,xx}+f^t w^t{}_{,xx})\Big)\Big]\Big] \tag{78m}$$

$$M^c_{xy_1} = -\frac{1}{5}c^2C^c_{66}u^b_{0,y}+\frac{1}{5}c^2C^c_{66}u^t_{0,y}+\frac{4}{15}c^3C^c_{66}\psi^c_{0,y}-\frac{1}{5}c^2C^c_{66}v^b_{0,x}+\frac{1}{5}c^2C^c_{66}v^t_{0,x} - \frac{4}{15}c^3C^c_{66}\phi^c_{0,x}+\frac{1}{5}c^2f^bC^c_{66}w^b{}_{,xy}+\frac{1}{5}c^2f^tC^c_{66}w^t{}_{,xy} \tag{78n}$$

$$M^c_{xy_2} = \frac{1}{5}c^3C^c_{66}u^b_{0,y}+\frac{4}{15}c^3C^c_{66}u^c_{0,y}+\frac{1}{5}c^3C^c_{66}u^t_{0,y}+\frac{1}{5}c^3C^c_{66}v^b_{0,x}+\frac{4}{15}c^3C^c_{66}v^c_{0,x} + \frac{1}{5}c^3C^c_{66}v^t_{0,x}-\frac{1}{5}c^3f^bC^c_{66}w^b{}_{,xy}+\frac{1}{5}c^3f^tC^c_{66}w^t{}_{,xy} \tag{78o}$$

$$M^c_{xy_3} = -\frac{1}{7}c^4C^c_{66}u^b_{0,y}+\frac{1}{7}c^4C^c_{66}u^t_{0,y}+\frac{4}{35}c^5C^c_{66}\psi^c_{0,y}-\frac{1}{7}c^4C^c_{66}v^b_{0,x}+\frac{1}{7}c^4C^c_{66}v^t_{0,x} - \frac{4}{35}c^5C^c_{66}\phi^c_{0,x}+\frac{1}{7}c^4f^bC^c_{66}w^b{}_{,xy}+\frac{1}{7}c^4f^tC^c_{66}w^t{}_{,xy} \tag{78p}$$

$$M^c_{yz_1} = \frac{1}{3}cC^c_{44}\Big[2v^b_0-4v^c_0+2v^t_0-(c+f^b)w^b_{,y}+(c+f^t)w^t{}_{,y}\Big] \tag{78q}$$

$$M^c_{yz_2} = \frac{1}{30}c^2C^c_{44}\Big[-18v^b_0+18v^t_0+16c\phi^c_0+8cw^c_{0,y}+3(2c+3f^b)w^b{}_{,y}+3(2c+3f^t)w^t{}_{,y}\Big] \tag{78r}$$

$$M^c_{xz_1} = \frac{1}{3}cC^c_{55}\Big[2u^b_0-4u^c_0+2u^t_0-(c+f^b)w^b{}_{,x}+(c+f^t)w^t{}_{,x}\Big] \tag{78s}$$

$$M^c_{xz_2} = \frac{1}{30}c^2C^c_{55}\Big[-18u^b_0+18u^t_0-16c\psi^c_0+8cw^c_{0,x}+3(2c+3f^b)w^b{}_{,x}+3(2c+3f^t)w^t{}_{,x}\Big] \tag{78t}$$

Appendix B

STATIC MODEL - GOVERNING EQUATIONS AND BOUNDARY CONDITIONS

$$\delta u_0^b : \frac{1}{2c^3}[2cM^c_{xz_1} + 3M^c_{xz_2} - cM^c_{xy_{2,y}} - M^c_{xy_{3,y}} - 2c^3N^b_{xy,y} - cM^c_{xx_{2,x}} - M^c_{xx_{3,x}} - 2c^3N^b_{xx,x}] - b_x = 0 \tag{79a}$$

$$\delta u_0^c : \frac{1}{c^2}[-2M^c_{xz_1} + M^c_{xy_{2,y}} - c^2N^c_{xy,y} + M^c_{xx_{2,x}} - c^2N^c_{xx,x}] - b_x = 0 \tag{79b}$$

$$\delta u_0^t : \frac{1}{2c^3}[2cM^c_{xz_1} - 3M^c_{xz_2} - cM^c_{xy_{2,y}} + M^c_{xy_{3,y}} - 2c^3N^t_{xy,y} - cM^c_{xx_{2,x}} + M^c_{xx_{3,x}} - 2c^3N^t_{xx,x}] - b_x = 0 \tag{79c}$$

$$\delta v_0^b : \frac{1}{2c^3}[2cM^c_{yz_1} + 3M^c_{yz_2} - cM^c_{yy_{2,y}} - M^c_{yy_{3,y}} - 2c^3N^b_{yy,y} - cM^c_{xy_{2,x}} - M^c_{xy_{3,x}} - 2c^3N^b_{xy,x}] - b_y = 0 \tag{79d}$$

$$\delta v_0^c : \frac{1}{c^2}[-2M^c_{yz_1} + M^c_{yy_{2,y}} - c^2N^c_{yy,y} + M^c_{xy_{2,x}} - c^2N^c_{xy,x}] - b_y = 0 \tag{79e}$$

$$\delta v_0^t : \frac{1}{2c^3}[2cM^c_{yz_1} - 3M^c_{yz_2} - cM^c_{yy_{2,y}} + M^c_{yy_{3,y}} - 2c^3N^t_{yy,y} - cM^c_{xy_{2,x}} + M^c_{xy_{3,x}} - 2c^3N^t_{xy,x}] - b_y = 0 \tag{79f}$$

$$\delta w^b : \frac{1}{4c^3}[4cM^c_{zz_1} + 2c^2N^c_{zz} - (2c(c+f)M^c_{yz_{1,y}} + (2c+3f)M^c_{yz_{2,y}}) + cfM^c_{yy_{2,yy}} + fM^c_{yy_{3,yy}} - 4c^3M^b_{yy,yy}(2c(c+f)M^c_{xz_{1,x}} + (2c+3f)M^c_{xz_{2,x}}) + 2cfM^c_{xy_{2,xy}}$$

$$+ 2fM^c_{xy_{3,xy}} - 8c^3 M^b_{xy,xy} - 4c^3 M^b_{xx,xx} + f(cM^c_{xx_{2,xx}} + 3M^c_{xx_{3,xx}})]$$

$$= q^b(x,y) + b_z \tag{79g}$$

$$\delta w^c_0 : \frac{1}{c^2}[-2M^c_{zz_1} + M^c_{yz_{2,y}} - c^2 N^c_{yz,y} + M^c_{xz_{2,x}} - c^2 N^c_{xz,x}] - b_z = 0 \tag{79h}$$

$$\delta w^t : \frac{1}{4c^3}\Big[2c(2M^c_{zz_1} - cN^c_{zz}) - (-2c(c+f)M^c_{yz_{1,y}} + (2c+3f)M^c_{yz_{2,y}})$$

$$- (cfM^c_{yy_{2,yy}} - fM^c_{yy_{3,yy}} + 4c^3 M^t_{yy,yy}) - (-2c(c+f)M^c_{xz_{1,x}} + (2c+3f)M^c_{xz_{2,x}})$$

$$- 2(cfM^c_{xy_{2,xy}} - fM^c_{xy_{3,xy}} + 4c^3 M^t_{xy,xy}) - (4c^3 M^t_{xx,xx} + cfM^c_{xx_{2,xx}} - fM^c_{xx_{3,xx}})\Big]$$

$$= q^t(x,y) + b_z \tag{79i}$$

The associated boundary conditions at $x = 0,\ a$ read as follows

$$u^b_0 = \tilde{u}^t \quad \text{or} \quad \tilde{N}^b_{xx} = \frac{cM^c_{xx_2} + M^c_{xx_3}}{2c^3} + N^b_{xx} \tag{80a}$$

$$u^c_0 = \tilde{u}^c \quad \text{or} \quad \tilde{N}^c_{xx} = N^c_{xx} - \frac{M^c_{xx_2}}{c^2} \tag{80b}$$

$$u^t_0 = \tilde{u}^t \quad \text{or} \quad \tilde{N}^t_{xx} = \frac{cM^c_{xx_2} - M^c_{xx_3}}{2c^3} + N^t_{xx} \tag{80c}$$

$$v^b_0 = \tilde{v}^b \quad \text{or} \quad \tilde{N}^b_{yy} = \frac{cM^c_{xy_2} + M^c_{xy_3}}{2c^3} + N^b_{xy} \tag{80d}$$

$$v^c_0 = \tilde{v}^c \quad \text{or} \quad \tilde{N}^c_{yy} = N^c_{xy} - \frac{M^c_{xy_2}}{c^2} \tag{80e}$$

$$v^t_0 = \tilde{v}^t \quad \text{or} \quad \tilde{N}^t_{yy} = \frac{cM^c_{xy_2} - M^c_{xy_3}}{2c^3} + N^t_{xy} \tag{80f}$$

$$w^b = \tilde{w}^b \quad \text{or} \quad \tilde{P}^b = \frac{1}{4c^3}\Big[4c^3 M^b_{xx,_x} + 4c^3 M^b_{xy,_y} + 4c^3 N^b_{xx} w^b{}_{,x} + 4c^3 N^b_{xy} w^b{}_{,y}$$

$$- cfM^c_{xx_{2,x}} - cfM^c_{xy_{2,y}} + 2c(c+f)M^c_{xz_1} + (2c+3f)M^c_{xz_2}$$

$$- fM^c_{xx_{3,x}} - fM^c_{xy_{3,y}}\Big] \tag{80g}$$

$$w^b{}_{,x} = \tilde{w}^b_{,x} \quad \text{or} \quad \tilde{M}^b = \frac{f(cM^c_{xx_2} + M^c_{xx_3}) - 4c^3 M^b_{xx}}{4c^3} \tag{80h}$$

$$w^c_0 = \tilde{w}^c \quad \text{or} \quad \tilde{P}^c = N^c_{xz} - \frac{M^c_{xz_2}}{c^2} \tag{80i}$$

$$\psi^c_0 = \tilde{\psi^c_0}^c \quad \text{or} \quad \tilde{M}^c = M^c_{xx_1} - \frac{M^c_{xx_3}}{c^2} \tag{80j}$$

$$w^t = \tilde{w}^t \quad \text{or} \quad \begin{aligned} \tilde{P}^t = & \frac{1}{4c^3}\Big[4c^3 M^t_{xx_{,x}} + 4c^3 M^t_{xy_{,y}} + 4c^3 N^t_{xx} w^t{}_{,x} + 4c^3 N^t_{xy} w^t{}_{,y} \\ & + cf M^c_{xx_{2,x}} + cf M^c_{xy_{2,y}} - 2c(c+f) M^c_{xz_1} + (2c+3f) M^c_{xz_2} \\ & - f M^c_{xx_{3,x}} - f M^c_{xy_{3,y}}\Big] \end{aligned} \tag{80k}$$

$$w^t{}_{,x} = \tilde{w}^t_{,x} \quad \text{or} \quad \tilde{M}^t = -\frac{4c^3 M^t_{xx} + cf M^c_{xx_2} - f M^c_{xx_3}}{4c^3} \tag{80l}$$

(80m)

where the tilde accent denotes the known external boundary values. Similar equations can be written for $y = 0,\ b$

Appendix C

DYNAMIC MODEL-STRESS RESULTANTS

$$\left\{\begin{array}{c}\left\{N\right\}\\ \left\{M\right\}\end{array}\right\} = \left[\begin{array}{cc}\left[A\right] & \left[B\right]\\ \left[B\right] & \left[D\right]\end{array}\right]\left\{\begin{array}{c}\left\{\epsilon^0\right\}\\ \left\{\epsilon^1\right\}\end{array}\right\} \tag{81}$$

where

$$(A_{ij}, B_{ij}, D_{ij}) = \sum_{k=1}^{N^{b,t}} \int_{z_k}^{z_{k+1}} Q_{ij}^{(k)}(1, \zeta, \zeta^2) dz \tag{82}$$

and

$$\zeta = \zeta^{b,t} = z \pm (c + \frac{f^{b,t}}{2}) \tag{83}$$

Also

$$\left\{\epsilon^0\right\} = \left\{\begin{array}{c}\epsilon_{xx}^0\\ \epsilon_{yy}^0\\ \gamma_{xy}^0\end{array}\right\} = \left\{\begin{array}{c}\frac{\partial u_0}{\partial x}\\ \frac{\partial v_0}{\partial y}\\ \frac{\partial u_0}{\partial y} + \frac{\partial v_0}{\partial x}\end{array}\right\} \tag{84}$$

and

$$\left\{\epsilon^1\right\} = \left\{\begin{array}{c}\epsilon_{xx}^1\\ \epsilon_{yy}^1\\ \gamma_{xy}^1\end{array}\right\} = \left\{\begin{array}{c}-\frac{\partial^2 w}{\partial x^2}\\ -\frac{\partial^2 w}{\partial y^2}\\ -\frac{\partial^2 w}{\partial x \partial y}\end{array}\right\} \tag{85}$$

For the core the following resultants are defined

$$\left\{N^c\right\} = \begin{Bmatrix} N^c_{xx} \\ N^c_{yy} \\ N^c_{zz} \\ N^c_{xy} \end{Bmatrix} = \int_{-c}^{c} \begin{Bmatrix} \sigma^c_{xx} \\ \sigma^c_{yy} \\ \sigma^c_{zz} \\ \sigma^c_{xy} \end{Bmatrix} dz \tag{86}$$

$$\begin{Bmatrix} Q^c_x \\ Q^c_y \end{Bmatrix} = \int_{-c}^{c} \begin{Bmatrix} \sigma^c_{xz} \\ \sigma^c_{yz} \end{Bmatrix} dz \tag{87}$$

Similarly, the following resultants are also defined for the core

$$\begin{Bmatrix} M^c_{xx} \\ M^c_{yy} \\ M^c_{zz} \\ M^c_{xy} \\ M^c_{xz} \\ M^c_{yz} \end{Bmatrix} = \int_{-c}^{c} \begin{Bmatrix} \sigma^c_{xx} \\ \sigma^c_{yy} \\ \sigma^c_{zz} \\ \sigma^c_{xy} \\ \sigma^c_{xz} \\ \sigma^c_{yz} \end{Bmatrix} z dz, \quad \begin{Bmatrix} R^c_{xx} \\ R^c_{yy} \\ R^c_{xy} \\ R^c_{xz} \\ R^c_{yz} \end{Bmatrix} = \int_{-c}^{c} \begin{Bmatrix} \sigma^c_{xx} \\ \sigma^c_{yy} \\ \sigma^c_{xy} \\ \sigma^c_{xz} \\ \sigma^c_{yz} \end{Bmatrix} z^2 dz, \quad \begin{Bmatrix} P^c_{xx} \\ P^c_{yy} \\ P^c_{xy} \end{Bmatrix} = \int_{-c}^{c} \begin{Bmatrix} \sigma^c_{xx} \\ \sigma^c_{yy} \\ \sigma^c_{xy} \end{Bmatrix} z^3 dz \tag{88}$$

$$I_i = \int_{-\frac{h}{2}}^{\frac{h}{2}} \rho(z)^i dz \quad (i = 0, 1, 2, 3..., 6) \tag{89}$$

where h represents the thickness of the bottom facesheet f^b, core $2c$ and the top facesheet f^t respectively.

Appendix D

DYNAMIC MODEL-GOVERNING DIFFERENTIAL EQUATIONS AND BOUNDARY CONDITIONS

$$\delta u_0^b: \quad 4\alpha_2 M_{xz}^c - 6\alpha_3 R_{xz}^c - N_{xy,y}^b + 2\alpha_3 P_{xy,y}^c - 2\alpha_2 R_{xy,y}^c - N_{xx,x}^b + 2\alpha_3 P_{xx,x}^c$$
$$- 2\alpha_2 R_{xx,x}^c + \beta_1 \ddot{u}_0^b - 2\beta_2 \ddot{u}_0^c + 4\beta_3 \ddot{u}_0^t + 2\beta_5 \ddot{\psi}_0^c - \beta_4 \ddot{w}_{,x}^b + 2f^t \beta_3 \ddot{w}_{,x}^t = 0 \quad (90a)$$

$$\delta v_0^b: \quad 4\alpha_2 M_{yz}^c - 6\alpha_3 R_{yz}^c - N_{yy,y}^b + 2\alpha_3 P_{yy,y}^c - 2\alpha_2 R_{yy,y}^c - N_{xy,x}^b + 2\alpha_3 P_{xy,x}^c$$
$$- 2\alpha_2 R_{xy,x}^c + \beta_1 \ddot{v}_0^b + 2\beta_2 \ddot{v}_0^c + 4\beta_3 \ddot{v}_0^t - 2\beta_5 \ddot{\phi}_0^c - \beta_4 \ddot{w}_{,y}^b + 2f^t \beta_3 \ddot{w}_{,y}^t = 0 \quad (90b)$$

$$\delta w^b: \quad 4\alpha_2 M_{zz}^c - \alpha_1 N_{zz}^c + (\alpha_1 + 2f^b\alpha_2)(M_{xz,x}^c + M_{yz,y}^c) - 2M_{xy,xy}^b - M_{xx,xx}^b$$
$$+ f^b\alpha_3(P_{xx,xx}^c + P_{yy,yy}^c + 2P_{xy,xy}^c) - f^b\alpha_2(R_{xx,xx}^c + R_{yy,yy}^c + 2R_{xy,xy}^c)$$
$$- R_{xz,x}^c(2\alpha_2 + 3f^b\alpha_3) + \beta_6 \ddot{w}^b - \beta_7 \ddot{w}_0^c - \beta_8 \ddot{w}^t + \beta_4(\ddot{u}_{0,x}^b + \ddot{v}_{0,y}^b)$$
$$+ f^b\beta_2(\ddot{u}_{0,x}^c + \ddot{v}_{0,y}^c) + 2f^b\beta_3(\ddot{u}_{0,x}^t + \ddot{v}_{0,y}^t) + f^b\beta_5(\ddot{\psi}_{0,x}^c - \ddot{\phi}_{0,y}^c)$$
$$+ f^b f^t \beta_3(\ddot{w}_{,xx}^t + \ddot{w}_{,yy}^t) - \beta_9(\ddot{w}_{,xx}^b + \ddot{w}_{,yy}^b) = q^b[x, y, t] \quad (90c)$$

$$\delta u_0^t: \quad 4\alpha_2 M_{xz}^c + 6\alpha_3 R_{xz}^c - N_{xy,y}^t - 2\alpha_3 P_{xy,y}^c - 2\alpha_2 R_{xy,y}^c - N_{xx,x}^t - 2\alpha_3 P_{xx,x}^c$$
$$- 2\alpha_2 R_{xx,x}^c + 4\beta_3 \ddot{u}_0^b + 2\xi_2 \ddot{u}_0^c + \xi_1 \ddot{u}_0^t + 2\xi_5 \ddot{\psi}_0^c - 2f^b\beta_3 \ddot{w}_{,x}^b + \xi_4 \ddot{w}_{,x}^t = 0 \quad (90d)$$

$$\delta v_0^t: \quad 4\alpha_2 M_{yz}^c + 6\alpha_3 R_{yz}^c - N_{yy,y}^t - 2\alpha_3 P_{yy,y}^c - 2\alpha_2 R_{yy,y}^c - N_{xy,x}^t - 2\alpha_3 P_{xy,x}^c$$
$$- 2\alpha_2 R_{xy,x}^c + 4\beta_3 \ddot{v}_0^b + 2\xi_2 \ddot{v}_0^c + \xi_1 \ddot{v}_0^t - 2\xi_5 \ddot{\phi}_0^c - 2f^b\beta_3 \ddot{w}_{,x}^b + \xi_4 \ddot{w}_{,x}^t = 0 \quad (90e)$$

$$\delta w^t: \quad 4\alpha_2 M_{zz}^c + \alpha_1 N_{zz}^c - (\alpha_1 + 2f^t\alpha_2)(M_{yz,y}^c - M_{xz,x}^c) - 2M_{xy,xy}^t - M_{xx,xx}^t$$
$$+ f^t\alpha_3(P_{yy,yy}^c + P_{xx,xx}^c + 2P_{xy,xy}^c) + f^t\alpha_2(R_{yy,yy}^c + 2R_{xy,xy}^c + R_{xx,xx}^c)$$

$$- R^c_{xz,x}(2\alpha_2 + 3\alpha_3 f^t) - \beta_8 \ddot{w}^b + \xi_7 \ddot{w}^c_0 + \xi_6 \ddot{w}^t + f^b f^t \beta_3 (\ddot{w}^b_{,yy} + \ddot{w}^b_{,xx})$$
$$- 2f^t \beta_3 (\ddot{u}^b_{0,x} + \ddot{v}^b_{0,x}) - f^t \xi_2 (\ddot{u}^c_{0,x} + \ddot{v}^c_{0,y}) - \xi_4 (\ddot{u}^t_{0,x} + \ddot{v}^t_{0,y})$$
$$- f^t \xi_5 (\ddot{\phi}^c_{0,y} + \ddot{\psi}^c_{0,x}) - \xi_9 (\ddot{w}^t_{,yy} + \ddot{w}^b_{,xx}) = q^t[x, y, t] \tag{90f}$$

$$\delta u^c_0 : \quad 8\alpha_2 M^c_{xz} + N^c_{xy,y} - 4\alpha_2 R^c_{xy,y} + N^c_{xx,x} - 4\alpha_2 R^c_{xx,x} - 2\beta_2 \ddot{u}^b_0 - \Delta_1 \ddot{u}^c_0 - 2\beta_2 \ddot{u}^t_0$$
$$- \Delta_2 \ddot{\psi}^c_0 + \beta_2 f^b \ddot{w}^b_{,x} - \beta_2 f^t \ddot{w}^t_{,x} = 0 \tag{90g}$$

$$\delta v^c_0 : \quad 8\alpha_2 M^c_{yz} + N^c_{yy,y} - 4\alpha_2 R^c_{yy,y} + N^c_{xy,x} - 4\alpha_2 R^c_{xy,x} - 2\beta_2 \ddot{v}^b_0 - \Delta_1 \ddot{v}^c_0 - 2\beta_2 \ddot{v}^t_0$$
$$+ \Delta_2 \ddot{\phi}^c_0 + \beta_3 f^b \ddot{w}^b_{,y} - \beta_3 f^t \ddot{w}^t_{,y} = 0 \tag{90h}$$

$$\delta w^c_0 : \quad 8\alpha_2 M^c_{zz} + Q^c_{y,y} - 4\alpha_2 R^c_{yz,y} + Q^c_{x,x} - 4\alpha_2 R^c_{xz,x} + \beta_7 \ddot{w}^b - \Delta_1 \ddot{w}^c_0 - \xi_7 \ddot{w}^t = 0 \tag{90i}$$

$$\delta \phi^c_0 : \quad - Q^c_y + 12 R^c_{yz} - M^c_{xy,x} + M^c_{yy,y} - 4\alpha_2 P^c_{yy,y} - 4\alpha_2 P^c_{xy,x} - 2\beta_5 \ddot{v}^b_0 - \Delta_2 \ddot{v}^c_0$$
$$+ 2\xi_5 \ddot{v}^t_0 + \Delta_4 \ddot{\phi}^c_0 + f^b \beta_5 \ddot{w}^b_{,y} + f^t \xi_5 \ddot{w}^t_{,y} = 0 \tag{90j}$$

$$\delta \psi^c_0 : \quad Q^c_x - 12 R^c_{xz} - M^c_{xy,y} - M^c_{xx,x} + 4\alpha_2 P^c_{xx,x} + 4\alpha_2 P^c_{xy,y} + 2\beta_5 \ddot{u}^b_0 + \Delta_2 \ddot{u}^c_0$$
$$+ 2\xi_5 \ddot{u}^t_0 + \Delta_4 \ddot{\psi}^c_0 - f^b \beta_5 \ddot{w}^b_{,x} + f^t \xi_5 \ddot{w}^t_{,x} = 0 \tag{90k}$$

Where

$$\alpha_1 = \frac{1}{2c} \qquad \alpha_2 = \frac{1}{4c^2} \qquad \alpha_3 = \frac{1}{4c^3}$$

$$\beta_1 = \frac{4c^6 I^b_0 + c^2 I^c_4 - 2c I^c_5 + I^c_6}{4c^6} \quad \beta_2 = \frac{c^4 I^c_2 - c^3 I^c_3 - c^2 I^c_4 + c I^c_5}{4c^6}$$
$$\beta_3 = \frac{c^2 I^c_4 - I^c_6}{16c^6} \qquad \beta_4 = \frac{8c^7 I^b_0 + 4c^6 f^b I^b_0 + 8c^6 I^b_1 + c^2 f^b I^c_4 - 2c f^b I^c_5 + f^b I^c_6}{8c^6}$$
$$\beta_5 = \frac{c^3 I^c_3 - c^2 I^c_4 - c I^c_5 + I^c_6}{4c^5} \qquad \beta_6 = \frac{4c^4 I^b_0 + c^2 I^c_2 - 2c I^c_3 + I^c_4}{4c^4}$$

$$\beta_7 = \frac{c^3 I_1^c - c^2 I_2^c - c I_3^c + I_4^c}{2c^4} \qquad \beta_8 = \frac{c^2 I_2^c - I_4^c}{4c^4}$$

$$\beta_9 = \frac{16c^8 I_0^b + 16c^7 f^b I_0^b + 4c^6 f^{b^2} I_0^b + 32c^7 I_1^b + 16c^6 f^b I_1^b + 16c^6 I_2^b + c^2 f^{b^2} I_4^c - 2c f^{b^2} I_5^c + f^{b^2} I_6^c}{16c^6}$$

$$\Delta_1 = \frac{c^4 I_0^c - 2c^2 I_2^c + I_4^c}{c^4}$$
$$\Delta_2 = \frac{c^4 I_1^c - 2c^2 I_3^c + I_5^c}{c^4}$$
$$\Delta_4 = \frac{c^4 I_2^c - 2c^2 I_4^c + I_6^c}{c^4}$$

$$\xi_1 = \frac{4c^6 I_0^t = c^2 I_4^c + 2c I_5^c + I_6^c}{4c^6}$$
$$\xi_2 = \frac{c^4 I_2^c + c^3 I_3^c - c^2 I_4^c - c I_5^c}{4c^6}$$
$$\xi_4 = \frac{8c^7 I_0^t + 4c^6 f^t I_0^t - 8c^6 I_1^t + c^2 f^t I_4^c + 2c f^t I_5^c + f^t I_6^c}{8c^6}$$
$$\xi_5 = \frac{c^4 I_3^c + c^3 I_4^c - c^2 I_5^c - c I_6^c}{4c^6}$$
$$\xi_6 = \frac{4c^4 I_0^t + c^2 I_2^c + 2c I_3^c + I_4^c}{4c^6}$$
$$\xi_7 = \frac{c^3 I_1^c + c^2 I_2^c - c I_3^c - I_4^c}{2c^4}$$
$$\xi_9 = \frac{16c^8 I_0^t + 16c^7 f^t I_0^t + 4c^6 f^{t^2} I_0^t - 32c^7 I_1^t - 16c^6 I_1^t + 16c^6 I_2^b + c^2 f^{t^2} I_4^c + 2c f^{t^2} I_5^c + f^{t^2} I_6^c}{16c^6}$$

The associated boundary conditions at $x = a$ read as follows

$$u_0^b = \tilde{u}^t \qquad \text{or} \qquad \tilde{N}_{xx}^b = \frac{c M_{xx_2}^c + M_{xx_3}^c}{2c^3} + N_{xx}^b$$

$$u_0^b = \tilde{u}^t \qquad \text{or} \qquad \tilde{N}_{xx}^b = N_{xx}^b - 2\alpha_3 P_{xx}^c + 2\alpha_2 R_{xx}^c$$

$$u_0^c = \tilde{u}^c \qquad \text{or} \qquad \tilde{N}_{xx}^c = N_{xx}^c - 4\alpha_2 R_{xx}^c$$

$$u_0^t = \tilde{u}^t \qquad \text{or} \qquad \tilde{N}_{xx}^t = N_{xx}^t + 2\alpha_3 P_{xx}^c + 2\alpha_2 R_{xx}^c$$

$$v_0^b = \tilde{v}^b \quad \text{or} \quad \tilde{N}_{yy}^b = N_{xy}^b - 2\alpha_3 P_{xy}^c + 2\alpha_2 R_{xy}^c$$

$$v_0^c = \tilde{v}^c \quad \text{or} \quad \tilde{N}_{yy}^c = N_{xy}^c - 4\alpha_2 R_{xy}^c$$

$$v_0^t = \tilde{v}^t \quad \text{or} \quad \tilde{N}_{yy}^t = N_{xy}^t + 2\alpha_3 P_{xy}^c + 2\alpha_2 R_{xy}^c$$

$$w^b = \tilde{w}^b \quad \text{or}$$

$$\begin{aligned}\tilde{Q_x}^b =& -\alpha_1 M_{xz}^c - 2\alpha_2 f^b M_{xz}^c + 2\alpha_2 R_{xz}^c + 3\alpha_3 f^b R_{xz}^c - \beta_4 \ddot{u}_0^b \\ & - f^b \beta_2 \ddot{u}_0^c - 2\beta_3 f^b \ddot{u}_0^t - \beta_5 \ddot{\psi}_0^c + M_{xy,y}^b - f^b \alpha_3 P_{xy,y}^c \\ & + \alpha_2 f^b R_{xy,y}^c + M_{xx,x}^b - \alpha_3 f^b P_{xx,x}^c + \alpha_2 f^b R_{xx,x}^c \\ & + \beta_9 \ddot{w}_{,x}^b + f^b f^t \beta_3 \ddot{w}_{,x}^t\end{aligned}$$

$$w^b{}_{,x} = \tilde{w}^b{}_{,x} \quad \text{or} \quad \tilde{M_{xx}}^b = -M_{xx}^b + \alpha_3 f^b P_{xx}^c - \alpha_2 f^b R_{xx}^c$$

$$w^b{}_{,y} = \tilde{w}^b{}_{,y} \quad \text{or} \quad \tilde{M_{xy}}^b = -M_{xy}^b + \alpha_3 f^b P_{xy}^c - \alpha_2 f^b R_{xy}^c$$

$$w_0^c = \tilde{w}^c \quad \text{or} \quad \tilde{Q_x}^c = Q_x^c - 4\alpha_2 R_{xz}^c$$

$$\psi_0^c = \tilde{\psi_0^c}^c \quad \text{or} \quad \tilde{M_{xx}}^c = M_{xx}^c - 4\alpha_2 P_{xx}^c$$

$$\phi_0^c = \tilde{\phi_0^c}^c \quad \text{or} \quad \tilde{M_{xy}}^c = -M_{xy}^c + 4\alpha_2 P_{xy}^c$$

$$w^t = \tilde{w}^t \quad \text{or}$$

$$\begin{aligned}\tilde{Q_x}^t =& \alpha_1 M_{xz}^c + 2\alpha_2 f^t M_{xz}^c + 2\alpha_2 R_{xz}^c + 3\alpha_3 f^t R_{xz}^c + 2 f^t \beta_3 \ddot{u}_0^b \\ & + f^t \xi_2 \ddot{u}_0^c + \xi_4 \ddot{u}_0^t + \xi_5 \ddot{\psi}_0^c + M_{xy,y}^t - f^t \alpha_3 P_{xy,y}^c \\ & - f^t \alpha_2 R_{xy,y}^c + M_{xx,x}^t - f^t \alpha_3 P_{xx,x}^c - f^t \alpha_2 R_{xx,x}^c \\ & - f^b f^t \beta_3 \ddot{w}_{,x}^b + \xi_9 \ddot{w}_{,x}^t\end{aligned}$$

$$w^t{}_{,x} = \tilde{w}^t{}_{,x} \quad \text{or} \quad \tilde{M_{xx}}^t = -M_{xx}^t + \alpha_3 f^t P_{xx}^c + \alpha_2 f^t R_{xx}^c$$

$$w^t{}_{,y} = \tilde{w}^t{}_{,y} \quad \text{or} \quad \tilde{M_{xy}}^t = -M_{xy}^t + \alpha_3 f^t P_{xy}^c + \alpha_2 f^t R_{xy}^c$$

where the tilde accent denotes the known external boundary values. Similar equations can be written for $y = 0, b$

Appendix E

NONLINEAR STATIC ANALYSIS RECTANGULAR PLATE

A nonlinear static analysis of a rectangular plate with $x = a$ and $y = \frac{a}{2}$ is presented for the following set of boundary conditions.

1. Simply Supported with moveable edges (Stress Free).
2. Simply Supported with fixed edges.
3. Clamped with moveable edges (stress free).
4. clamped with fixed edges.

For movable (stress-free) boundary condition in-plane displacements along the normal direction to the boundary are allowed whereas the out-of-plane displacement is restricted. Similarly, for immovable boundary conditions, the plate is prevented from both in-plane and out-of-plane displacements along the edges.

The analysis technique employed is the same as explained above in Section 3.3 for a square plate. Following geometric properties were used.

- The top facesheet has a thickness of $f^t = 2mm$.
- The bottom facesheet has a thickness of $f^b = 2mm$.

- The core thickness is $2c = 16\ mm$.
- The total thickness of the plate is defined to be $h_{tot} = 2f + 2c$.
- The width of the plate is $a = 20h_{tot}$.
- The depth of the plate is $b = \frac{a}{2}$.

The material properties are the same as highlighted in Section 3.3.

E.1 Simply Supported with Moveable Edges

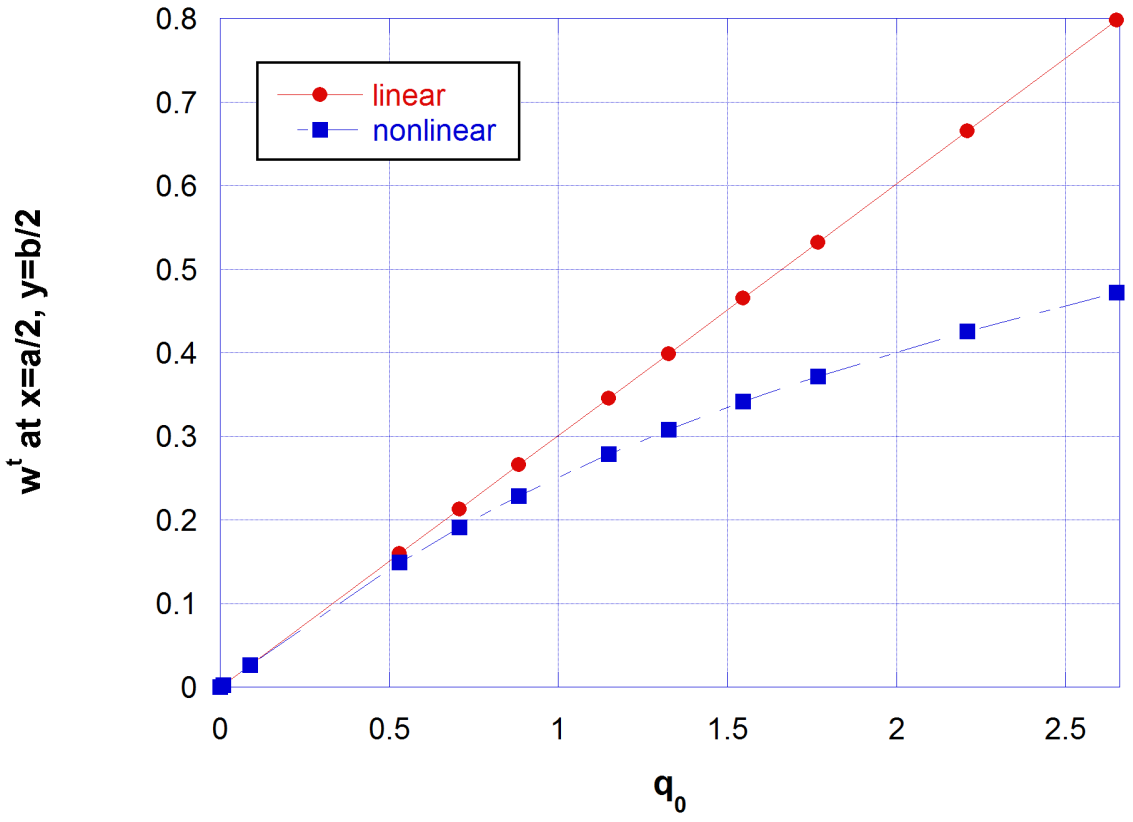

Figure 50: w^t for simply supported rectangular plate with moveable edges-linear vs nonlinear Solution

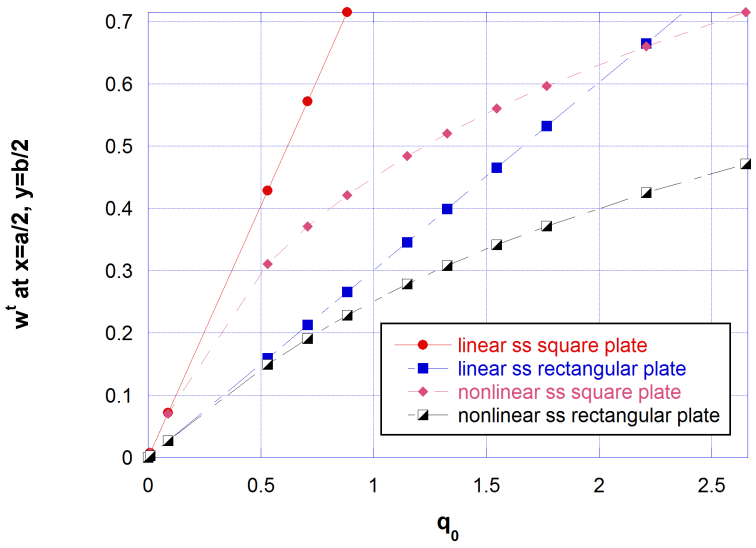

Figure 51: w^t for simply supported rectangular plate with moveable edges-linear square plate vs linear rectangular plate vs nonlinear square plate vs nonlinear rectangular Plate

E.2 Simply Supported with Fixed Edges

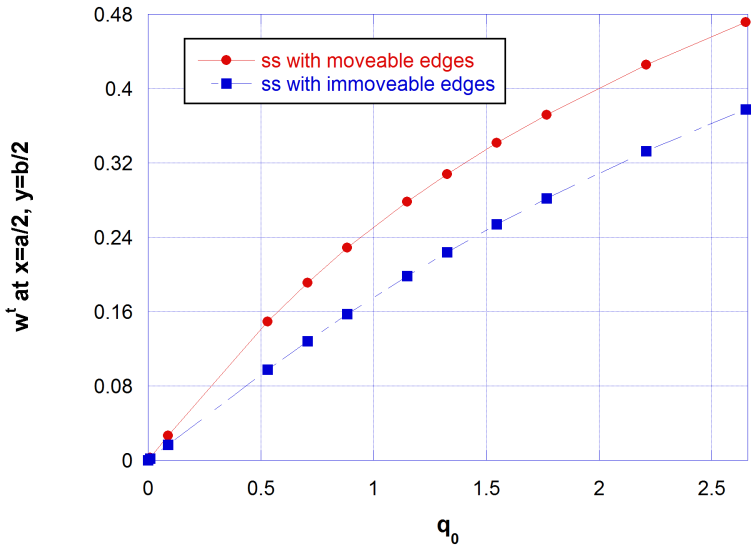

Figure 52: w^t for simply supported rectangular plate with fixed edges-simply supported with free edges vs simply supported with fixed edges

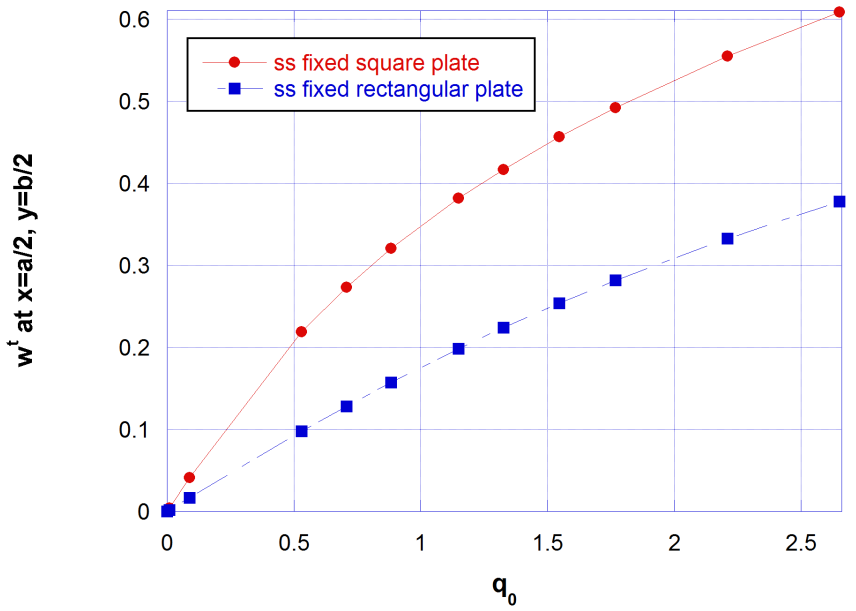

Figure 53: w^t for simply supported rectangular plate with fixed edges-square plate vs rectangular Plate

E.3 Clamped with Moveable Edges

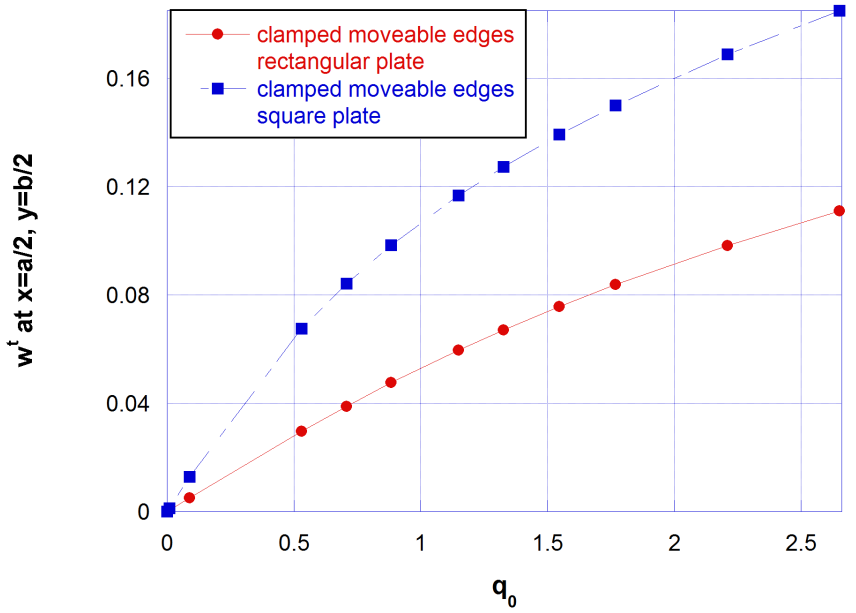

Figure 54: w^t for a clamped rectangular plate with moveable edges-square vs rectangular Plate

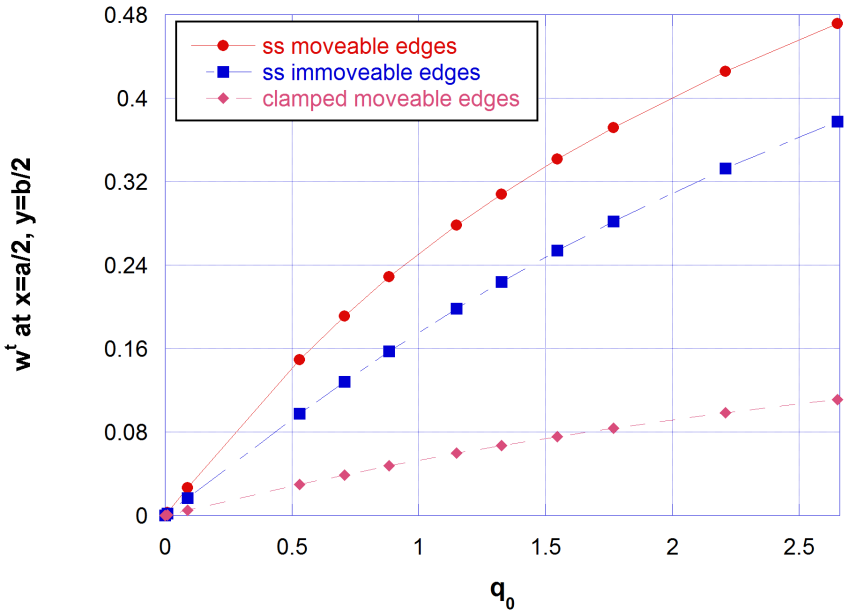

Figure 55: w^t for a clamped rectangular plate with moveable edges-simply supported with moveable edges vs simply supported with fixed Edges vs clamped with moveable edges

E.4 Clamped with Fixed Edges

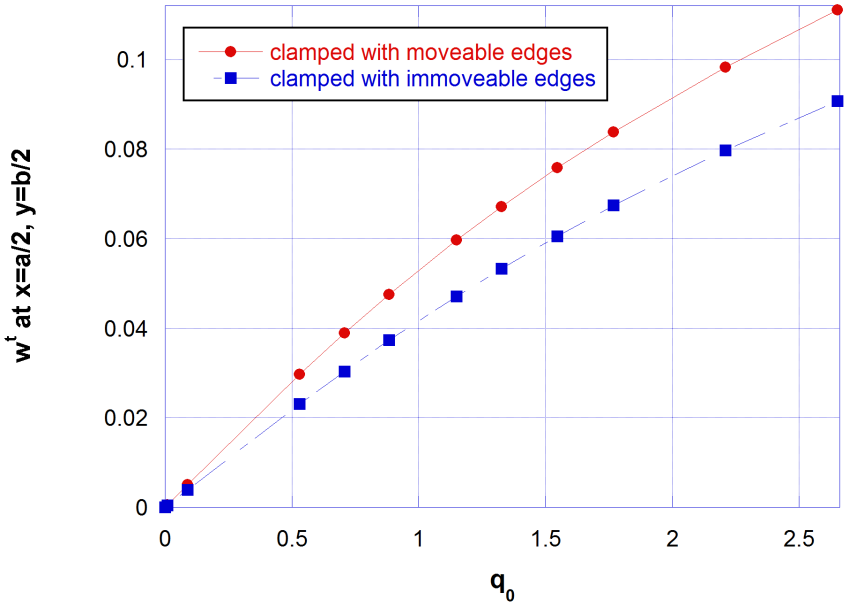

Figure 56: w^t for a clamped rectangular plate with fixed edges-clamped with moveable edges vs clamped with fixed edges

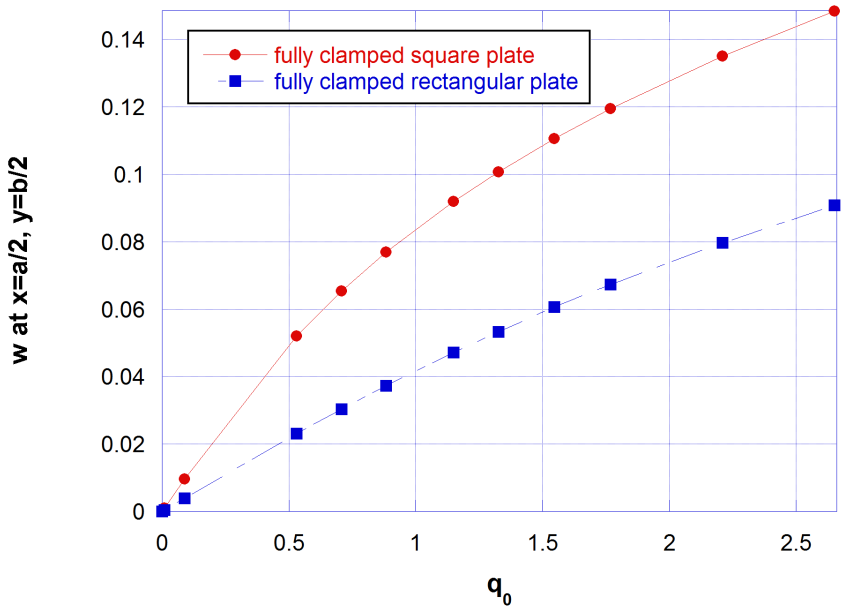

Figure 57: w^t for a clamped rectangular plate with fixed edges-square vs rectangular plate

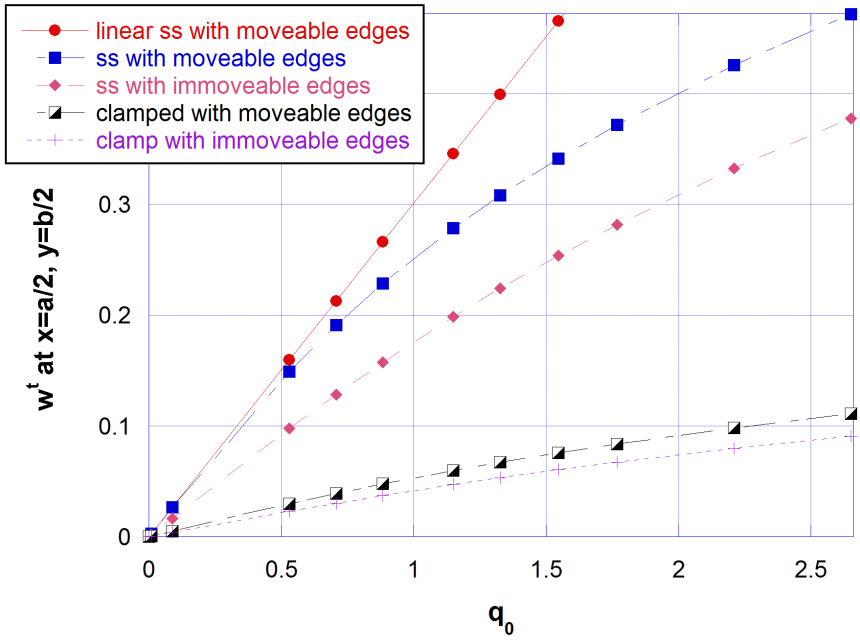

Figure 58: w^t for a clamped rectangular plate with fixed edges-linear simply supported with moveable edges vs nonlinear simply supported with moveable edges vs simply supported with fixed edges vs clamped with moveable Edges vs clamped with fixed edges

REFERENCES

[1] Luciano Demasi and Wenbin Yu. Assess the accuracy of the variational asymptotic plate and shell analysis using the generalized unified formulation. *Mechanics of Advanced Materials and Structures*, 20(3):227–241, 2013.

[2] Catherine N. Phan, Y. Frostig, and George A. Kardomateas. Analysis of sandwich beams with a compliant core and with in-plane rigidity-extended high-order sandwich panel theory versus elasticity. *Journal of Applied Mechanics*, 79(4):041001, 2012.

[3] Y. Frostig, M. Baruch, O. Vilnay, and I. Sheinman. Highorder theory for sandwichbeam behavior with transversely flexible core. *Journal of Engineering Mechanics*, 118:1026, 1992.

[4] N.J. Pagano. Exact solutions for rectangular bidirectional composites and sandwich plates. *Journal of Composite Materials*, 4:20–34, January 1970.

[5] G.A. Kardomateas. Three dimensional elasticity solution for sandwich plates with orthotropic phases: The positive discriminant case. *Journal of Applied Mechanics*, 76:014505, January 2009.

[6] F.J. Plantema. *Sandwich Construction*. Wiley, New York, 1966.

[7] H.J. Allen. *Analysis and Design of Structural Sandwich Panels*. Pergamon, Oxford, 1969.

[8] J. Vinson. *The behavior of sandwich structures of isotropic and composite materials*. CRC, 1999.

[9] A.K. Noor. Free vibrations of multilayered composite plates. *AIAA J*, 11:1038–9, 1973.

[10] G. Kirchoff. Über das gleichgewicht und die bewegung einer elastishen scheibe. *Journ f d reine und angewandte Math*, 40:51–88, 1850.

[11] E. Reissner. The effect of transverse shear deformation on teh bending of elastic plates. *Journal of Applied Mechanics*, 12:69–76, 1945.

[12] Zhen Wu, YK Cheung, SH Lo, and Wanji Chen. Effects of higher-order global–local shear deformations on bending, vibration and buckling of multilayered plates. *Composite Structures*, 82(2):277–289, 2008.

[13] T Kant and K Swaminathan. Free vibration of isotropic, orthotropic, and multilayer plates based on higher order refined theories. *Journal of Sound and Vibration*, 241(2):319–327, 2001.

[14] K Swaminathan and SS Patil. Analytical solutions using a higher order refined computational model with 12 degrees of freedom for the free vibration analysis of antisymmetric angle-ply plates. *Composite Structures*, 82(2):209–216, 2008.

[15] H Murakami. Laminated composite plate theory with improved in-plane responses. *Journal of Applied Mechanics*, 53(3):661–666, 1986.

[16] JG Ren. A new theory of laminated plate. *Composites Science and Technology*, 26(3):225–239, 1986.

[17] JG Ren. Bending theory of laminated plate. *Composites science and technology*, 27(3):225–248, 1986.

[18] L Libresku. Improved linear theory of elastic anisotropic multilayered shells. part 1. *Polymer Mechanics*, 11(6):885–896, 1975.

[19] ME Fares and M Kh Elmarghany. A refined zigzag nonlinear first-order shear deformation theory of composite laminated plates. *Composite Structures*, 82(1):71–83, 2008.

[20] KN Cho, CW Bert, and AG Striz. Free vibrations of laminated rectangular plates analyzed by higher order individual-layer theory. *Journal of Sound and Vibration*, 145(3):429–442, 1991.

[21] Asghar Nosier, Rakesh K Kapania, and JN Reddy. Free vibration analysis of laminated plates using a layerwise theory. *AIAA journal*, 31(12):2335–2346, 1993.

[22] DH Robbins and JN Reddy. Modelling of thick composites using a layerwise laminate theory. *International Journal for Numerical Methods in Engineering*, 36(4):655–677, 1993.

[23] Junuthula Narasimha Reddy. *Mechanics of laminated composite plates and shells: theory and analysis*. CRC press, 2004.

[24] JN Reddy. An evaluation of equivalent-single-layer and layerwise theories of composite laminates. *Composite Structures*, 25(1):21–35, 1993.

[25] Masoud Tahani. Analysis of laminated composite beams using layerwise displacement theories. *Composite Structures*, 79(4):535–547, 2007.

[26] N. Gardner, E. Wang, P. Kumar, and A. Shukla. Blast mitigation in a sandwich composite using graded core and polyurea interlayer. *Experimental Mechanics*, pages 1–15, 2011.

[27] M. Jackson and A. Shukla. Performance of sandwich composites subjected to sequential impact and air blast loading. *Composites Part B: Engineering*, 42(2):155–166, 2011.

[28] S. Nemat-Nasser, W. Kang, J. McGee, W. Guo, and J. Isaacs. Experimental investigation of energy-absorption characteristics of components of sandwich structures. *International journal of impact engineering*, 34(6):1119–1146, 2007.

[29] S. Tekalur, A. Bogdanovich, and A. Shukla. Shock loading response of sandwich panels with 3-d woven e-glass composite skins and stitched foam core. *Composites Science and Technology*, 69(6):736–753, 2009.

[30] E. Wang, N. Gardner, and A. Shukla. The blast resistance of sand- wich composites with stepwise graded cores. *International Journal of Solids and Structures*, 46(18):3492–3502, 2009.

[31] E. Carrera and S. Brischetto. A survey with numerical assessment of classical and refined theories for the analysis of sandwich plates. *Applied mechanics reviews*, 62:010803, 2009.

[32] E. Carrera. Theories and finite elements for multilayered plates and shells:a unified compact formulation with numerical assessment and benchmarking. *Archives of Computational Methods in Engineering*, 10(3):215–296, 2003.

[33] V. Berdichevsky. An asymptotic theory of sandwich plates. *International Journal of Engineering Science*, 48(3):383–404, 2010.

[34] V. Berdichevsky. Nonlinear theory of hard-skin plates and shells. *International Journal of Engineering Science*, 48(3):357–369, 2010.

[35] Wenbin Yu, Dewey H Hodges, and Vitali V Volovoi. Asymptotic construction of reissner-like composite plate theory with accurate strain recovery. *International Journal of Solids and Structures*, 39(20):5185–5203, 2002.

[36] Wenbin Yu, Dewey H Hodges, and Vitali V Volovoi. Asymptotically accurate 3-d recovery from reissner-like composite plate finite elements. *Computers & structures*, 81(7):439–454, 2003.

[37] Wenbin Yu and Dewey H. Hodges. An asymptotic approach for thermoelastic analysis of laminated composite plates. *Journal of Engineering Mechanics*, 130(5):531–540, 2004.

[38] Wenbin Yu and Dewey H Hodges. A simple thermopiezoelastic model for smart composite plates with accurate stress recovery. *Smart materials and structures*, 13(4):926, 2004.

[39] Wenbin Yu, Jun-Sik Kim, Dewey H Hodges, and Maenghyo Cho. A critical evaluation of two reissner–mindlin type models for composite laminated plates. *Aerospace Science and Technology*, 12(5):408–417, 2008.

[40] R.B. Nelson and D.R. Lorch. A refined theory for laminated orthotropic plates. *ASME Journal of Applied Mechanics*, 41(1):177–183, 1974.

[41] F.B. Hildebrand, E. Reissner, and G.B. Thomas. Notes on the foundations of the theory of small displacements of orthotropic shells. *NACA*, TN 1833, 1949.

[42] J. Hohe, L. Librescu, and S.Y. Oh. Dynamic buckling of flat and curved sandwich panels with transversely compressible core. *Composite Structures*, 74(1):10–24, July 2006.

[43] R. Li and G.A. Kardomateas. Nonlinear high-order core theory for sandwich plates with orthotropic phases. *AIAA Journal*, 46(11), November 2008.

[44] Victor Birman and Charles W Bert. Wrinkling of composite-facing sandwich panels under biaxial loading. *Journal of Sandwich Structures and Materials*, 6(3):217–237, 2004.

[45] GS Gough, CF Elam, and NA De Bruyne. The stabilization of a thin sheet by a continuous supporting medium. *JR Aeronaut. Soc*, 44(349):12–43, 1940.

[46] Nicholas John Hoff. The buckling of sandwich-type panels. *Journal of the Aeronautical Sciences (Institute of the Aeronautical Sciences)*, 12(3), 2012.

[47] Dan Zenkert. *An introduction to sandwich construction*. Engineering materials advisory services, 1997.

[48] Jack R Vinson. *The behavior of sandwich structures of isotropic and composite materials*. CRC Press, 1999.

[49] Y Frostig. Buckling of sandwich panels with a flexible core—high-order theory. *International Journal of SOLIDS and STRUCTURES*, 35(3):183–204, 1998.

[50] DJ Dawe and WX Yuan. Overall and local buckling of sandwich plates with laminated faceplates, part i: Analysis. *Computer methods in applied mechanics and engineering*, 190(40):5197–5213, 2001.

[51] WX Yuan and DJ Dawe. Overall and local buckling of sandwich plates with laminated faceplates, part ii: Applications. *Computer methods in applied mechanics and engineering*, 190(40):5215–5231, 2001.

[52] Walter K Vonach and Franz G Rammerstorfer. A general approach to the wrinkling instability of sandwich plates. *Structural Engineering and Mechanics*, 12(4):363–376, 2001.

[53] JB Dafedar, YM Desai, and AA Mufti. Stability of sandwich plates by mixed, higher-order analytical formulation. *International journal of solids and structures*, 40(17):4501–4517, 2003.

[54] GA Kardomateas. Wrinkling of wide sandwich panels/ beams with orthotropic phases by an elasticity approach. *Journal of applied mechanics*, 72(6):818–825, 2005.

[55] Maria Antonieta Aiello and Luciano Ombres. Buckling load design of sandwich panels made with hybrid laminated faces and transversely flexible core. *Journal of Sandwich Structures and Materials*, 9(5):467–485, 2007.

[56] Ahmed K Noor, Jeanne M Peters, and W Scott Burton. Three-dimensional solutions for initially stressed structural sandwiches. *Journal of engineering mechanics*, 120(2):284–303, 1994.

[57] F.B. Hildebrand, E. Reissner, and G.B. Thomas. Note on the foundations of the theory of small displacements of orthotropic shells. *NACA*, pages TN–1833, 1949.

[58] R.B. Nelson and D.R. Lorch. A refined theory for laminated orthotropic plates. *ASME J Appl Mech*, 41:177–83, 1974.

[59] L. Librescu. Elastostatics and kinematics of anisotropic and heterogeneous shell type structures. *The Netherlands: Noordhoff*, 1975.

[60] K.H. Lo, R.M. Christensen, and E.M. Wu. A higher order theory of plate deformation, part 1: Homogeneous plates. *ASME J Appl Mech*, 44(4):663–8., 1977.

[61] K.H. Lo, R.M. Christensen, and E.M. Wu. A higher order theory of plate deformation, part 2: Laminated plates. *ASME J Appl Mech*, 44(4):669–76, 1977.

[62] J.N. Reddy. A simple higher order theory for laminated composite plates. *ASME J Appl Mech*, 51:745–52., 1984.

[63] M. Levinson. An accurate simple theory of the statics and dynamics of elastic plates. *Mech Res Commun*, 7, 1980.

[64] M.V.V. Murthy. An improved transverse shear deformation theory for laminated anisotropic plates. *NASA Technical Paper*, 1981.

[65] N.R. Senthilnathan and K.H. Lim. Buckling of shear deformable plates. *AIAA J*, 25(9):1268–71., 1987.

[66] J.N. Reddy and N.D. Phan. Stability and vibration of isotropic and laminated plates according to higher order shear deformation theory. *J Sound Vibration*, 98:157–70., 1985.

[67] Chang-Yong Lee and Dewey H. Hodges. Dynamic variational-asymptotic procedure for laminated composite shells - part II: High-frequency vibration analysis. *Journal of Applied Mechanics*, 76, 2009.

[68] P Malatkar. *Nonlinear vibrations of cantilever beams and plates.* PhD thesis, Virginia Polytechnic Institute and State University, USA, 2003.

[69] A Israr. *Vibration analysis of cracked aluminium plates.* PhD thesis, University of Glasgow, Glasgow, UK, 2008.

[70] Von Karman. Festigkeitshprobleme im machinenbau. *Encyklopadie der Mathematishen Wissenchaften*, IV:349, 1910.

[71] H.M Berger. A new approach to the analysis of large deflections of plates. *Journal of Applied Mechanics*, 22:465–472, 1955.

[72] T Wah. Large amplitude flexural vibration of rectangular plates. *International Journal of Mechanical Sciences*, 5:425–438, 1963.

[73] C.S. Huang and A.W. Leissa. Vibration analysis of rectangular plates with side cracks via the ritz method. *Journal of Sound and Vibration*, 323:974–988, 2009.

[74] Dewey H. Hodges, Atilgan, Ali R., , and Donald A. Danielson. A geometrically nonlinear theory of elastic plates. *J. Applied Mechanics*, 60:109–116, March 1993.

[75] C.Y. Chia. *Nonlinear analysis of plates*. McGraw-Hill, London, 1980.

[76] Ali H. Nayfeh and Dean T. Mook. *Nonlinear Oscillations*. Wiley, March, 1995.

[77] M Sathyamoorthy. Effects of large amplitude, shear and rotatory inertia on vibration of rectangular plates. *Journal of Sound and Vibration*, 63:161–167, 1979.

[78] E. Riks. Bifurcation and stability, a numerical approach. *National Aerospace Laboratory NLR*, NLR(MP):84078u, 1984.

[79] M.S. Gadala and G. AE. Oravas. Numerical solutions of nonlinear problems of continua-i. *Computers & Structures*, 19:865–877, 1984.

[80] R. Szilard. Critical load and post-buckling analysis by fem using energy balancing technique. *Computers & Structures*, 20(1-3):277–286, 1985.

[81] E. Carnoy. Postbuckling analysis of elastic structures by the finite element method. *Computer Methods in Applied Mechanics and Engineering*, 23:143–174, 1980.

[82] D. Karamanlidis and E.E. McEwen. Improved finite pre-and postbuckling analysis of thin-walled structures. *ASME*, 2:211–218, 1985.

[83] G.A. Thurston, F.A. Brogan, and P. Stehlin. Postbuckling analysis using a general-purpose code. *AIAA*, 24(6), 1986.

[84] Newton's method. `http://mathworld.wolfram.com/NewtonsMethod.html`. Accessed: 2015-02-10.

[85] Renfu Li, George A. Kardomateas, and George J. Simitses. Point-wise impulse (blast) response of a composite sandwich plate including core compressibility effects. *International Journal of Solids and Structures*, 46:2216–2223, 2009.

[86] Haiying Huang and George A. Kardomateas. Buckling and initial postbuckling behavior of sandwich beams including transverse shear. *AIAA Journal*, 40(11):2331–2335, 2002.

[87] Luciano Demasi and Wenbin Yu. Assess the accuracy of the variational asymptotic plate and shell analysis using the generalized unified formulation. *Mechanics of Advanced Materials and Structures*, 20:227–241, 2013.

[88] V. L. Berdichevsky. Variational-asymptotic method of constructing a theory of shells. *PMM*, 43(4):664–687, 1979.